THE UNIVERSITY OF CALGARY

PERFORMANCE EVALUATION OF PASSIVE OPTICAL FIBER LOCAL AREA NETWORKS

by

Abraham Olatunji Fapojuwo

A THESIS

SUBMITTED TO THE FACULTY OF GRADUATE STUDIES

IN PARTIAL FULFILLMENT OF THE REQUIREMENTS FOR THE

DEGREE OF MASTER OF SCIENCE

DEPARTMENT OF ELECTRICAL ENGINEERING

CALGARY, ALBERTA

DECEMBER, 1985

ISBN Ø-315-29943-6

THE UNIVERSITY OF CALGARY

FACULTY OF GRADUATE STUDIES

The undersigned certify that they have read, and recommended to the Faculty of Graduate Studies for acceptance, a thesis entitled, "*Performance Evaluation of Passive Optical Fiber Local Area Networks*" submitted by Abraham Olatunji Fapojuwo in partial fulfillment of the requirements for the degree of Master of Science.

David Irvine-Halliday
Supervisor - Dr. D. Irvine-Halliday
Dept. of Electrical Engineering

Wah Chun Chan
Dr. W.C. Chan
Dept. of Electrical Engineering

Ronald H. Johnston
Dr. R.H. Johnston
Dept. of Electrical Engineering

Graham Birtwistle
Dr. G.M. Birtwistle
Dept. of Computer Science

Date: 13 Dec. 1985

Abstract

A methodology for evaluating the performance of passive optical fiber local area networks is presented. Five network performance parameters are considered. These include the total network path length, the allowable attenuation, the dynamic range requirement of the network, the network bandwidth capability, and the network traffic handling characteristics.

The implementation of a passive optical fiber local area network topology for each of the conventional local area network topologies - star, linear bus and loop is presented. Equations, algorithms and procedures for evaluating the performance parameters with respect to each passive optical fiber local area network topology are also presented.

A versatile fiber optic network design simulation package capable of facilitating the analysis and design of planned passive optical fiber local area networks is developed.

The simulator is used to select the optimum network topology in terms of path length, network attenuation, dynamic range, bandwidth and traffic characteristics. The simulator running speed on the CYBER 205 Supercomputer is approximately 100 cpu seconds for a 6-node network and the results obtained so far indicate that the star topology exhibits superior performance over the linear bus and loop topologies.

Acknowledgements

It is a great pleasure at this time to acknowledge others who have contributed immensely to the successful completion of this work.

First, I give great thanks to God who has granted me the wisdom and good health throughout the period of this study.

I am particularly grateful to my Supervisor, Dr. Dave Irvine-Halliday for his constant encouragement and guidance. I appreciate his suggestions, constructive criticisms and the numerous stimulating discussions we have had during the course of this study, and more importantly, his invaluable friendship to me will ever be remembered.

Many thanks are due to all my friends who have done so much to help establish a convivial environment in which to work or who have provided the needed moral support during the difficult stages of this work.

I am indebted to Kristen Mollin for her constant help in facilitating my use of the CDC CYBER 205 Supercomputer and for vectorizing the Traffic Modules of the network design software package developed in this thesis.

Financial assistance received from the University of Calgary in the form of graduate assistantships is greatly acknowledged.

Thanks are due to Ms. Laura Smyth for formatting the thesis.

To Victoria, my wife, I owe much for her unending patience, encouragement and understanding without which I could hardly have completed this work.

To my parents

Table of Contents

Page No.

Table of Contents vi
List of Tables viii
List of Figures ix
List of Symbols xii
1. INTRODUCTION 1
1.1. Introduction and Purpose of the Thesis 1
1.2. Optical Fiber Local Area Network Components 3
1.2.1. Electrical-to-Optical Conversion Components 3
1.2.1.1. Source Output Power 3
1.2.1.2. Source Spectrum 6
1.2.1.3. Source Extinction Ratio 6
1.2.2. Optical Fiber 8
1.2.2.1. Fiber Attenuation 8
1.2.2.2. Fiber Dispersion 9
1.2.3. Digital Optical Receiver 11
1.2.3.1. Receiver Sensitivity Analysis 12
1.2.3.2. Receiver Sensitivity Penalty 14
1.3. Scope of the Thesis 16
2. IMPLEMENTATION OF POFLAN TOPOLOGIES 18
2.1. Introduction 18
2.2. Models of Optical Interconnecting Components 19
2.2.1. Unidirectional Coupler 19
2.2.2. Transmissive Star Coupler 21
2.2.3. Optical Connectors 24
2.3 POFLAN Implementations 24
2.3.1. Loop Topology 26
2.3.1.1. Transmission Loss Analysis 26
2.3.2. Linear Bus Topology 31
2.3.2.1. Transmission Loss Analysis 31
2.3.3. Star Topology 34
2.3.3.1. Transmission Loss Analysis 34
2.4. Summary 34
3. ANALYSIS OF POFLAN PERFORMANCE PARAMETERS 37
3.1. Introduction 37
3.2. POFLAN Performance Parameters 37
3.2.1. Total Fiber Length Required 37
3.2.2. Network Attenuation 38

Table of Contents (continued)

3.2.3. Network Dynamic Range Requirement 39
3.2.4. Network Bandwidth Capability 40
3.2.5. Network Traffic Characteristics 45
3.2.5.1. Implications of the stated Assumptions 47
3.2.5.2. Description of the CSMA/CD Access Protocol 48
3.2.5.3. Implementation of the Network Traffic Model 51
3.2.5.4. Definition of the Network Traffic Parameters 53
3.3. Summary 54
4. EVALUATION OF POFLAN PERFORMANCE BY COMPUTER SIMULATION 55
4.1. Introduction 55
4.2. Salient Features and Capabilities of the FONSIM Package 56
4.3. FONSIM Description 58
4.3.1. Level 1 Subroutines 58
4.3.2. Level 2 Subroutines 66
4.3.3. Level 3 Subroutines 67
4.4. FONSIM Verification and Validation 76
4.5. Application of the FONSIM Package 85
4.5.1. Simulation Experiments 85
4.5.2. Selected Network Parameters 89
4.5.3. Simulation Results and Discussion 89
4.5.3.1. Network Size 94
4.5.3.2. Transmission Loss and Dynamic Range 99
4.5.3.3. Maximum Fiber Attenuation Coefficient 99
4.5.3.4. Network Bandwidth Capacity 108
4.5.3.5. Basic Performance Parameters for the 6-node Network 115
4.5.3.6. Network Throughput 117
4.5.3.7. Average Packet Delay 123
4.5.3.8. The Effects of Different Backoff Algorithms 130
4.5.3.9. Backlog Clearing Time 131
4.6. Summary 137
5. CONCLUSIONS AND SUGGESTIONS FOR FUTURE DEVELOPMENTS 138
5.1. Conclusions 138
5.2. Suggestions for Future Developments 141
References 143
Appendix 147

List of Tables

Table No.	Title	Page No.
2.1	Minimum and Maximum excess losses of an N x N passive Transmissive Star Coupler	25
4.1	Classification of the FONSIM Package modules into different levels	60
4.2	Ethernet Parameters	83
4.3	Distance Matrix (in km) of the 6-node Network Example	87
4.4a	Selected Network Parameter Values	90
4.4b	Selected Typical LED Data	91
4.4c	Selected Typical Fiber Parameters	92
4.4d	Selected typical SiAPD and TZ amplifier parameters	93
4.5	Basic Performance Parameters for the 6-node Network example	116

List of Figures

Figure No.	Title	Page No.
1.1a	Basic Star LAN Topology	2
1.1b	Basic Linear Bus LAN Topology	2
1.1c	Basic Loop LAN Topology	2
1.2(a)	Typical LED diode Output Power/Drive Current Characteristic	4
1.2(b)	Typical LASER Output Power/Drive Current Characteristic	5
1.3(a)	Typical LED source Spectra	7
1.3(b)	Typical LASER source Spectra	7
1.4	Typical Loss Versus Wavelength characteristics for a Silica multimode graded-index fiber	10
2.1(a)	Schematic Operation of a Unidirectional Coupler in the Transmitting Mode	20
2.1(b)	Schematic Operation of a Unidirectional Coupler in the Receiving Mode	20
2.1(c)	Schematic Operation of two Unidirectional Couplers at a nodal access point on the broadcast channel	20
2.2	Transmissive Star Coupler Model	22
2.3(a)	Implementation of passive, broadcast optical fiber Loop Topology	27
2.3(b)	Implemented Loop topology indicating the signals at various points on the common channel	28
2.3c	Implementation of the double Loop Topology	29
2.4	Implementation of passive, broadcast optical fiber Linear Bus Topology	32
2.5	Implementation of passive, broadcast optical fiber Star Topology	35
3.1	Section of an Optical fiber showing input and output signals	41
3.2	Network Traffic Simulation Model	46
3.3	Operational flowchart of the 1-persistent CSMA/CD access protocol	52
4.1	General Organization of the FONSIM package	59
4.2	The inverse-transform approach for an exponential random variable	63
4.3(a)	Operational flowchart of TRAFIC	69
4.3(b)	Operational flowchart of PKTARV	70
4.3(c)	Operational flowchart of COLCHK	74
4.3(d)	Operational flowchart of PKTDEP	75
4.4	M/M/1 Queueing System	77
4.5(a)	Average number of packets in the Nodal Queue Versus offered load	79
4.5(b)	Average number of packets in the M/M/1 System Versus offered load	80
4.6(a)	Average Packet Delay in the Nodal Queue Versus offered load	81
4.6(b)	Average Packet Delay in the M/M/1 System Versus offered load	82
4.7	Comparison of Experimental and simulated values of Ethernet throughput-offered load characteristics	84
4.8	Configuration of the 6-node Network example	86

4.9(a) Network Size Versus Operating bit rate 95
4.9(b) Effect of Degradation factors on Network size for STARNET 96
4.9(c) Effect of Degradation factors on Network size for LOOPNET 97
4.9(d) Effect of Degradation factors on Network size for BUSNET 98
4.10(a) Minimum Transmission Loss Versus Network size 100
4.10(b) Maximum Transmission Loss Versus Network size 101
4.10(c) Network Dynamic Range Versus Network size 102
4.11(a) Maximum attenuation coefficient Versus operating bit rate 103
4.11(b) Variation of the maximum attenuation coefficient with operating bit rate for STARNET 104
4.11(c) Variation of the maximum attenuation coefficient with network size for STARNET 105
4.11(d) Variation of the maximum attenuation coefficient with network size for LOOPNET 106
4.11(e) Variation of the maximum attenuation coefficient with network size for BUSNET 107
4.12(a) Maximum Network Bandwidth Versus maximum link distance for $\alpha = 3$ dB/km , $N = 6$ 109
4.12(b) Maximum Network Bandwidth Versus maximum link distance for $\alpha = 5$ dB/km , $N = 6$ 110
4.12(c) Maximum Network Bandwidth Versus maximum link distance for $\alpha = 3$ dB/km , $N = 12$ 111
4.12(d) Effect of Bandwidth Length dependence factor on maximum Network Bandwidth for STARNET 112
4.12(e) Effect of Bandwidth Length dependence factor on maximum Network Bandwidth for LOOPNET 113
4.12(f) Effect of Bandwidth Length dependence factor on maximum Network Bandwidth for BUSNET 114
4.13(a) Network Throughput Versus Offered load for B = 1 Mb/s, $\frac{1}{\mu} = 2000$ bits 118
4.13(b) Network Throughput Versus Offered load for B = 10 Mb/s, $\frac{1}{\mu} = 2000$ bits 119
4.13(c) Effect of varying the channel capacity on Network Througput for STARNET 120
4.13(d) Network Throughput Versus Offered load for B = 1 Mb/s, $\frac{1}{\mu} = 256$ bits 121
4.13(e) Effect of varying the mean packet length on Network Throughput for STARNET 122
4.14(a) Average Packet Delay Versus Offered load for B = 1 Mb/s, $\frac{1}{\mu} = 2000$ bits 125
4.14(b) Average Packet Delay Versus Offered load for B = 10 Mb/s, $\frac{1}{\mu} = 2000$ bits 126
4.14(c) Effect of varying the channel capacity on Average packet delay for STARNET 127
4.14(d) Average Packet Delay Versus Offered load for B = 1 Mb/s, $\frac{1}{\mu} = 256$ bits 128
4.14(e) Effect of varying the mean packet length on Average packet delay for STARNET 129
4.15(a) Effect of Backoff Algorithm on Network Throughput for STARNET 132
4.15(b) Effect of Backoff Algorithm on Average packet Delay for STARNET 133
4.16(a) Backlog Clearing time Versus Offered load for B = 1 Mb/s, $\frac{1}{\mu} = 2000$ bits 134
4.16(b) Effect of higher channel capacity on backlog clearing time 135

4.16(c) Effect of lower mean packet length on backlog clearing time 136

LIST OF SYMBOLS

A	Optical pulse energy
A_i	Optical pulse energy of the input pulse into the fiber
A_o	Optical pulse energy of the output pulse from the fiber
APD	Avalanche Photodiode
B	Operating Bit rate
BEB	Binary Exponential Backoff algorithm
BER	Bit Error Rate
BJT	Bipolar Junction Transistor
BW	Optical Bandwidth
BWL	Bandwidth-Length product
c	Velocity of light in vacuum
C	Channel Capacity
C_A	Absorption Loss function
C_{gd}	Gate-to-drain Capacitance of the Field Effect Transistor
C_{gs}	Gate-to-source Capacitance of the Field Effect Transistor
C_M	Microbending Loss
cpu	Central Processing Unit
C_p	Coupling Coefficient of the Unidirectional Coupler
C_{phd}	Photodiode Capacitance
$C_{p_{opt}}$	Optimum Coupling Coefficient
C_R	Rayleigh Loss Coefficient
CSMA/CD	Carrier Sense Multiple Access with collision detection
C_T	Total input Capacitance of the amplifier
D	Fiber Length

D_B	Distance between the two furthest nodes in a Linear Bus Topology
$D_{B_{\min}}$	Distance between the two closest nodes in a Linear Bus Topology
D_{jc}	Distance from a node to the Star Coupler
D_L	Distance between the two furthest nodes in a Loop Topology
$D_{L_{\min}}$	Distance between the two closest nodes in a Loop Topology
$D_{\max}$	Distance between the two furthest nodes in a network
$D_{\min}$	Distance between the two closest nodes in a network
D_S	Distance between the two furthest nodes in a Star Topology
$D_{S_{\min}}$	Distance between the two closest nodes in a Star Topology
D_{TB}	Total fiber length required by the Linear Bus topology
D_{TL}	Total fiber length required by the Loop topology
D_{TS}	Total fiber length required by the Star topology
$E_R(0)$	Average energy received which represents a 'zero' data bit
$E_R(1)$	Average energy received which represents a 'one' data bit
$E(Q_m)$	Expected number of packets in the queue of the $M/M/1$ system
$E(X)$	Expected number of packets in the $M/M/1$ system
f	Frequency
f_{3dB}	3 dB Optical Bandwidth
FET	Field Effect Transistor
$F(x)$	Probability distribution function of x
g_m	Field Effect Transistor transconductance
GRC	Gaussian - Raised Cosine receiver input - output pulse shapes
h	Planck's constant
$H_{FM}(\omega)$	Fiber Transfer function
$H_n(\omega)$	Normalized baseband Transfer function

$H_{out}'(f)$	Normalized Fourier Transform of the optical pulse shape at the receiver output
$H_p'(f)$	Normalized Fourier Transform of the optical pulse shape at the receiver input
HZ	High impedance amplifier design
I	Input Drive Current of the Light Source
I_{dm}	Bulk Leakage Current of the Avalanche photodiode
I_{du}	Unmultiplied Dark Current of the photodiode
I_L	Sum of the gate leakage current of the Field Effect transistor and the surface leakage current of a photodiode
I_{th}	Threshold current of the avalanche photodiode
I_{tho}	Threshold current of the APD at a temperature T_o
I_2	Normalized weighting integral for an arbitrary input optical pulse shape
I_2'	Normalized weighting integral for a narrow input optical pulse shape
$I_2^{(GRC)}$	Normalized weighting integral for a Gaussian optical pulse at the receiver input and a raised Cosine optical pulse at the receiver output
I_3	Normalized weighting integral for an arbitrary input optical pulse shape
I_3'	Normalized weighting integral for a narrow input optical pulse shape
$I_3^{(GRC)}$	Normalized weighting integral for a Gaussian optical pulse at the receiver input and a raised Cosine optical pulse at the receiver output
j	complex variable parameter
k_B	Boltzmann's constant
K_z	Proportionality factor between the minimum received power and the optical bandwidth
$K_z^{(APD)}$	K_z for the Avalanche photodiode
$K_z^{(PIN)}$	K_z for the PIN photodiode

L	Time-average number of packets in the $M/M/1$ system
LI	Lower confidence-interval limit
L_{DR}	Network dynamic range
$L_{e_{\max}}$	Maximum excess loss of the star coupler
$L_{e_{\min}}$	Minimum excess loss of the star coupler
L_F	Total Fiber loss
L_M	System Loss margin
$L_{\max}^{NET}$	Maximum network attenuation
$L_{\max}^{TRX}$	Maximum transmission loss
$L_{\min}^{TRX}$	Minimum transmission loss
L_q	Time-average number of packets in the nodal queue of the $M/M/1$ system.
L_s	Splitting loss of the Star Coupler
M	Exponentially distributed (Markovian) process
$M/M/1$	A queueing system with exponentially distributed interarrival and service times, only one server, infinite capacity and first-in, first-out queueing discipline
M_a	Avalanche gain of the APD
$min(a,b)$	Minimum value between a and b
M_m	m^{th} central moment of an optical pulse
M_{mh}	m^{th} central moment of the normalized baseband fourier transform of an optical pulse
M_{mi}	m^{th} central moment of the input optical pulse shape into the fiber
M_{mo}	m^{th} central moment of the output optical pulse shape from the fiber
N	Number of nodes in a network
$N_{\max}$	Maximum number of nodes in a network
N_{pe}	Number of photogenerated electrons generated per bit period

$N_{pe}^{(PIN)}$	Number of photogenerated electrons by a PIN photodiode
N_s	Number of independent simulation runs
OH^-	Hydroxyl Ion
pkt.	Packet
POFLAN	Passive Optical Fiber Local Area Network
$\overline{P}$	Minimum average optical power required at the detector input for a specified bit error rate
P_B	Power budget
P_{co}	Power output from a unidirectional coupler output port
P_i	Power input to a unidirectional coupler input port
$\overline{P}_i$	Ideal Optical Sensitivity
$\overline{P}_{I_{dm} \neq 0}$	Nonideal Optical sensitivity due to nonzero bulk leakage current
PIN	p - intrinsic - n (dopants)
$P_{\max}$	Maximum power received by a node
$P_{\max_{opt}}$	Optimum maximum power received by a node
$P_{\min}$	Minimum received power by a node
$P_{\min_{opt}}$	Optimum minimum power received by a node
P_n	Steady state probability that a system is in state n
$\overline{P}_n$	Nonideal Optical sensitivity
P_o	Optical output power from the light source
P_{oj}	Difference between P_{roj} and the insertion loss of a unidirectional coupler connecting node j to the fiber channel
P_{roj}	Power remaining in the fiber channel after a fraction has been tapped by node j
P_R	Power tapped into a network node by the unidirectional coupler
P_{Ri}	Power received at node i
P_T	Coupled Power into the fiber by a transmitting node

P_{Ti}	Coupled power into the fiber by node i
$\overline{P}_{\gamma \neq 1}$	Nonideal Optical sensitivity due to intersymbol interference
$\overline{P}_{\varepsilon \neq 0}$	Nonideal Optical sensitivity due to nonzero extinction ratio
$P(D)$	Optical power at a fiber length D
$P(0)$	Coupled power into the fiber at a fiber length D equal to zero
q	Electronic charge
Q	Bit error rate parameter
Q_m	Random variable that counts the number of packets waiting in the queue for transmission
R_F	Feedback resistance of the Transimpedance amplifier
R_F–B	Feedback resistance-Operating bit rate product
rms	root mean square
s_r	Power splitting ratio of the Star Coupler
$s(t)$	Optical pulse shape
$S^2(N_s)$	Sample variance of N_s observations
$S(\omega)$	Fourier transform of an optical pulse
S_I	Equivalent input noise current spectral density
$S_i(\omega)$	Fourier transform of the optical pulse shape at the fiber input
$S_o(\omega)$	Fourier transform of the optical pulse shape at the fiber output
S_{tx}	Spectral relative intensity of the source
S_V	Equivalent input noise voltage spectral density
t	Time
$t_{N_s-1,\,1-\frac{\kappa}{2}}$	Upper $1-\dfrac{\kappa}{2}$ critical point for the t-distribution with (N_s-1) degrees of freedom
T	Operating temperature
t_c	Central time of an optical pulse

t_{ci}	Central time of the input optical pulse into the fiber
t_{co}	Central time of the output optical pulse from the fiber
t_d	Transit delay along the fiber
T_o	Characteristic temperature
TZ	Transimpedance Amplifier design
UI	Upper confidence-interval limit
$U(0,1)$	Uniformly distributed random number chosen between 0 and 1
W	Average packet delay in the $M/M/1$ system
W_q	Average packet delay in the nodal queue of the $M/M/1$ system
x	Excess noise parameter of the APD
X	Random variate
$\overline{Y}(N_s)$	Sample mean of N_s observations
Z	Signal independent noise parameter of the amplifier and the photodiode
Z_i	Signal independent noise parameter for the case $I_2 = I'_2$ and $I_3 = I'_3$
α	Frequency independent attenuation coefficient
α_c	Fraction of the optical power transmitted through a connector
$\alpha(\lambda_s)$	Fiber attenuation coefficient at a wavelength λ_s
$\alpha(\omega)$	Attenuation coefficient at a frequency ω
β	Factor which accounts for the insertion loss of the unidirectional coupler
$\beta(\omega)$	Phase parameter at a frequency ω
Γ	Factor appearing in the spectral density of voltage noise generator of the Field Effect transistor
γ	Fraction of the optical pulse contained within the bit period (occupancy factor)
δ	Chromatic dispersion parameter of the fiber

$\Delta\lambda_s$	Source root mean square linewidth
$\Delta\overline{P}$	Optical Sensitivity penalty
ε	Source extinction ratio
ζ	Photodiode responsivity
η_c	Light source coupling efficiency
η_e	Photodiode external quantum efficiency
η_q	Light source external quantum efficiency
Θ	Ambient temperature (kelvins)
κ	Confidence interval parameter
λ	Mean packet arrival rate
λ_s	Source operating wavelength
λ_o	Center operating wavelength of the light source
$\frac{1}{\mu}$	Average packet length
ξ	Optical bandwidth length dependence factor
ρ	Normalized offered load
σ^2	Second central moment of the optical pulse
σ_c	rms width of the fiber impulse response due to chromatic dispersion
σ_m	rms width of the fiber impulse response due to modal dispersion
σ_h	rms width of the normalized baseband transfer function
σ_i	rms width of the input optical pulse into the fiber
σ_o	rms width of the output optical pulse from the fiber
σ_s	rms width of the source output pulse
σ_p	rms width of the optical pulse at the detector input
τ	Branch-to-branch coupling ratio of the star coupler
ϕ	Mean of the exponential distribution

ψ	Parameter relating the occupancy factor and extinction ratio
ω	Angular frequency
$\lfloor z \rfloor$	The greatest integer that is less than or equal to the real number z
$\lvert ( ) \rvert$	Magnitude of ( )
$\int$	Integration
$\sum$	Summation

CHAPTER 1

INTRODUCTION

1.1. Introduction and Purpose of the Thesis

In recent years, a great deal of interest has centered on the design of optical fiber local area networks (LAN's) due to the unique characteristics of the optical fiber compared to conventional metallic cables. A number of these characteristics include extremely low transmission loss, very large bandwidth and total immunity to electromagnetic interference [1].

Current application trends of optical fiber LAN's are extending into various fields, such as in offices, factories, laboratories and University Campuses. Several results have been reported on the performance of installed optical fiber LAN's [2,3,4].

However, one of the challenging problems still facing designers of optical fiber LAN's is the performance evaluation of a planned network. To assess the performance of a network that is planned, a predictive technique, is necessary. Such a technique must be flexible, easy to use and must allow the consideration of different network alternatives.

The basic goal of this thesis is the development of a methodology, named FONSIM (Fiber Optic Network SIMulator) to be used for predicting the performance of planned passive optical fiber local area networks (POFLAN's). The performance of the conventional LAN topologies shown in Fig.1.1 are investigated. These topologies are studied in terms of five network performance criteria, namely, total fiber length, network attenuation, network dynamic range requirement, network bandwidth capability and network traffic characteristics.

The use of a design package such as FONSIM will provide the necessary insights into the performance of planned POFLAN's before they are installed and facilitate their graceful evolution in the future.

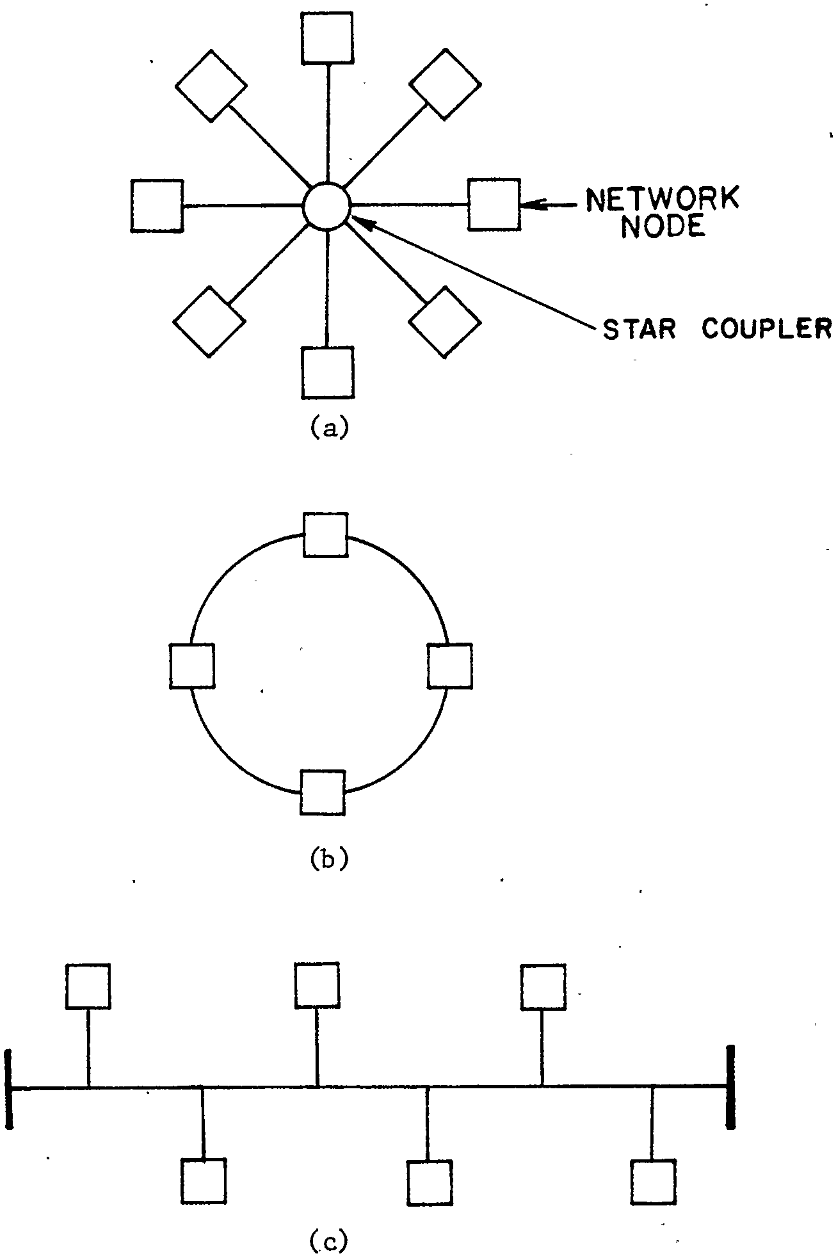

Fig. 1.1 (a) Basic Star LAN Topology

(b) Basic Loop LAN Topology

(c) Basic Linear Bus LAN Topology

1.2. Optical Fiber Local Area Network Components

In the context of this thesis, an optical fiber local area network is defined as a network for data communications among nodes such as computers, terminals and other devices, operating within a geographical area (typically less than 10 *km* in diameter) and at high data rates (typically greater than or equal to 1*Mbps*). A passive optical fiber LAN does not incorporate regenerators along the signal transmission path between any two network nodes so as to enhance the network reliability.

An optical fiber LAN consists mainly of electrical-to-optical conversion components, the optical fiber, optical-to-electrical conversion components, optical connectors and couplers. The characteristics of the first three listed devices are described below while a discussion on the last two devices is deferred till the second chapter.

1.2.1. Electrical-to-Optical Conversion Components

Current optical fiber LAN's employ either light emitting diodes (LED's) or injection laser diodes (ILD's) as the electrical-to-optical conversion component (light source). In the design of digital POFLAN's, three important parameters of the light source have significant effects on the overall network performance and must be accurately modeled, these are the source output power, the source spectral width, and the source extinction ratio.

1.2.1.1. Source Output Power

Fig.1.2 shows the typical source output power/input current characteristics. The LED output power is described by [5]

$$P_o \;=\; a_1 I + a_2 I^2 + ... + a_n I^n \tag{1.1}$$

where a_j , $j \in \{ 1,2,....,n \}$ are arbitrary constants. Equation (1.1) is usually approximated by the linear law

$$P_o \;\approx\; a_1 I \tag{1.2}$$

The ILD, being a threshold component, has an output power described by [6]

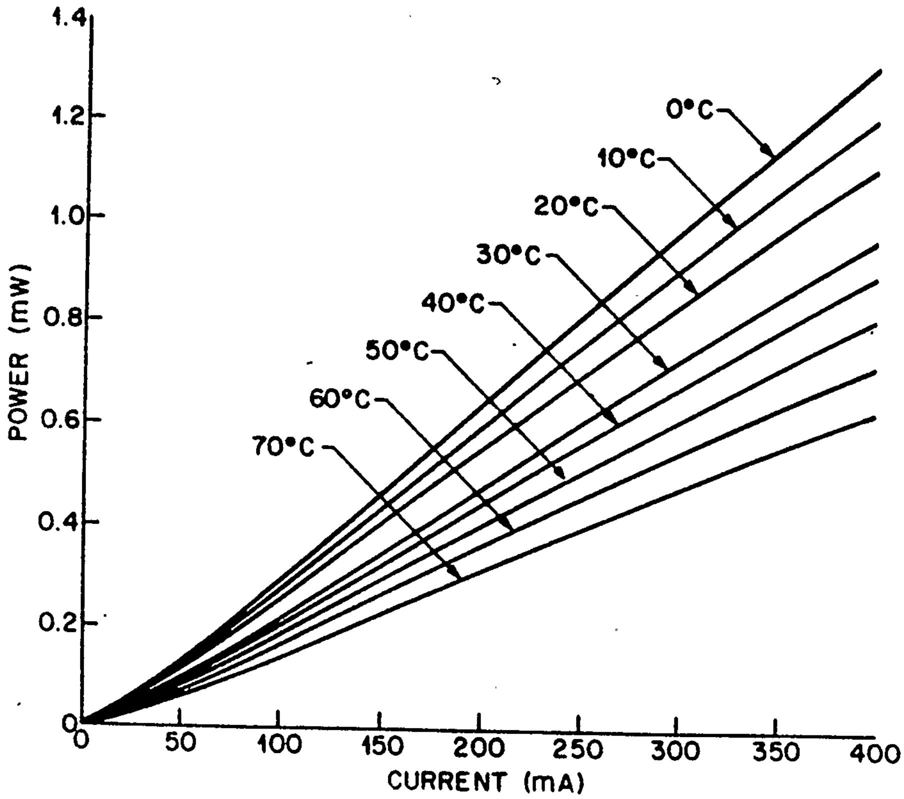

Fig. 1.2 (a) Typical LED Output Power/Drive Current Characteristics

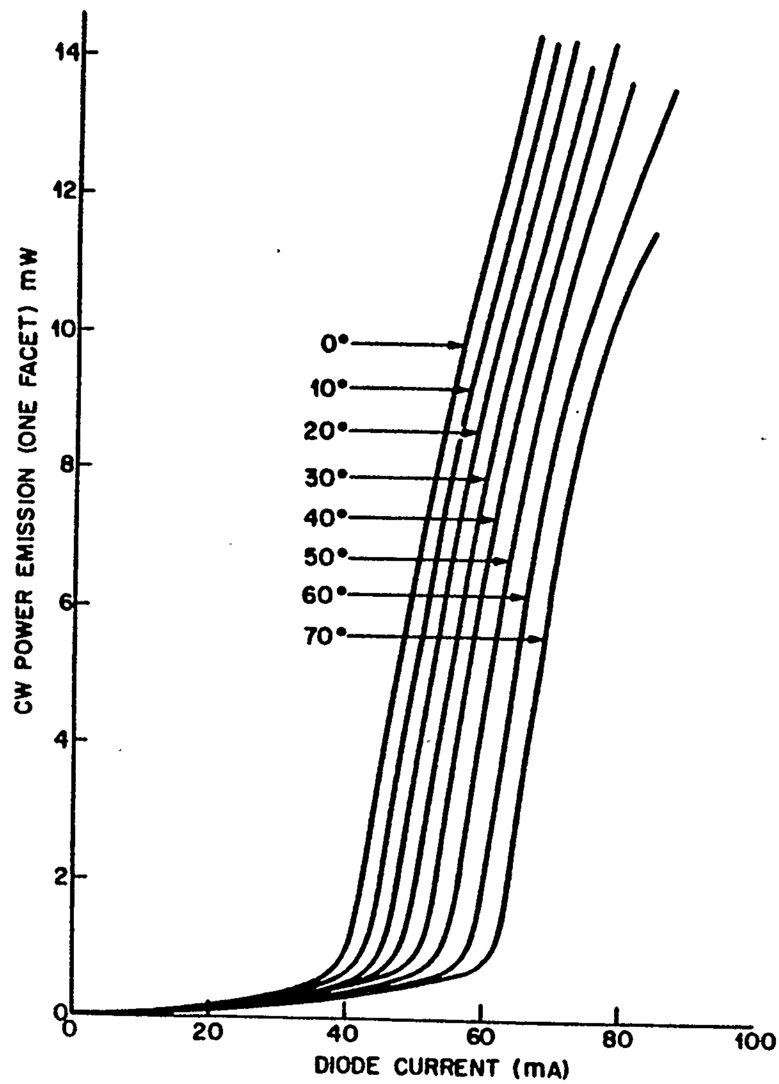

Fig. 1.2 (b) Typical LASER Output Power/Drive Current Characteristics

$$P_o = \eta_q \frac{hc}{q\lambda_s} (I - I_{th}) \tag{1.3}$$

The temperature dependence of the threshold current, I_{th}, is expressed in terms of the characteristic temperature, T_o, and defined by

$$I_{th} = I_{tho} e^{\frac{T}{T_o}} \tag{1.4}$$

The amount of power that is actually coupled into the optical fiber is the product of the source output power and its coupling efficiency. ILD's usually emit higher output power than LED's.

1.2.1.2. Source Spectrum

The typical time average spectra for the light sources are depicted in Fig.1.3. The spectra of both light sources are often modeled as a normalized Gaussian waveform [7]

$$S_{tx} = \frac{1}{\sigma_s\sqrt{2\pi}} \exp\left[-\frac{(\lambda_s - \lambda_o)^2}{2\sigma_s^2}\right] \tag{1.5}$$

The source spectrum is important in the evaluation of the fiber attenuation and dispersion. ILD's have a narrower spectrum than LED's.

1.2.1.3. Source Extinction Ratio

When a 'zero' data bit is transmitted by the light source, the optical energy received at the optical receiver may not be equal to zero if the light source is not completely extinguished. The ratio of the average energy received which represents a 'zero' data bit, $E_R(0)$, to that received which corresponds to a 'one' data bit, $E_R(1)$, is known as the source extinction ratio, ε [8],

$$\varepsilon = \frac{E_R(0)}{E_R(1)} \tag{1.6}$$

For an ideal light source, ε is equal to zero, however, this is not the case with ILD's biassed near threshold.

The other requirements of the light sources are stable operation over a wide temperature range,

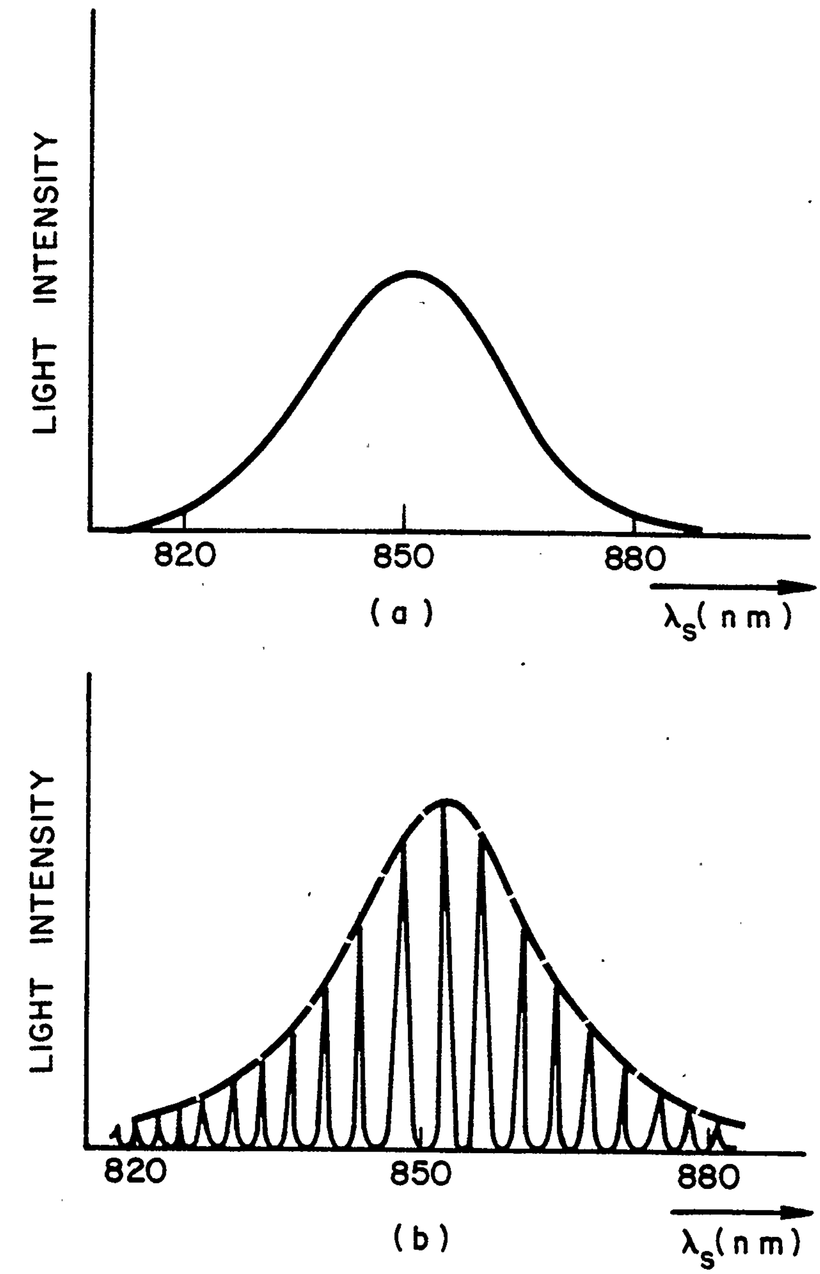

Fig. 1.3 (a) Typical LED Source Spectrum

(b) Typical LASER Source Spectra

high reliability, and low cost. LED's are normally superior to ILD's in terms of these requirements.

In summary, either an LED or an ILD may be selected for a POFLAN design. The choice depends on the type of application in which the POFLAN is designed to serve. Generally speaking, ILD's are more suitable for long haul and high data rate applications, while LED's are more appropriate for small to medium size and small to medium data rate networks.

1.2.2. Optical Fiber

Two types of optical fiber are available for use in the design of POFLAN's, they are the multimode fiber (step or graded-index) which allows the propagation of typically hundreds of separate optical modes and the single mode fiber (step-index) where only 'one' mode exists. Current optical fiber LAN's generally employ multimode graded-index fiber because its larger core diameter results in easier splicing, lower splicing loss and simplifies power splitting at tapping points. As a result, it is only this type of fiber that is considered in this thesis. The two vital characteristics of the graded-index multimode fiber which must be appropriately modeled are the fiber attenuation and dispersion.

1.2.2.1. Fiber Attenuation

The decrease of the optical power along the fiber length is governed by the relation [9]

$$P(D) = P(0)10^{-\frac{\alpha(\lambda_s)D}{10}} \tag{1.7}$$

Attenuation along the fiber is characterized by the attenuation coefficient, $\alpha(\lambda_s)$, which accounts for the various loss mechanisms inherent in the fiber. The loss mechanisms include Rayleigh scattering, impurity and dopant absorption (hydroxyl ion, Fe^{2+}, Cr^{3+}), infra-red molecular lattice absorption, ultra-violet atomic absorption and microbending. The fiber attenuation coefficient is generally modeled by [10]

$$\alpha(\lambda_s) = C_R\lambda_s^{-4} + C_A(\lambda_s) + C_M \tag{1.8}$$

A typical loss versus wavelength characteristic for a silica multimode graded-index fiber is illustrated in Fig.1.4 where the contribution of the different loss components are shown. It is observed that the loss coefficient is minimum in the long operating wavelength regions (1.1 - 1.3 μm) and (1.5 - 1.55 μm). The total fiber loss in decibels, L_F, is determined by weighting $\alpha(\lambda_s)$ by the source spectrum, $S_\alpha(\lambda_s)$ to obtain [11]

$$L_F = 10\log_{10}[\int S_\alpha(\lambda_s)10^{-\frac{\alpha(\lambda_s)D}{10}}d\lambda_s] \tag{1.9}$$

Usually, $S_\alpha(\lambda_s)$ is normalized such that $\int S_\alpha(\lambda_s)d\lambda_s = 1$; this normalization makes the total fiber loss evaluated from Equation (1.9) to be equivalent to that computed from Equation (1.7). The attenuation coefficient is one of the parameters which determines the quality of optical fibers and in particular, fibers with lower loss coefficients are generally more expensive than those with higher loss coefficients.

1.2.2.2. Fiber Dispersion

Dispersion in graded-index multimode fibers arises from differential mode delay (multimode dispersion), wavelength dependent material (chromatic dispersion) and waveguide effects.

(i) Multimode Dispersion: The modal delay spread along a fiber is determined from the transfer function of the fiber illuminated by a coherent source such as a laser diode. For analytical studies, the fiber transfer function approximates a Gaussian distribution which is described by [7]

$$H_{FM}(\omega) = \frac{1}{\sigma_m\sqrt{2\pi}}\exp[-\frac{\sigma_m^2\omega^2}{2} - j\omega t_d] \tag{1.10}$$

where σ_m is the root mean square (rms) width of the fiber impulse response representing the modal delay spread of the optical pulse.

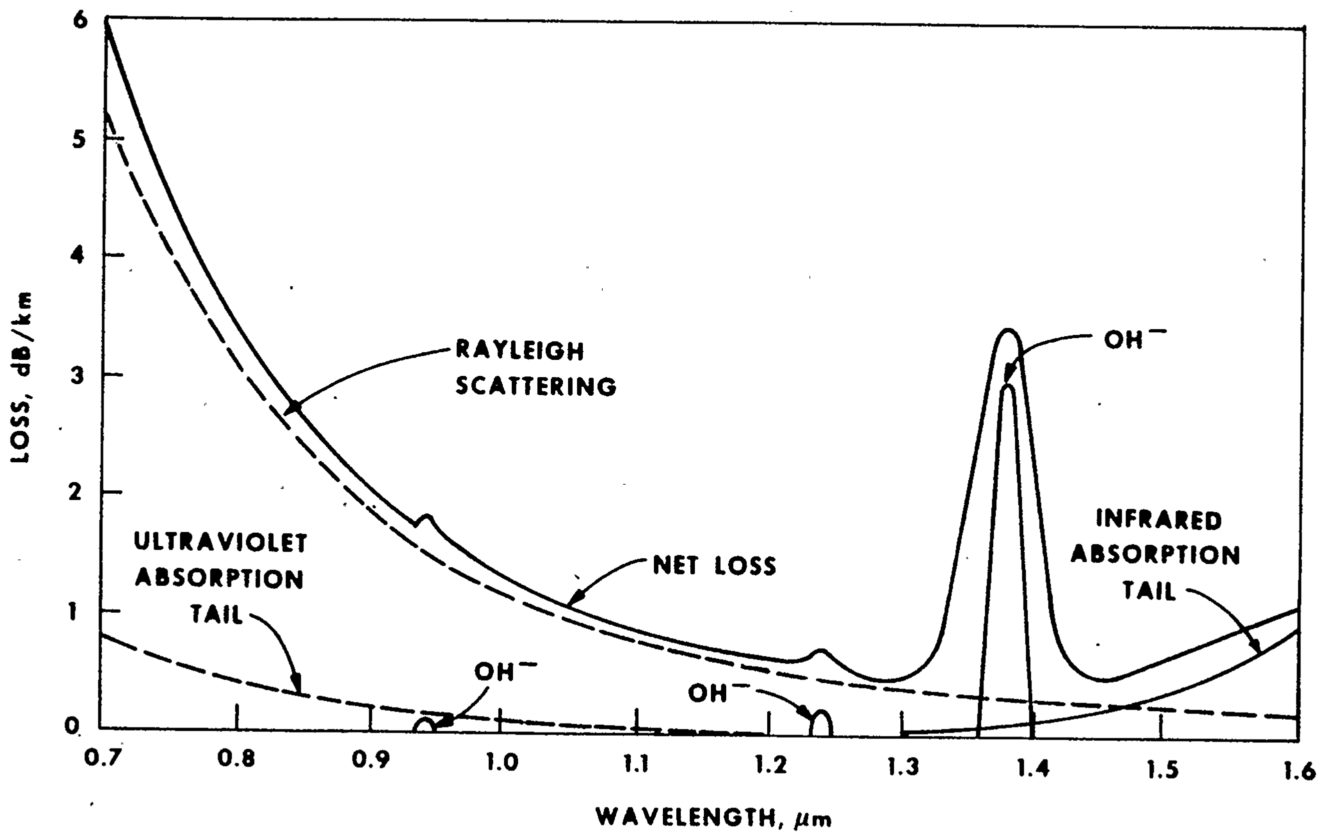

Fig. 1.4 Typical Loss Versus Wavelength Characteristics for a Silica multimode graded-index fiber.

(ii) Chromatic Dispersion: Personick has shown that the optical pulse spread along the fiber due to the wavelength dependent chromatic dispersion is given by [7]

$$\sigma_c = \delta \cdot D \cdot (\Delta\lambda_s) \tag{1.11}$$

A characteristic feature of the chromatic dispersion is the zero crossing near 1.3 μm, a wavelength which is also close to a local minimum in fiber loss.

It is important to note that the modal delay spread and the chromatic dispersion effects are independent, hence they contribute to the overall fiber *rms* impulse response width as the square root of the sum of squares. In addition, over the typical range of the bandwidth-length product of multimode graded-index fibers, the chromatic dispersion is the dominant component in the short wavelengths ($0.8 - 0.9\mu m$) when an LED source is employed and in the long wavelengths ($1.3 - 1.55\mu m$), the modal dispersion is the larger component. For a laser diode operating at both short and long wavelengths, the chromatic dispersion is usually masked by the multimode dispersion. The chromatic and modal dispersion effects limit the optical bandwidth of multimode graded-index fibers.

1.2.3. Digital Optical Receiver

The main component in the digital optical receiver is the optical- to-electrical conversion component (photodetector) which is either a PIN photodiode or an avalanche photodiode (APD). The other receiver components include the following: (i) the amplifier stage, which can be either a transimpedance (TZ) or a high impedance (HZ) design that incorporates either a bipolar junction transistor (BJT) or a field effect transistor (FET) as the front end active device; (ii) the equalization circuitry which removes the unwanted intersymbol interference and (iii) the decision and timing circuitry which regenerates the transmitted data. For POFLAN applications, the optical receiver must have a high optical sensitivity and a wide dynamic range. The optical sensitivity is the minimum optical power required at the photodetector input to achieve a specified bit error rate (BER) while the receiver dynamic range is the difference in decibels between the optical sensitivity and the maximum allowable optical power level at the receiver input.

1.2.3.1. Receiver Sensitivity Analysis

A comprehensive analysis of the receiver sensitivity for digital fiber optical communication systems has been reported by Personick [12]. A simpler and accurate method based on Personick's work was subsequently reported by Smith and Garrett [13]. The difference in the two approaches lies in how the shot noise voltage is evaluated. While Personick carried out a detailed analysis that evaluated the shot noise voltage as a function of time within the bit period, Smith and Garrett proposed a simplification of Personick's expressions by relating the mean square shot noise voltage at the decision time to the average unity gain photocurrent over the bit period. The latter approach is employed in this thesis because of its reduced computational difficulty. In the following, a synopsis of the important optical receiver relationships which are relevant to this study is presented.

The minimum average optical power, $\overline{P}$, required at the receiver input to achieve a desired bit error rate value is given by [14]

$$\overline{P} = B\frac{q}{\zeta}\,\frac{N_{pe}}{2}\,\frac{(1+\varepsilon)}{(1-\varepsilon)^2} \tag{1.12}$$

where the expression for the number of photogenerated electrons, N_{pe}, is derived under the assumption that the BER is evaluated using the standard Gaussian approximation. With this assumption and taking into account the effects of degradation factors, N_{pe} is expressed as [14]

$$N_{pe} = (2-\psi)Q^2 I_2 M_a^x + 2\frac{Q}{M_a}\left[(1-\psi)Q^2 I_2 (M_a^{2+x})^2 + (1-\varepsilon)^2 \left(I_2 \frac{I_{dm}}{Bq} M_a^{2+x} + Z\right)\right]^{1/2} \tag{1.13}$$

The photodiode responsivity, ζ, is defined by

$$\zeta = \eta_e \frac{q\lambda_s}{hc} \tag{1.14}$$

and the parameter ψ, is related to the occupancy factor, γ, and the source extinction ratio, ε, by

$$\psi = \gamma(1-\varepsilon) \tag{1.15}$$

Z is the dimensionless, signal-independent receiver noise parameter. For a transimpedance amplifier design incorporating a FET active device, Z is described to a good approximation by [13]

$$Z = \frac{I_2}{Bq^2}\left[S_I + \frac{2k_B\Theta}{R_F} + \frac{S_V}{R_F^2}\right] + \left(\frac{2\pi C_T}{q}\right)^2 BI_3S_V \tag{1.16}$$

where the equivalent input noise current density, S_I, and the voltage spectral density, S_V, are described by

$$S_I = qI_L \tag{1.17}$$

and

$$S_V = \frac{2k_B\Theta\Gamma}{g_m} \tag{1.18}$$

respectively. The TZ-FET amplifier design combination for the optical receiver gives high sensitivity and wide dynamic range. I_2 and I_3 are the normalized weighting functions which depend on the optical pulse shape at the receiver input and the desired optical pulse shape at the receiver output and these are given by [13]

$$I_2 = \int_{-\infty}^{\infty}\left|\frac{H_{out}'(f)}{H_p'(f)}\right|^2 df \tag{1.19}$$

$$I_3 = \int_{-\infty}^{\infty}\left|\frac{H_{out}'(f)}{H_p'(f)}\right|^2 f^2 df \tag{1.20}$$

As an illustration, for a Gaussian pulse at the receiver input whose normalized Fourier transform is given by

$$H_p'(f) = \exp\left[-\frac{(2\pi\sigma_p f)^2}{2}\right] \tag{1.21a}$$

and a raised cosine pulse at the receiver output described by,

$$H_{out}'(f) = Cos^2(\frac{\pi f}{2}) \tag{1.21b}$$

the expressions for I_2 ans I_3 are obtained as

$$I_2^{(GRC)} = \frac{4}{\pi}\int_0^{\frac{\pi}{2}} e^{16\sigma_p^2 x^2} Cos^4 x dx \tag{1.22a}$$

$$I_3^{(GRC)} = \frac{16}{\pi^3}\int_0^{\frac{\pi}{2}} e^{16\sigma_p^2 x^2} x^2 Cos^4 x dx \tag{1.22b}$$

The values of $I_2^{(GRC)}$ and $I_3^{(GRC)}$ are computed by numerical integration.

It is important to note that Equation (1.13) is applicable to both avalanche and PIN photodiodes. For the PIN photodiode, the avalanche gain is equal to unity and the bulk leakage current is equal to zero. This simplification gives

$$N_{pe}^{(PIN)} = (2-\psi)Q^2 I_2 + 2Q\left[(1-\psi)Q^2 I_2 + (1-\varepsilon)^2 Z\right]^{\frac{1}{2}} \tag{1.23}$$

and as a result of the manner in which N_{pe} depends on M_a in Equation (1.13), the receiver sensitivity of the APD must be evaluated at its optimum avalanche gain.

1.2.3.2. Receiver Sensitivity Penalty

The optical receiver sensitivity is degraded by the source extinction ratio, the intersymbol interference due to the broadening of the transmitted optical pulses along the fiber and the bulk leakage current of the photodiode.

The ideal sensitivity is obtained when $\varepsilon = 0$, $\gamma = 1$ and $I_{dm} = 0$. Substitution of these conditions into Equation (1.12) gives

$$\overline{P}_i = \frac{B}{2}\frac{q}{\zeta}\left[Q^2 I_2 M_a^x + 2\frac{Q}{M_a} Z_i^{\frac{1}{2}}\right] \tag{1.24}$$

where Z_i is now described by

$$Z_i = \frac{I'_2}{Bq^2}\left[S_I + \frac{2k_B\Theta}{R_F} + \frac{S_V}{R_F^2}\right] + \left(\frac{2\pi C_T}{q}\right)^2 B I'_3 S_V \tag{1.25}$$

and the integrals I'_2 and I'_3 are calculated for a narrow optical input pulse shape such as a unit impulse and a raised cosine output pulse shape. The values of I'_2 and I'_3 for these pulse shapes are found to be 0.75 and *zero* respectively.

The expressions for the degraded sensitivity due to the effect of each degradation factor are summarized as follows:

(i) Extinction Ratio Effect: $\varepsilon \neq 0$, $\gamma = 1$, $I_{dm} = 0$

$$\bar{P}_{\varepsilon \neq 0} = \frac{B}{2}\frac{q}{\zeta}\left[(1+\varepsilon)Q^2 I'_2 M_a^x + 2\frac{Q}{M_a}W^{1/2}\right]\frac{(1+\varepsilon)}{(1-\varepsilon)^2} \tag{1.26}$$

where the constant W is given by

$$W = \varepsilon Q^2 I'_2 (M_a^{2+x})^2 + (1-\varepsilon)^2 Z_i$$

(ii) Intersymbol Interference Effect: $\varepsilon = 0$, $\gamma \neq 1$, $I_{dm} = 0$

$$\bar{P}_{\gamma \neq 1} = \frac{B}{2}\frac{q}{\zeta}\left[(2-\gamma)Q^2 I_2 M_a^x + 2\frac{Q}{M_a}Y^{1/2}\right] \tag{1.27}$$

where the constant Y is defined by

$$Y = (1-\gamma)Q^2 I_2 (M_a^{2+x})^2 + Z$$

(iii) Bulk Leakage Current Effect: $\varepsilon = 0$, $\gamma = 1$, $I_{dm} \neq 0$

$$\bar{P}_{I_{dm} \neq 0} = \frac{B}{2}\frac{q}{\zeta}\left[Q^2 I'_2 M_a^x + 2\frac{Q}{M_a}(N_{dm} + Z_i)^{1/2}\right] \tag{1.28}$$

where the constant N_{dm} is given by

$$N_{dm} = I'_2 \frac{I_{dm}}{Bq} M_a^{2+x}$$

The sensitivity penalty in decibels, $\Delta\bar{P}$, associated with each degradation factor is defined as

$$\Delta\overline{P} = 10\log_{10}\left[\frac{\overline{P}_n}{\overline{P}_i}\right] \tag{1.29}$$

where $\overline{P}_n$ is the non-ideal sensitivity due to the effect of each degradation factor.

From the above equations, it is seen that the optical sensitivity of the receiver depends on the operating bit rate, the source extinction ratio, the bit error rate, the dispersion along the fiber, the amplifier thermal noise and the photodiode parameters and furthermore, the actual optical sensitivity at the receiver input is reduced by a penalty which arises from one or a combination of the degradation factors. A desirable requirement in optical system design is to have a minimum sensitivity penalty since the optical sensitivity together with the optical power coupled into the fiber determine the system power budget. The power budget must be high enough to accommodate all the losses in the system. For a given light source, the coupled power into a fiber is essentially fixed and a high power budget therefore depends upon having a high optical sensitivity at the receiver.

1.3. Scope of the Thesis

This chapter describes the essential characteristic models of the main components of POFLAN's and these models are used in the analysis presented in later chapters.

In Chapter Two, the theory of operation of the POFLAN interconnecting optical components is presented and each of the conventional LAN configurations is then implemented as a POFLAN topology. The advantages and disadvantages of each POFLAN topology are subsequently discussed.

In Chapter Three, an analysis of the POFLAN performance parameters considered in this thesis is given and the expressions derived and the algorithms employed for each POFLAN topology are presented. The important network design problems which are associated with each performance parameter are highlighted.

In Chapter Four, the features, capabilities and the structure of the network simulation software package developed are described. To illustrate the usefulness of this package, it is then applied to the design of two network examples and the results obtained together with the discussions on these results are presented.

Chapter Five contains the conclusions and suggestions for future developments.

The Appendix contains the derivations of some of the expressions used.

In summary, the main contributions of this thesis are:

(1) the performance evaluation of POFLAN topologies in terms of five network performance parameters.

(2) the development of a flexible and easy to use software tool named FONSIM, that can be employed for predicting the performance of planned POFLAN's.

Although the goal of this thesis is to provide the user of FONSIM with the optimum network topology in terms of each performance parameter, it is important to note that the optimum topology is also dependent upon the particular application, the geographical distribution of the network nodes and the costs involved.

CHAPTER 2

IMPLEMENTATION OF POFLAN TOPOLOGIES

2.1. Introduction

Topology refers to the basic physical configuration of a network. Local area networks, in general, are classified by the topology as well as by the access protocol. The basic LAN topologies used in fiber optic local area network applications are the ring or loop network, the linear bus network and the star network. For broadcast POFLAN applications, each of these topologies is implemented with optoelectronic devices, optical fiber, and optical interconnecting components such as couplers and connectors.

Two very important factors must be taken into consideration in the network implementation development process: (1) the losses of the interconnecting components and (2) the access protocol to be used by the network nodes. Carrier sense multiple access with collision detection (CSMA/CD) is the access protocol implemented for all the POFLAN topologies considered in this thesis. A vital requirement for this choice is that all the network configurations implemented must be able to detect collision occurrence, this requirement is taken into consideration during the network implementation process.

In this Chapter, a discussion on the models of the interconnecting components employed is first presented and this is then followed by the implementation developed for each of the basic LAN topologies. Analytical expressions are derived for the transmission loss of the realized POFLAN topologies and the advantages and disadvantages of each topology are then summarized.

2.2. Models of Optical Interconnecting Components

2.2.1. Unidirectional Coupler

The unidirectional coupler is the main interconnecting component which is used in the realization of the loop and the linear bus topologies. A method that is widely used for fabricating this device is the fused biconical tapered technology where the fabrication process entails the twisting together of a pair of fibers which are then fused. The operation of the unidirectional coupler is shown in schematic form in Figure 2.1 [3]. The coupler operation is in either of two modes: the transmitting mode or the receiving mode. In the transmitting mode, the power entering into one of the coupler input ports is coupled into the main fiber (Figure 2.1a) while in the receiving mode, power is coupled from the main fiber into one of the coupler output ports (Figure 2.1b).

Based on Figure 2.1, equations relating the powers at each tapping junction can be written:

MODE 1: Transmitting mode

$$P_{co} = \beta C_p P_T \tag{2.1a}$$

$$P_R = \beta(1 - C_p)P_T \tag{2.1b}$$

MODE 2: Receiving mode

$$P_R = \beta C_p P_i \tag{2.2a}$$

$$P_{co} = \beta(1 - C_p)P_i \tag{2.2b}$$

The superposition of these two modes gives the power matrix equation which is expressed as

$$\begin{bmatrix} P_R \\ P_{co} \end{bmatrix} = \begin{bmatrix} \beta(1 - C_p) & \beta C_p \\ \beta C_p & \beta(1 - C_p) \end{bmatrix} \begin{bmatrix} P_T \\ P_i \end{bmatrix} \tag{2.3}$$

where C_p is the fraction of the power coupled between fibers (coupling ratio) and β is the factor which accounts for the insertion loss of the unidirectional coupler.

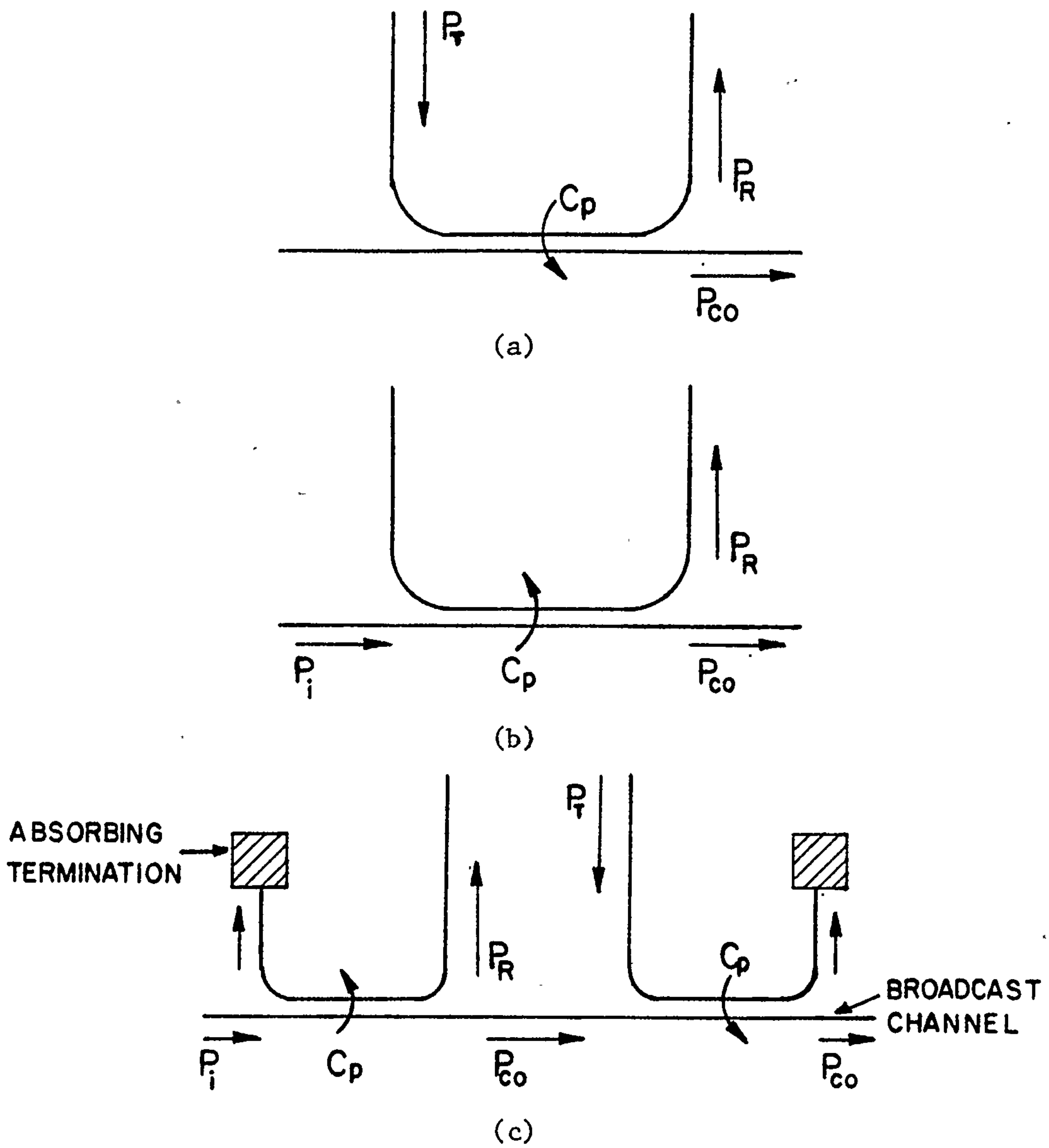

Fig. 2.1 (a) Schematic Operation of a Unidirectional Coupler in the Transmitting mode

(b) Schematic Opearion of a Unidirectional Coupler in the Receiving mode

(c) Schematic Operation of two Unidirectional Couplers at a nodal access point on the broadcast channel.

To detect collision occurrence, it is assumed that a signal transmitted by a node is not received by the same node. With this assumption and from Figure 2.1c, Equations (2.1) and (2.2) can be rewritten for the two modes:

In the transmitting mode, ($P_i = 0$), if only one node in the network transmits, Equation (2.1) then becomes

$$P_{co} = \beta C_p P_T \tag{2.4}$$

while in the receiving mode, ($P_T = 0$), Equation (2.2) becomes

$$P_R = \beta C_p P_i \tag{2.5a}$$

$$P_{co} = \beta(1 - C_p)P_i \tag{2.5b}$$

While Equation (2.4) accounts for the amount of power that is coupled onto the common fiber channel by the coupler operation, Equation (2.5a) represents the fractional power tapped off the bus by a node and Equation (2.5b) represents the amount of power remaining on the fiber channel to be passed on to other nodes. Equations (2.4) and (2.5) form the basis of the derivation of the transmission losses for the loop and linear bus topologies.

2.2.2. Transmissive Star Coupler

Figure 2.2 shows the transmissive star coupler model used in the implementation of the star network. The coupler is fabricated by using the same fused biconical tapered fiber technology described for the unidirectional couplers. The relationship between the input power to the star coupler and the output power from the coupler can be expressed by the power scattering matrix

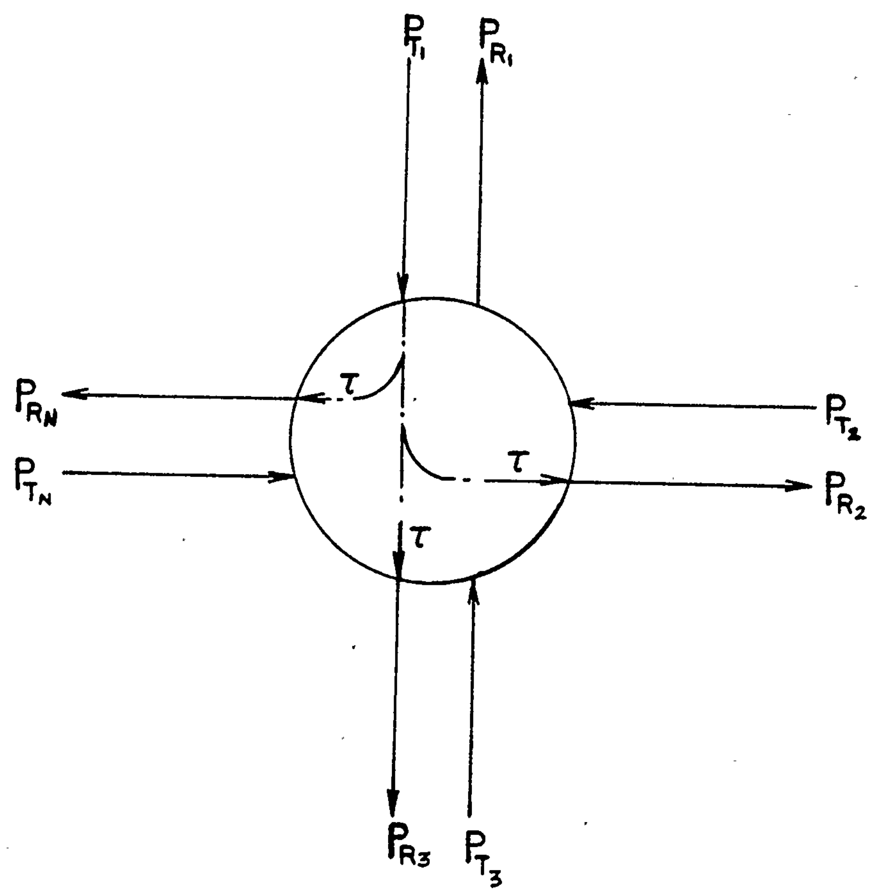

Fig. 2.2 Transmissive Star Coupler Model

$$\begin{bmatrix} P_{R_1} \\ P_{R_2} \\ P_{R_3} \\ \cdot \\ \\ P_{R_N} \end{bmatrix} = \begin{bmatrix} 0 & \tau & \tau & & & \tau \\ \tau & 0 & \tau & & & \\ \tau & \tau & 0 & & & \\ & & & & & \\ & & & & & \\ \tau & \tau & \tau & \tau & \tau & 0 \end{bmatrix} \begin{bmatrix} P_{T_1} \\ P_{T_2} \\ P_{T_3} \\ \\ \\ P_{T_N} \end{bmatrix} \tag{2.6}$$

The diagonal elements of the $(N \times N)$ matrix are zero. This confirms the requirement that the optical signal transmitted by a node must not be coupled back to the same node. The detection of collision occurrence is therefore rendered possible. The power received at the other ports due to a transmission from one node, P_{T_1} say, is given by

$$\begin{aligned} P_{R_2} &= \tau P_{T_1} \\ P_{R_3} &= \tau P_{T_1} \\ P_{R_N} &= \tau P_{T_1} \end{aligned} \tag{2.7}$$

Under equilibrium conditions and assuming that the insertion loss of the star coupler is negligible, then the power transmitted by a node must be equal to the sum of the powers received by the other $(N - 1)$ nodes in the star network, that is,

$$P_{T1} = \tau (N - 1) P_{T1} \tag{2.8}$$

so that τ, the star coupler coupling ratio, is then given by

$$\tau = \frac{1}{(N - 1)} \tag{2.9a}$$

and for a large number of network nodes, Equation (2.9a) can be expressed to good approximation by

$$\tau \approx \frac{1}{N} \tag{2.9b}$$

The power splitting ratio between a transmitting port and a receiving port is defined by

$$s_r = \frac{P_{Rj}}{P_{Ti}} \quad i{\neq}j \tag{2.10}$$

Applying Equation (2.7) and Equation (2.9b) in Equation (2.10) gives the splitting loss (in decibels) of the star coupler as

$$L_s \approx 10\log_{10}(N) \tag{2.11}$$

In addition to the splitting loss, there is also the excess loss inherent in the star coupler, which depends on the number of nodes supported by the star coupler. This loss is determined during the fabrication process. As an example, Table 2.1 lists the minimum and maximum excess losses reported for the CANSTAR Communications TCS $N \times N$ passive transmission star couplers [15].

2.2.3. Optical Connectors

Optical connectors are necessary at the input/output ends of each optical device. Due to the insertion loss of the connector, only a fraction of the power at the connector input appears at its output, where this loss is accounted for by the parameter α_c, which represents the fraction of the optical power transmitted through the optical connector.

2.3. POFLAN Implementations

The following assumptions are made regarding the implementation development:

(i) All the network nodes use identical sources.

(ii) All the unidirectional couplers employed in the implementation of the loop and linear bus topologies have identical coupling coefficients.

(iii) As a first approximation, the fiber loss is not included in the expressions derived for the transmission loss of each topology.

NUMBER OF PORTS (N)	MINIMUM EXCESS LOSS (dB)	MAXIMUM EXCESS LOSS (dB)
4	0.0	2.0
8	0.0	2.0
16	0.5	3.5
32	0.5	3.5
64	1.0	5.0
100	1.0	6.8

Table 2.1 Minimum and Maximum excess losses of an $N \times N$ passive Transmissive Star Coupler

2.3.1. Loop Topology

The implementation developed for the loop topology is shown in Figure 2.3(a). Each node in the network is connected to the common ring bus with two unidirectional couplers and the signal transmitted by a node propagates in only one direction.

2.3.1.1. Transmission Loss Analysis

The maximum received power in the loop network occurs between the two closest nodes. By following a similar approach used in [3], the maximum received power is given by (Figure 2.3b)

$$P_{\max} = \alpha_c^2\beta^2 C_p^2 P_T \tag{2.12}$$

The minimum received power occurs between the two furthest nodes in the network and this is derived as follows:

Consider a transmission from node 1 to node 3, the following equations can be written:

$$P_{o1} = \alpha_c \beta C_p P_T$$

$$P_{ro2} = \alpha_c^2\beta^2 C_p(1 - C_p)P_T$$

$$P_{o2} = \alpha_c^3\beta^3 C_p(1 - C_p)^2 P_T$$

The power received at node 3 is given by

$$P_{R3} = \alpha_c^4\beta^4 C_p^2(1 - C_p)^2 P_T$$

Similarly, consider a transmission from node 1 to node 4

$$P_{ro3} = \alpha_c^4\beta^4 C_p(1 - C_p)^3 P_T$$

$$P_{o3} = \alpha_c^5\beta^5 C_p(1 - C_p)^4 P_T$$

The power received at node 4 is given by

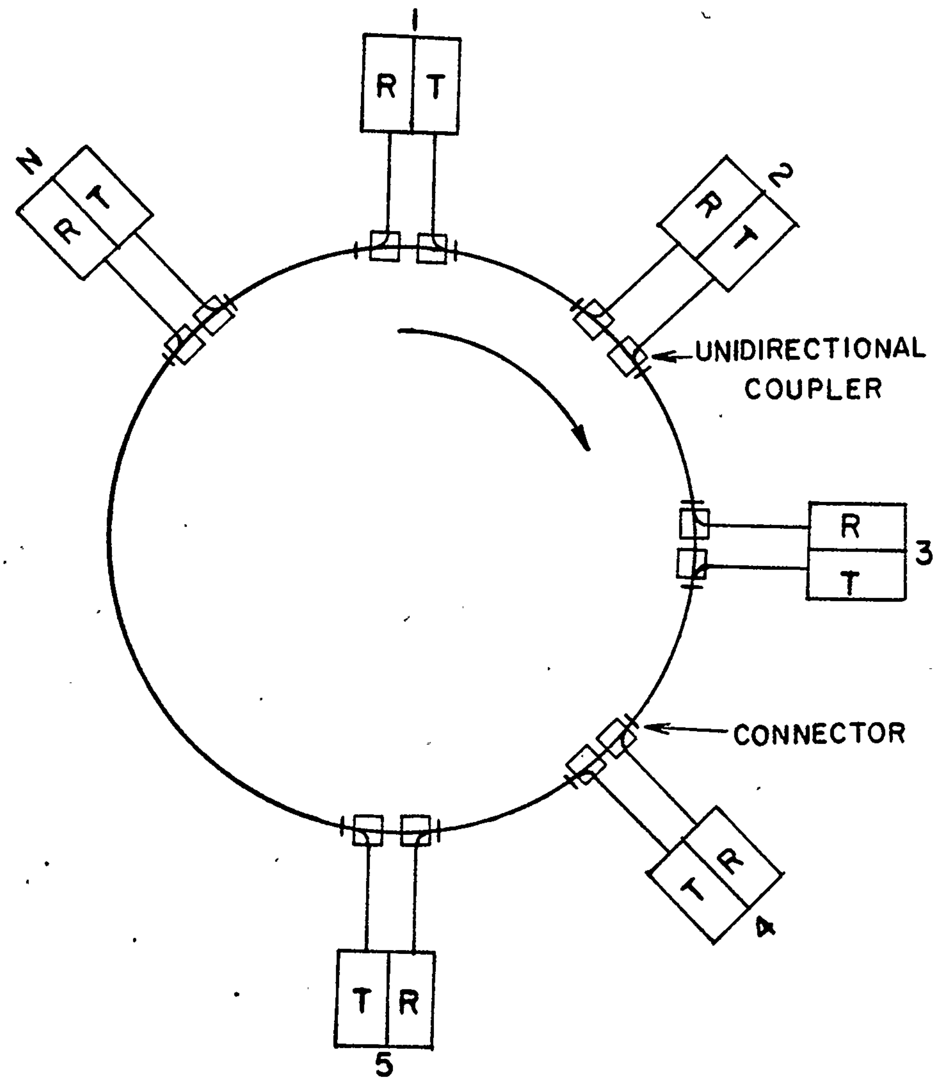

Fig. 2.3 (a) Implementation of passive, broadcast optical fiber Loop Topology

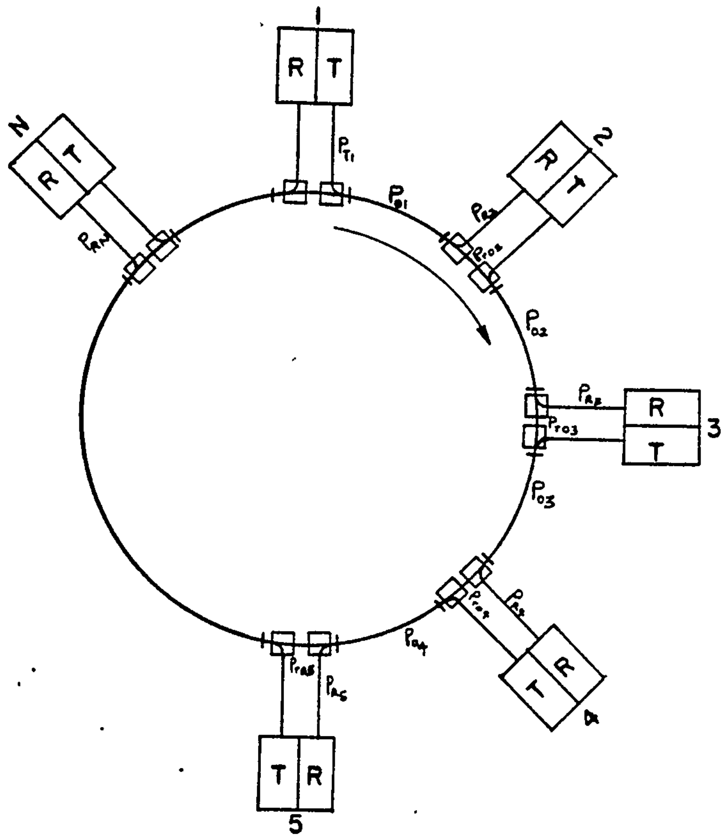

Fig. 2.3 (b) Implemented Loop topology indicating the signals at various points on the common channel

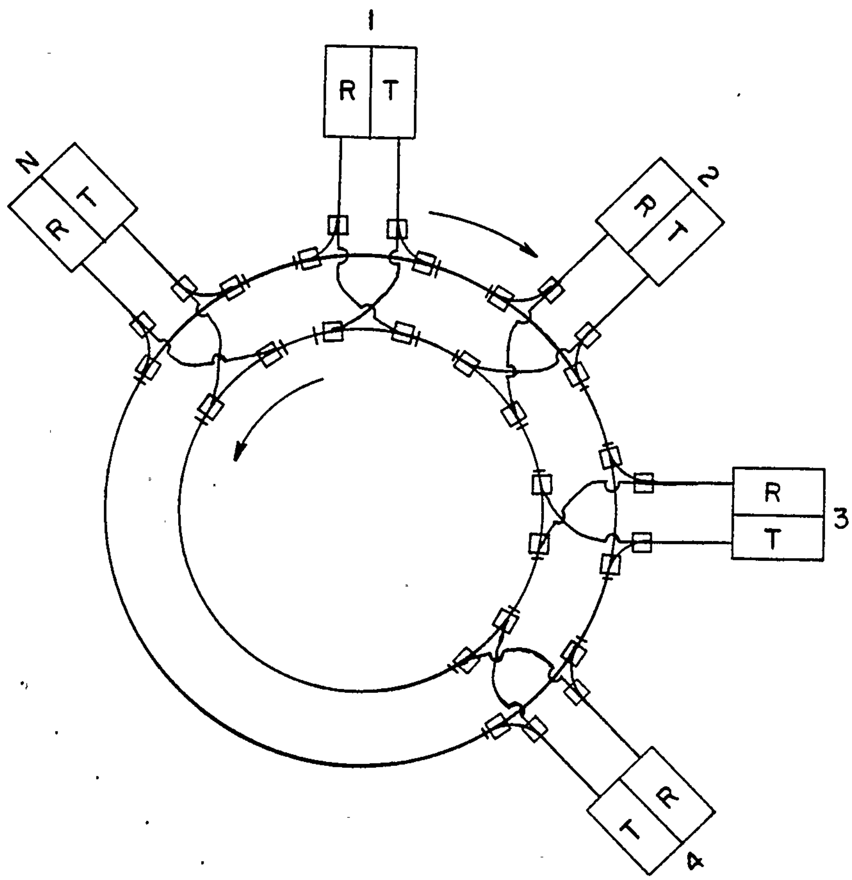

Fig. 2.3 (c) Implementation of the double Loop Topology

$$P_{R4} = \alpha_c^6\beta^6C_p^2(1 - C_p)^4P_T$$

Furthermore, consider a transmission from node 1 to node 5

$$P_{ro4} = \alpha_c^6\beta^6C_p(1 - C_p)^5P_T$$

$$P_{o4} = \alpha_c^7\beta^7C_p(1 - C_p)^6P_T$$

The power received at node 5 is given by

$$P_{R5} = \alpha_c^8\beta^8C_p^2(1 - C_p)^6P_T$$

In general, the minimum received power at node N due to a transmission from node 1 is given by

$$P_{\min} = \alpha_c^{(2N-2)}C_p^2(1 - C_p)^{(2N-4)}\beta^{(2N-2)}P_T \tag{2.13}$$

By differentiating $P_{\min}$ with respect to C_p and equating the result to zero, the optimum coupling coefficient which maximizes the minimum optical power received is given by

$$C_{p_{opt}} = \frac{1}{(N-1)} \tag{2.14}$$

Substituting $C_{p_{opt}}$ into Equations (2.12) and (2.13) gives the optimal maximum and minimum received powers as

$$P_{\max_{opt}} = \alpha_c^2\beta^2\left[\frac{1}{N-1}\right]^2P_T \tag{2.15}$$

$$P_{\min_{opt}} = \alpha_c^{(2N-2)}\beta^{(2N-2)}\frac{(N-2)^{(2N-4)}}{(N-1)^{(2N-2)}}P_T \tag{2.16}$$

Expressed in decibels, the minimum transmission loss for the loop network is given by

$$\begin{aligned} L_{\min}^{TRX} &= -10\log_{10}\left[\frac{P_{\max_{opt}}}{P_T}\right] \\ L_{\min}^{TRX} &= -20\log_{10}(\alpha_c) - 20\log_{10}(\beta) - 20\log_{10}(\frac{1}{N-1}) \end{aligned} \tag{2.17}$$

and the maximum transmission loss is also given by

$$L_{\max}^{TRX} = -10\log_{10}\left[\frac{P_{\min_{opt}}}{P_T}\right]$$

$$L_{\max}^{TRX} = -(2N-2)10\log_{10}(\alpha_c) - (2N-2)10\log_{10}(\beta) - 10\log_{10}\left[\frac{(N-2)^{(2N-4)}}{(N-1)^{(2N-2)}}\right] \qquad (2.18)$$

It is seen from Equation (2.18) that the maximum transmission loss increases with the number of nodes in the network. It is also important to state that the configuration of Figure 2.3a may not be very reliable because a break at any point on the loop bus results in total network failure. The reliability can be enhanced by using a double loop configuration as shown in Figure 2.3(c) where one loop is active and the other remains inactive until a failure occurs. The double loop configuration obviously requires greater fiber length than the single loop implementation.

Network upgradability may be difficult with the loop topology as the addition of more nodes involves opening up the ring and this disturbs transmission among the existing nodes.

2.3.2. Linear Bus Topology

The implementation developed for the linear bus topology is shown in Figure 2.4. The signal transmitted by a node is propagated in both directions and is received by all the other nodes.

2.3.2.1. Transmission Loss Analysis

By employing the same technique used for the loop network, the maximum power received by a node in a linear bus network is given by

$$P_{\max} = \alpha_c^2\beta^4C_p^4P_T \qquad (2.19)$$

while the minimum power received at node N due to a transmission from node 1 is derived as

$$P_{\min} = \alpha_c^{(2N-2)}\beta^{2N}C_p^4(1 - C_p)^{(2N-4)}P_T \qquad (2.20)$$

The coupling coefficient which maximizes the minimum optical power is then obtained as

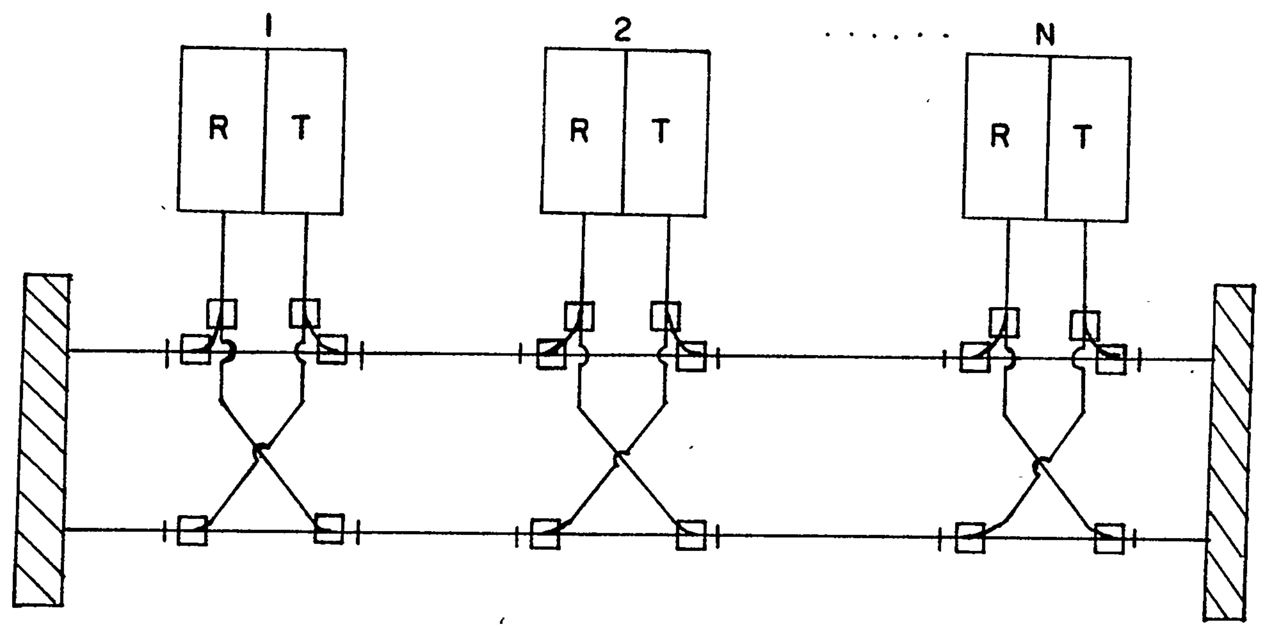

Fig. 2.4 Implementation of passive, broadcast optical fiber Linear Bus Topology

$$C_{P_{opt}} = \frac{2}{N} \tag{2.21}$$

Substitution of $C_{P_{opt}}$ into Equation (2.19) and Equation (2.20) gives the optimal maximum and minimum powers received as

$$P_{\max_{opt}} = \alpha_c^2 \beta^4 (\frac{2}{N})^4 P_T \tag{2.22}$$

and

$$P_{\min_{opt}} = 16 \alpha_c^{(2N-2)} \beta^{2N} N^{-2N} (N-2)^{(2N-4)} P_T \tag{2.23}$$

respectively. The transmission loss in decibels suffered by the strongest received signal is given by

$$\begin{aligned} L_{\min}^{TRX} &= -10\log_{10}\left[\frac{P_{\max_{opt}}}{P_T}\right] \\ L_{\min}^{TRX} &= -20\log_{10}(\alpha_c) - 40\log_{10}(\beta) - 40\log_{10}(\frac{2}{N}) \end{aligned} \tag{2.24}$$

while the loss suffered by the weakest received signal is expressed by

$$\begin{aligned} L_{\max}^{TRX} &= -10\log_{10}\left[\frac{P_{\min_{opt}}}{P_T}\right] \\ L_{\max}^{TRX} &= -10\log_{10}(16) - (2N-2)10\log_{10}(\alpha_c) - \\ &\quad - 2N(10\log_{10}(\beta)) - (2N-4)10\log_{10}(N-2) + (2N)10\log_{10}(N) \end{aligned} \tag{2.25}$$

As in the loop network, the transmission loss of the linear bus network also increases with the number of nodes on the bus and this places severe constraint on the network size. Unlike the loop network, nodes may be added or removed, depending upon their location, without affecting the other nodes on the linear bus. A break on the bus will not cause total network breakdown, it will merely divide the bus into two functional halves. It is these attributes of the linear bus network which make it superior to the loop network.

2.3.3. Star Topology

The implementation developed for the star topology is shown in Figure 2.5 where the signal transmitted by a node is distributed by the star coupler to the other network nodes.

2.3.3.1. Transmission Loss Analysis

The minimum and maximum losses of the star network are given by

$$L_{\min}^{TRX} = -4[10\log_{10}(\alpha_c)] + L_{e_{\min}} + 10\log_{10}(N) \tag{2.26}$$

$$L_{\max}^{TRX} = -4[10\log_{10}(\alpha_c)] + L_{e_{\max}} + 10\log_{10}(N) \tag{2.27}$$

Note that the fiber loss is not yet included in the derivation, this will be considered in a later Chapter. It is seen from Equations (2.26) and (2.27) that the minimum and maximum losses increase logarithmically with the number of nodes in a star network.

The passive star implementation offers several important advantages over the linear bus and loop realizations. First, due to the uniform distribution of the coupling and connector losses among the nodes in the Star network, the dynamic range to be processed at the nodal receivers is reduced compared to the large values which are to be processed by the loop and linear bus topologies. Secondly, the maximum loss between the two furthest nodes is significantly reduced compared to the maximum losses in the linear bus and the loop networks and this means that for a given power budget, a greater number of network nodes can be connected to a star network than to the bus or loop. A break in any of the fiber links only cuts off the node connected by this link. The main disadvantage of the star network is the greater length of fiber required for a given topology but this drawback is normally offset by the aforementioned advantages.

2.4. Summary

In this Chapter, the POFLAN implementations of the conventional LAN topologies are developed. Expressions for the transmission loss are also derived for each of the realized topolo-

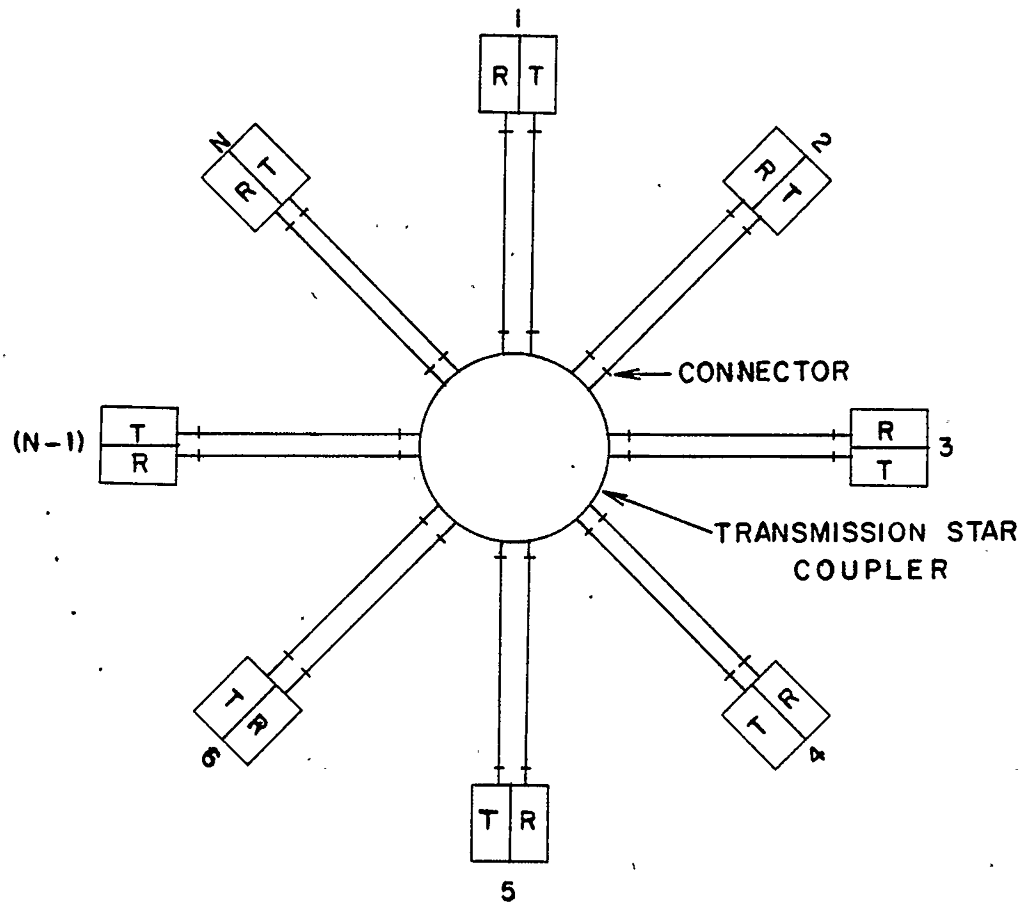

Fig. 2.5 Implementation of passive, broadcast Optical fiber Star Topology.

gies. These expressions are required in the computation of the network attenuation and the network dynamic range. The analysis for these two criteria and for the other network performance parameters is the topic of the next Chapter.

CHAPTER 3

ANALYSIS OF POFLAN PERFORMANCE PARAMETERS

3.1. Introduction

The behavior of the POFLAN topologies is evaluated with respect to five performance parameters where these are the total fiber length required by each topology, the network attenuation, the network dynamic range requirement, the bandwidth capability and the traffic characteristics. In this Chapter, the equations, algorithms and procedures that are used in the evaluation of these parameters are presented. Several design problems which are associated with the performance parameters are highlighted.

3.2. POFLAN Performance Parameters

3.2.1. Total Fiber Length Required

The total fiber length required by each POFLAN topology is the minimum fiber length which connects all of the network nodes where this length depends upon the type of network topology. The computational procedure for each of the POFLAN topologies is described as follows:

The total fiber length required by the star topology, D_{TS}, can be written as

$$D_{TS} = 2 \sum_{j=1}^{N} D_{jc} \tag{3.1}$$

where D_{jc} is the distance from a node to the Star coupler. For the linear bus topology, the total fiber length required, D_{TB}, is the sum of the link lengths which connect all of the network nodes along a single open path, while for the loop topology, the fiber length required, D_{TL}, is equal to the sum of the link lengths which join all of the network nodes along a simple closed path.

The optimum topology is the one which requires the overall minimum fiber length.

3.2.2. Network Attenuation

The network attenuation is the total loss between the two furthest nodes in a network and it consists of the transmission loss, the fiber loss and a small system margin which allows for the degradation of the optical components. The attenuation is expressed by

$$L_{\max}^{NET} = L_{\max}^{TRX} + \alpha D_{\max} + L_M \tag{3.2}$$

Note that $D_{\max}$ in the fiber loss term ($\alpha D_{\max}$) is the distance between the two furthest nodes in a given topology and not the total path length as incorrectly stated for the Star topology in [16-17].

The power budget of an optical network system is the difference between the coupled power into the fiber by the light source and the minimum allowable receiver power (optical receiver sensitivity). The power budget is given by

$$P_B = P_T - \overline{P} \tag{3.3}$$

which, in effect, is the maximum permissible attenuation between a source and a photodiode in the network. The network attenuation criterion is satisfied if the total loss between the two furthest nodes is less than or equal to the power budget and applying the worst case of this constraint gives

$$P_T - \overline{P} = L_{\max}^{TRX} + \alpha D_{\max} + L_M \tag{3.4}$$

It was pointed out in Chapter One that the receiver sensitivity, $\overline{P}$, is a function of parameters such as the bit rate, the type of photodiode employed, and the sensitivity degradation factors. The analysis presented in Chapter Two also showed that the maximum transmission loss depends on the number of nodes supported by a network topology. Important network design problems can be formulated from Equation (3.4) and some of these are itemized as follows:

(i) Given that the coupled power, the fiber loss and the system margin are fixed, what is the maximum number of nodes, $N_{\max}$, which can be supported by the network as a function of the operating bit rate?

(ii) For the same specifications as in (i), what is the effect of using different light sources and/or different photodiodes?

(iii) How is the maximum number of nodes supported by a network affected by the receiver parameters such as M_a, I_{dm}, ε, γ, and Z?

(iv) Given that $\overline{P}$, P_T, and L_M are fixed, how does the fiber attenuation coefficient vary with N?

(v) For the same parameters as in (iv), which network topology experiences the greatest loss?

(vi) By varying N while the other design parameters are fixed, what is the maximum transmission loss?

3.2.3. Network Dynamic Range Requirement

The dynamic range, L_{DR}, to be processed by the receiver at any of the network nodes is the difference between the maximum network loss, $L_{\max}^{NET}$, and the minimum network loss, $L_{\min}^{NET}$, incurred by each network topology. L_{DR} is expressed by

$$L_{DR} = L_{\max}^{NET} - L_{\min}^{NET} \tag{3.5}$$

where $L_{\max}^{NET}$ is given by Equation (3.2) and $L_{\min}^{NET}$ is defined by

$$L_{\min}^{NET} = L_{\min}^{TRX} + \alpha D_{\min} + L_M \tag{3.6}$$

$D_{\min}$ is the distance between the two closest nodes in the network. From Equation (3.6), two design problems can be addressed:

(i) What is the variation of the dynamic range as a function of the network topology?

(ii) What is the variation of the dynamic range as a function of the number of nodes in the network?

3.2.4. Network Bandwidth Capability

A measure of the information carrying capability of an optical fiber is usually defined as its optical bandwidth. As mentioned in Chapter One, the optical bandwidth of a graded-index multimode fiber is limited by the multimode and chromatic dispersion effects. In this section, the expression for the 3 *dB* optical bandwidth of a graded-index multimode fiber is derived and the relationship between the optical bandwidth of the fiber and the receiver sensitivity is shown. This relationship provides some necessary insights regarding the limitations of the bandwidth/attenuation performance of an optical system.

From Figure (3.1), the transfer function of the given optical fiber section can be expressed by [18]

$$H_{FM}(\omega) = \frac{S_o(\omega)}{S_i(\omega)} \tag{3.7}$$

Equation (3.7) can be represented by the generalized normalized transfer function

$$H_{FM}(\omega) = \exp[-\alpha(\omega) - j\beta(\omega)] \tag{3.8}$$

By definition, the Fourier transform of an optical pulse , $s(t)$, is given by

$$S(\omega) = \int_{-\infty}^{\infty} s(t)\exp(-j\omega t)dt \tag{3.9}$$

The right hand side of Equation (3.9) can be expanded in terms of the pulse characteristics such as the pulse energy, the pulse central time and its m^{th} central moment. The characteristic function of Equation (3.9) is then derived to be

$$S(\omega) = A\exp[-j\omega t_c - \frac{\omega^2}{2} M_2 + j\frac{\omega^3}{6} M_3 + \frac{\omega^4}{24} (M_4 - 3M_2^2) \pm ....] \tag{3.10}$$

where A, the optical pulse energy, t_c, the optical pulse central time and M_m, the m^{th} central moment of the optical pulse are described respectively by

$$A = \int_{-\infty}^{\infty} s(t)dt \tag{3.11a}$$

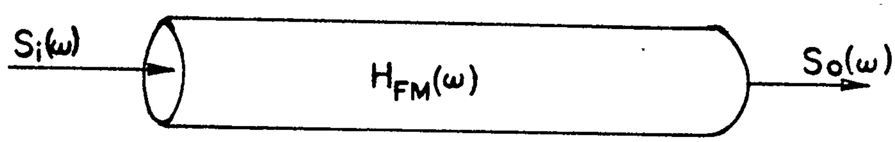

Fig. 3.1 Section of an Optical fiber showing input and output signals

$$t_c = \frac{1}{A}\int_{-\infty}^{\infty} ts(t)dt \tag{3.11b}$$

$$M_m = \frac{1}{A}\int_{-\infty}^{\infty}(t - t_c)^m s(t)dt \tag{3.11c}$$

It is usual to denote the second central moment of the optical pulse, M_2, by σ^2, thus by substituting Equation (3.10) into Equation (3.7), we obtain

$$\begin{aligned} H_{FM}(\omega) = \frac{A_o}{A_i} \exp[- \frac{\omega^2}{2} (\sigma_o^2 - \sigma_i^2) \\ - j\omega(t_{co} - t_{ci}) - j\frac{\omega^3}{6} (M_{3o} - M_{3i}) \pm ..] \end{aligned} \tag{3.12}$$

Comparison of Equation (3.8) with Equation (3.12) shows that

$$\alpha(\omega) = \ln(\frac{A_i}{A_o}) + \frac{\omega^2}{2}(\sigma_o^2 - \sigma_i^2) \pm .... \tag{3.13a}$$

and

$$\beta(\omega) = \omega(t_{co} - t_{ci}) - \frac{\omega^3}{6}(M_{3o} - M_{3i}) \pm .... \tag{3.13b}$$

From Equation (3.13), the frequency independent attenuation parameter and the transit delay of the propagating modes along the fiber are given by

$$\alpha = \ln\left[\frac{A_i}{A_o}\right] \tag{3.14a}$$

and

$$t_d = t_{co} - t_{ci} \tag{3.14b}$$

respectively. The normalized baseband transfer function is defined by

$$H_n(\omega) = \frac{H_{FM}(\omega)}{\exp(- \alpha - j\omega t_d)} \tag{3.15}$$

which gives

$$H_n(\omega) = \exp[-\frac{\omega^2}{2}\sigma_h^2 + j\frac{\omega^3}{6}M_{3h} + \frac{\omega^4}{24}(M_{4h} - 3\sigma_h^4) \pm \cdots] \tag{3.16}$$

where

$$\sigma_h^2 = \sigma_o^2 - \sigma_i^2 \tag{3.17a}$$

and

$$M_{mh} = M_{mo} - M_{mi} \tag{3.17b}$$

From Equation (3.16), the relationship between the root mean square (rms) pulse spread along the fiber, σ_h, and the 3 *dB* optical bandwidth of the fiber can be derived. The 3 *dB* optical bandwidth of the fiber is defined as the frequency at which the normalized baseband transfer function has fallen to half of the zero frequency value, this is given by

$$\left|H_n(2\pi(f_{3dB}))\right| = 0.5 \tag{3.18}$$

From Equations (3.16) and (3.18), it can then be shown that

$$BW = f_{3dB} \approx \frac{(2\ln 2)^{1/2}}{2\pi\sigma_h}[1 + \frac{\ln 2}{4}(\frac{M_{4h}}{3\sigma_h^4} - 1) \pm ...] \tag{3.19}$$

Equation (3.19) is the general expression which gives the bandwidth of the optical fiber in terms of the parameters of the optical pulse defined by $s(t)$. As it is usual to assume that the optical pulse is Gaussian in shape, then it is easily shown that Equation (3.19) reduces to

$$BW \approx \frac{(2\ln 2)^{1/2}}{2\pi\sigma_h} \tag{3.20}$$

The parameter σ_h, accounts for the optical pulse spread along the fiber, where this arises from the modal and chromatic dispersive effects. As already stated in Chapter One, these two effects are independent, and from probability theory their resultant effect is expressed by [19]

$$\sigma_h^2 = \sigma_m^2 + \sigma_c^2 \tag{3.21}$$

and the parameter σ_h is very useful in determining the bandwidth-length product of a given optical fiber.

In addition to the bandwidth-length product that is specified for a given fiber, it is also essential in network design to determine the optical bandwidth limitation due to the losses in the system. Baues has shown that the optical receiver sensitivity is related to the optical bandwidth by [1]

$$\bar{P} = K_z \cdot (BW) \tag{3.22}$$

where the proportionality factor, K_z, depends largely on the total receiver noise, the specified bit error rate probability and the gain of the photodiode.

The above approaches are used to investigate the dependence of the maximum optical bandwidth on the maximum link distance for the POFLAN topologies considered in this thesis. From Equation (1.24), the expression for K_z can be written for the two types of photodiodes: For the APD,

$$K_z^{(APD)} = \frac{q}{2\zeta}[Q^2 I_2 M_a^x + \frac{2Q}{M_a} Z_i^{1/2}] \tag{3.23a}$$

while for the PIN photodiode

$$K_z^{(PIN)} = \frac{q}{2\zeta}[Q^2 I_2 + 2QZ_i^{1/2}] \tag{3.23b}$$

$\bar{P}$ is computed from Equation (3.4) as the difference between the coupled power and all the losses in the system, with K_z evaluated from Equation (3.23), the corresponding values of bandwidth can then be determined.

Several design problems relating to the bandwidth parameter are outlined as follows:

(i) For a given number of nodes, what is the maximum bandwidth as a function of the maximum link distance in a network topology?

(ii) Given a fixed maximum link distance, what is the maximum optical bandwidth of a network topology?

(iii) How does the bandwidth vary with different values of the bandwidth-length dependence factor?

3.2.5. Network Traffic Characteristics

The two main parameters which determine the traffic characteristics of local area networks are the network throughput and the average packet delay where these two parameters are evaluated as a function of the offered load on the network. Analytical models for traffic studies of LAN's which use CSMA/CD as the access protocol have been formulated [20-21]. Though such analytical models are concerned with only the media access protocol, a number of approximations are required to obtain tractable results. To obtain more accurate results for complex networks it is necessary to resort to simulation. In this thesis, the discrete-event simulation technique is used in evaluating the traffic parameters of the POFLAN topologies. The network traffic model constructed for the simulation is shown in Figure 3.2 where each of the network nodes is modeled by a queue. The assumptions made during the development of the network traffic simulation model include the following:

(i) The packet arrival at each of the N nodes in the network follows a Poisson process, that is, the packet interarrival time is exponentially distributed with an equal mean arrival rate of λ at each of the nodes.

(ii) Packet lengths are chosen from an exponential distribution with a constant mean packet length for all the nodes.

(iii) All nodal buffers are assumed to be infinite in length.

(iv) Nodal processing delays are assumed to be negligible in comparison with the packet transmission time.

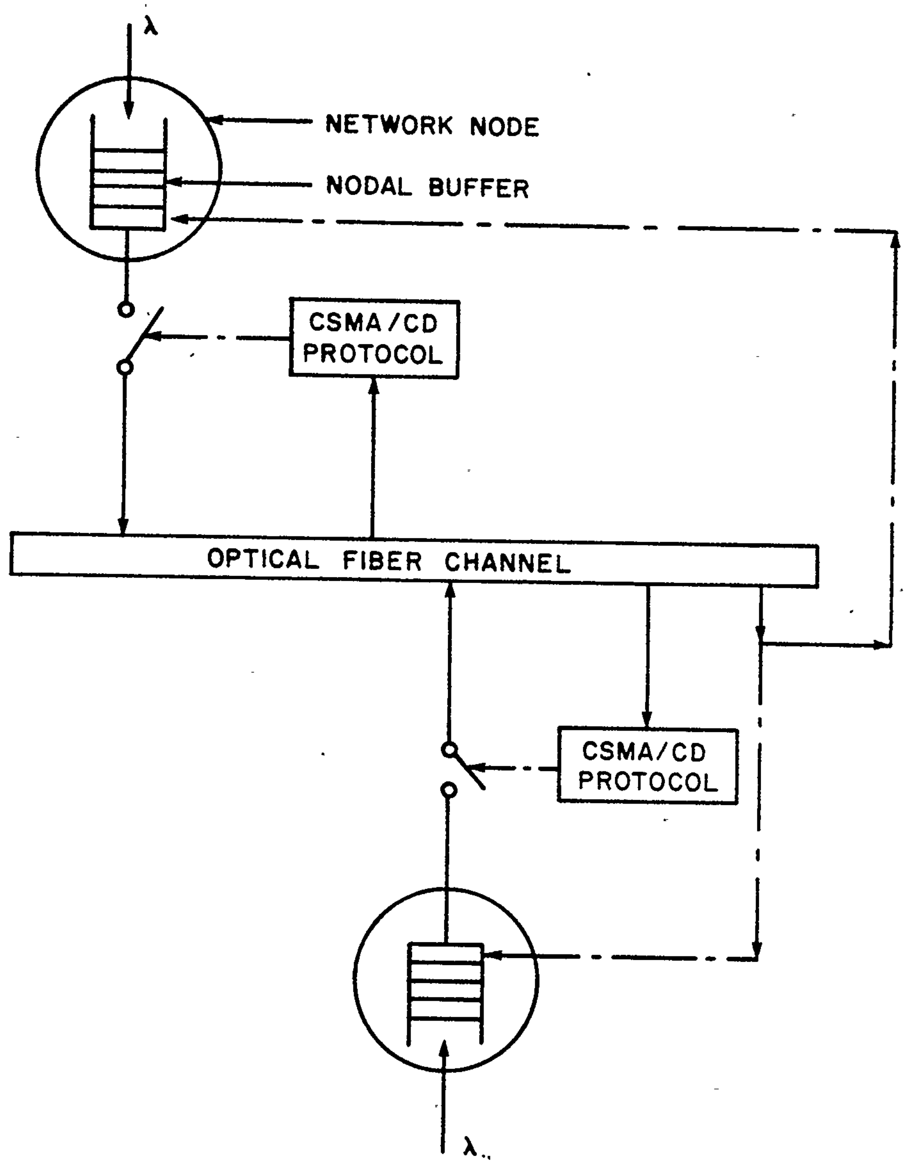

Fig. 3.2 Network Traffic Simulation Model

(v) The optical channel is noise free.

(vi) The propagation delay is very much less than the average packet transmission time. (The propagation delay is defined as the ratio of the distance between the two furthest nodes in the network to the velocity of light in the fiber while the average packet transmission time is equal to the ratio of the average packet length to the channel capacity. The ratio of the propagation delay to the average packet transmission time is called the normalized propagation delay parameter).

(vii) The effects of packet overhead, that is, packet header, acknowledgement and error control bits, are ignored in the simulation.

3.2.5.1. Implications of the stated Assumptions

There are two important implications derivable from the assumptions that the packet interarrival time and the packet length are exponentially distributed (assumptions (i) and (ii)). The first implication is explained by the fact that most of the values of an exponentially distributed random variable are smaller than the mean value of the random variable. With respect to the interarrival time, this means that the majority of the randomly selected interarrival times are less than its mean value. The net effect of this is that a number of packets arrive in a short period of time, thereby creating a queue at each of the network nodes. This is followed by a long interval during which time no new packets arrive, thus leading to a reduction in the size of the nodal queues during this interval. In terms of the packet length (which is a measure of the packet transmission time), the bulk of the packets generated will have lengths which are less than the mean packet length and thus the majority of the packets will have small transmission times which in effect reduces the nodal queue buildup.

The second implication of these assumptions is explained by the "memoryless" (Markovian) property of the exponential distribution. Based on this property, the time to the next packet arrival at a node is independent of the time since the last arrival. With respect to the packet transmission time, the time required to complete the transmission of a packet from a particular node cannot be predicted by any of the other nodes even if the time that packet has already been under transmission is known.

Assumption (iii) allows the potential queue length buildups to be observed as this provides useful information for computing the backlog clearing time. No restriction is placed on the size of the nodal buffers so that none of the arriving packets shall be refused during the network operating time.

By assuming the optical channel to be noise free, the only source of error arises from the collision of packets along the optical channel; this assumption being necessary in the implementation of the CSMA/CD access protocol. The assumption that the propagation delay is very much less than the average packet transmission time ensures the efficient use of the optical channel which leads to high network throughput. Assumption (vii) implies that the traffic characteristics results reported in this thesis are the upper bound performance of the network topologies simulated.

3.2.5.2. Description of the CSMA/CD Access Protocol

The CSMA/CD protocol is a random access technique which is designed to address the problem of how a common broadcast transmission medium is to be shared by the different network nodes. The protocol is an improved version of the earliest developed multiaccess techniques - ALOHA and CSMA. The CSMA/CD operates in either of three modes and the operating rules for each mode are listed as follows [22]:

Mode 1: Nonpersistent CSMA/CD

(i) If the medium is idle, transmit.

If a collision is detected during transmission, immediately cease transmitting the packet, and transmit a brief jamming signal, wait a random amount of time, then attempt to transmit again.

(ii) If the medium is busy, wait an amount of time drawn from a probability distribution and repeat step (i).

Mode 2: 1-persistent CSMA/CD

(i) If the medium is idle, transmit.

If a collision is detected during transmission, immediately cease transmitting the packet, and transmit a brief jamming signal, wait a random amount of time, then attempt to transmit again.

(ii) If the medium is busy, continue to listen until the channel is sensed idle, then repeat step (i).

Mode 3: *p*-persistent CSMA/CD

(i) If the medium is idle, transmit with probability p or delay transmission by one time unit with probability $(1 - p)$ (one time unit is equal to the maximum propagation delay).

If there is a transmission then

If a collision is detected, immediately cease transmitting the packet, and then transmit a brief jamming signal, wait a random amount of time, and attempt to transmit again,

else if transmission is delayed, repeat step (i) after the delay of one time unit.

(ii) If the medium is busy, continue to listen until the channel is idle and repeat step (i).

From the above rules, the following remarks can be made:

The nonpersistent CSMA/CD reduces the probability of collisions but has the drawback of high channel idle time following a prior transmission. The 1-persistent CSMA/CD reduces the channel idle time but it is a greedy algorithm and a collision is guaranteed if two or more nodes are waiting to transmit. A compromise intended to reduce collisions and simultaneously reduce idle time is the p-persistent CSMA/CD. But the question arises as to what should be the effective value of p. The main problem to avoid is one of instability under heavy load where there are many collisions and very few packets being successfully transmitted. In a network where n nodes are attempting to transmit, it is required that np must be less than unity or p be made very small to reduce the number of collisions. It has been shown that out of these three modes, the most common choice is the 1-persistent CSMA/CD because the wasted time due to collisions is very short (if the packet transmission time is very much greater than the propagation delay) and with random backoff the nodes involved in a collision are unlikely to collide on their next tries. To ensure that backoff maintains stability, an algorithm known as the binary exponential backoff (BEB) is used in selecting the retransmission delay of colliding packets. In the BEB algorithm, a node will attempt to transmit repeatedly in the face of repeated collisions, but after each collision, the mean value of the random delay is doubled and after sixteen unsuccessful attempts the node will give up and report an error. The binary exponential backoff algorithm is defined by the Institute of Electrical and Electronics Engineers (IEEE BEB) thus [23]: "*The delay is an integral multiple of slot time. The number of slot times to delay before the n^{th} retransmission attempt is chosen as a uniformly distributed random integer r in the range* $(0 \leq r \leq 2^k)$ *, where* $k = min(n,10)$." In essence, the retransmission delay is doubled for each of the first ten retransmissions, but then stays constant up to the sixteenth retransmission. In most cases, the slot time is usually taken to be twice the end-to-end maximum propagation delay. The beauty of the 1-persistent CSMA/CD with binary exponential backoff is that it is efficient over a wide range of loads. At low loads, 1-persistence guarantees that a node can seize the channel as soon as it goes idle, in contrast to the non- and p-persistent schemes, and at high loads, it is at least as stable as the other techniques. The drawback of the BEB algorithm is that it has a last-in, first-out effect where the nodes with no or few collisions will have a chance to transmit before nodes which have waited longer. The operational flowchart of the 1-persistent CSMA/CD access protocol is shown in Figure 3.3.

3.2.5.3. Implementation of the Network Traffic Model

In the implementation of the network traffic model, three main events must be modeled:

(i) Arrival of packets into the network

(ii) Checking for collision during transmissions

(iii) Departure of packets from the network

(i) Packet arrival: All arriving packets into the network are placed in their respective nodal buffers and these packets are transmitted according to a first-in, first-out discipline. Any packet that is unsuccessful in a transmission attempt continues to try until it is successfully transmitted. A packet at the top of a nodal queue which senses the channel idle (assuming no transmission period is already in progress) initiates a new transmission period. The packet which initiates the new transmission period first experiences a propagation delay after which a check is made for collisions, this statement implying that a worst case condition is considered for the CSMA/CD protocol implementation.

(ii) Collision Checking: Collision on the channel is checked at the end of the propagation delay of the packet which initiated the current transmission period. If a packet from any other network nodes accesses the channel during the propagation delay, it sets the collision variable to indicate a collision occurrence.

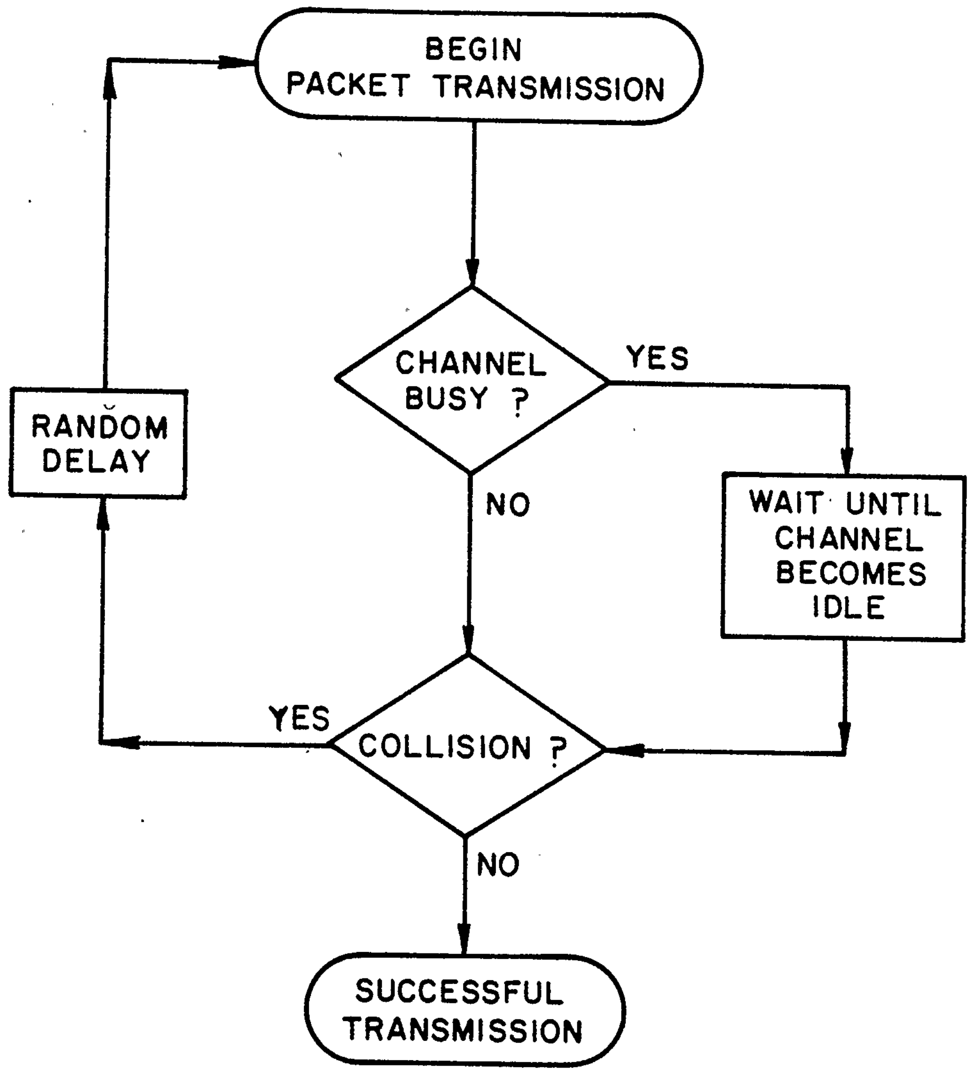

Fig. 3.3 Operational Flow Chart of the 1-persistent CSMA/CD access protocol

Should a collision be detected at the end of the propagation delay (more than one packet on the channel) then further transmission is stopped and all the colliding packets are rescheduled. If however no collision occurs, then the packet which initiated the transmission period is guaranteed a successful transmission and a departure event is scheduled for this packet. Any other packet which arrives while the channel is in use, but after the propagation delay simply waits (1-persistent) for the channel to be free.

(iii) Packet Departure: A packet that has been successfully transmitted is removed from the channel and from its nodal queue and statistics on the number of packets that have been successfully transmitted are gathered.

3.2.5.4. Definition of the Network Traffic Parameters

The network traffic parameters to be determined and their definitions are as follows:

(i) Normalized network Throughput: The actual number of packets successfully transmitted by all the nodes (per second) divided by the network unidirectional channel capacity.

(ii) Average packet end-to-end Delay: The average time between packet arrival at a node and its successful departure from the network.

(iii) Offered Traffic: The total amount of packets requiring transmission, both new and rescheduled.

(iv) Backlog Clearing Time: The amount of time it takes to transmit the queued packets at all of the network nodes after the entry of new packets into the network is terminated at a specified simulation time.

The design problem associated with the traffic characteristics is mainly concerned with the evaluation of the throughput/delay characteristics for different loads on the network. Simply put: at what load must the network operate to guarantee a high network throughput and an acceptable average packet delay?

3.3. Summary

In this Chapter, the procedures for evaluating the network performance parameters have been described and several design problems relating to these parameters have been highlighted. The actual implementation of these procedures and the development of a network design tool which will aid the task of finding solutions to the problems that have been raised form the topic of Chapter Four.

CHAPTER 4

EVALUATION OF POFLAN PERFORMANCE BY COMPUTER SIMULATION

4.1. Introduction

Digital computer simulation is one of the most powerful design tools for evaluating the performance of various systems [24]. Simulation as a design tool certainly improves the designer's understanding of a system beyond what intuition or analytical tools alone can provide. The analytical technique is an alternative design tool but for most complex systems it often leads to intractable equations, one reason for this being the large number of parameters associated with such systems coupled with the constraints on these parameters. In many cases, it is often difficult to formulate suitable equations which accurately describe the behavior of such systems and even when the describing equations are written, approximate solutions are only obtainable after many simplifying assumptions are made and these may render the results hardly acceptable. The simulation technique is one feasible method that is generally employed to predict the performance of complex systems. The technique entails the design of a computerized model of a system and conducting experiments with this model for the purpose of either understanding the behavior of the real system or evaluating various strategies for the operation of the real system. Although the simulation technique may require a large processing time, the results obtained from this technique closely approach the results from a real system because they are not based on as many assumptions as are analytical techniques.

In this Chapter, the application of the simulation technique in the design of planned passive optical fiber local area networks (POFLAN's) is discussed. The objective of the simulation is to compare the performance of the different POFLAN topologies with respect to the different network performance parameters thus providing useful insights to network designers. This objective is realized in this thesis through the development of a software package named Fiber Optic Network

SIMulator (FONSIM) [25]. As mentioned in Chapter Three, five network performance parameters form the basis for comparing the performance of the network topologies considered. While pure simulation models are developed for investigating the traffic handling characteristics, analytical expressions form the basis for studying network attenuation, dynamic range, bandwidth capability, and path length performance parameters. In essence, the FONSIM package is a hybrid package which consists of the mathematical analysis of the first four performance parameters and the pure simulation of the network traffic characteristic parameter. The salient features and capabilities of the FONSIM package are discussed in the next section. Section 4.3 presents the general structure of the software package. Verification and validation techniques are described in Section 4.4 while in Section 4.5 several results obtained from the application of the software package in the design of two network examples are presented. The results depict several interesting properties of the different POFLAN topologies.

4.2. Salient Features and Capabilities of the FONSIM Package

The FONSIM program was implemented in FORTRAN 77 language and executed on a VAX 11/780 under the UNIX operating system and on a CDC CYBER 205 Supercomputer under the Virtual Storage operating system (VSOS). The package, which is in modular form, consists of a library of performance evaluation subprograms and it provides a flexible, versatile, and easy-to-use means to assess the performance of planned POFLAN's. The simulation software package was designed to be user friendly and it only requires a user to specify the inputs and the type of performance measure to be investigated for a particular network topology. The inputting of the input data is done either in dialogue form or through the use of a data file and the results computed are then displayed on the screen or printed out on a line printer. The FONSIM package provides answers to all of the design problems highlighted in Chapter Three and in particular, it can be used to determine the following parameters for each of the POFLAN topologies:

(1) the variation of the network size as a function of the operating bit rate

(2) the effect of the degradation factors on the network size for different operating bit rates

(3) the minimum and maximum transmission losses incurred

(4) the network dynamic range required for different network sizes

(5) the optical fiber quality (in terms of the maximum attenuation coefficient) which is required for interconnecting the network nodes

(6) the dependence of the maximum fiber attenuation coefficient on network size

(7) the network bandwidth capability

(8) the total fiber length that will interconnect all the network nodes

(9) the network throughput as a function of the offered traffic on the network

(10) the average packet delay as a function of the offered load on the network

(11) the queue buildups at the different network nodes in the network

(12) the clearing time of all the backlogged packets at different network nodes

(13) the sensitivity of the throughput-delay characteristics on the variations in the bit rate, the mean packet length, the propagation delay and the backoff algorithm.

(14) the optimum network topology in terms of each of the performance parameters. By manipulating the input data, sensitivity studies can be performed on the performance measures and the performance of different network alternatives can be compared from which the optimum

network topology is selected.

4.3. FONSIM Description

The general organization of the simulation program is as shown in Figure 4.1. The flowchart consists of an input section, the simulator processing section and an output section. All the network input parameters are specified in the input section, the processing section includes the performance evaluation blocks and the results of the computer processing are displayed by the output section. The feedback path signifies that some of the chosen input data may be varied so that the sensitivity of the output parameters to such variations can be observed. The three sections are further broken down into modules which are arranged in three levels: Level 1 consists of subroutines for reading in the input data, random number generators which generate the driving inputs for the discrete-event simulation section, statistical subroutines used for the analysis of simulation output results, and the report subroutine which prints the output results; Level 2 consists of subprograms responsible for queue management and a subroutine for monitoring the status of all the network nodes at any time during the course of simulation while Level 3 comprises the performance evaluation modules where each module is designed for one performance measure. The classification of these subroutines according to the three levels is shown in Table 4.1. In all, the simulation program consists of 24 subroutines, 5 function subprograms and one main (calling) program. The simulation program requires a store of about 300 kilobytes and consists of 4000 lines of FORTRAN code. A brief description of these subroutines is presented as follows:

4.3.1. Level 1 Subroutines

These are divided into four categories, namely, the input parameter routines, the random number generators, the statistical routines and the output routines.

(i) Input Parameter Routines: There are two routines in this category - NETINP and INTCMP. Subroutine NETINP performs the reading of all the network input parameters required in the simulation while subroutine INTCMP computes various intermediate parameters. The net-

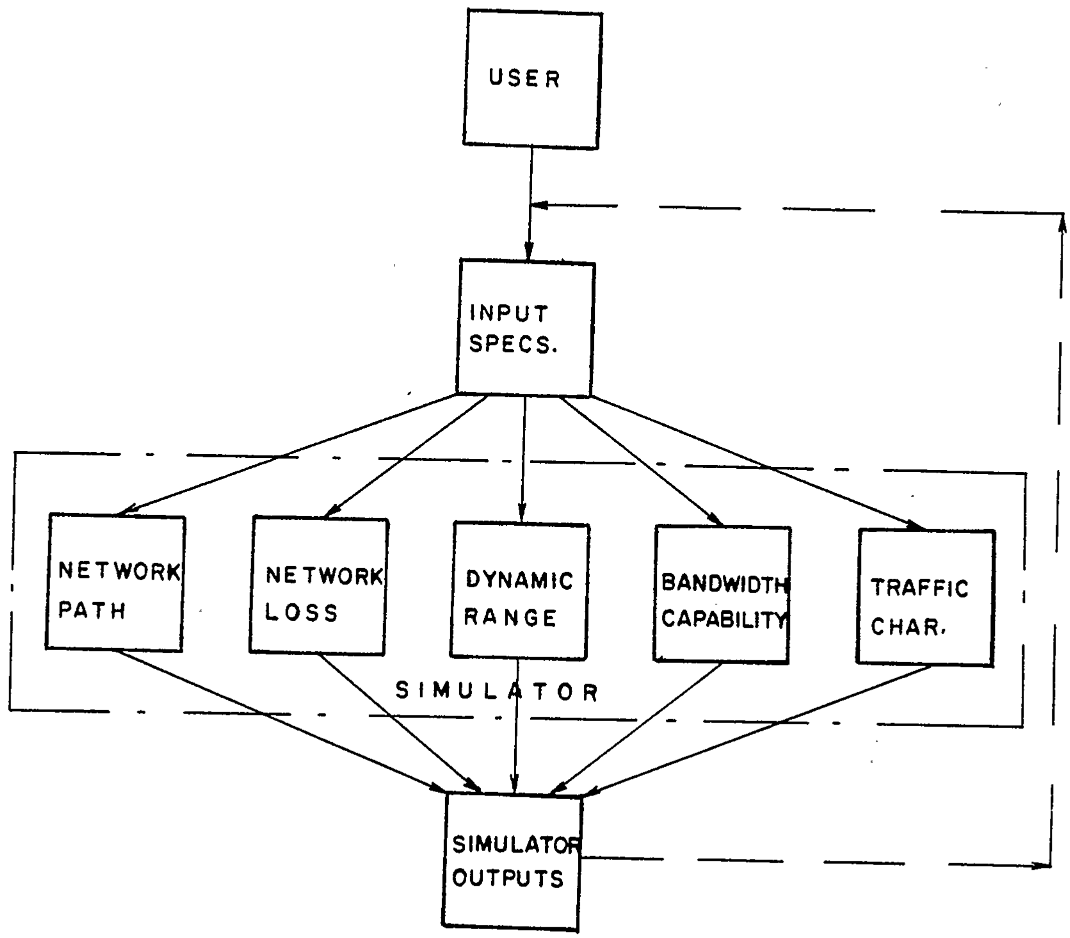

Fig. 4.1 General Organization of the FONSIM package

LEVEL 1	LEVEL 2	LEVEL 3
NETINP	INITLZ	PATH
INTCMP	FILPKT	TRXLOS
URAND	RMVPKT	DYRNGE
EXPON	CNCPKT	BNDWDT
DUNIFM	NXTPKT	TRAFIC
UNIFRM	DLTPKT	RCVR
SMPSTA	MONITR	PKTARV
TIMSTA	CPYPKT	PKTDEP
QUESTA		COLCHK
REPORT		SINK
CINTVL		

Table 4.1 Classification of the FONSIM Package modules into different levels.

work input parameters can be read either on an interactive basis or by initially storing the input data in an input data file which is then read during program execution. The general network data that must be inputted are the total number of network nodes, the distance matrix, the channel capacity of the fiber required for network interconnection, the operating bit rate, the allowable system margin, the type of network topology to be simulated and the performance parameter to be investigated. The input data associated with the light source at each of the network nodes include the type of light source required, the operating wavelength, the source output power, the coupling efficiency of the light source to the fiber and the source extinction ratio. For the optical fiber, its attenuation coefficient, the bandwidth-length product and the bandwidth-length dependence factor must be specified. The required input data for the receiver include the type of detector suitable at each network node, the quantum efficiency, the detector capacitance and the bit error rate. For avalanche photodiodes, the avalanche gain, the excess noise factor and the multiplied dark current must be specified. The input data that are required for the transimpedance amplifier design include the front-end active device parameters and the bit rate-feedback resistance product. For the access couplers, the coupling ratio and the insertion loss parameter must be specified. The input data required for traffic analysis include the mean packet arrival rate at each of the network nodes, the mean packet length, the total number of packets to be transmitted or the network operating time (simulation time), the backoff algorithm required for rescheduling colliding packets, the jam time (channel clearing time) and the seed values for the random number streams.

After the entry of all the input data, subroutine INTCMP then computes other parameters which are required for subsequent calculations where these intermediate parameters include the coupling loss, the insertion loss, the coupled power into the fiber, the connector loss, the insertion loss of the access coupler, the amplifier feedback resistance, the Q-factor of the photodiode, the input traffic intensity, the maximum end-to-end distance of the network topology considered, the maximum propagation delay and the slot time.

(ii) Random Number Generators: Pure simulation study of any system requires the generation of random numbers according to a given probability distribution. In the FONSIM package, four function subprograms, namely, URAND, EXPON, DUNIFM, and UNIFRM are written to perform the generation of random variates. URAND generates independent and uniformly distributed random numbers between zero and one, U(0,1), by the multiplicative congruential method for a specified random number stream. Using the inverse transform method, the U(0,1) generated numbers are then converted to any other desired probability distributions [26].

EXPON generates an exponential random variate for a parameter from that parameter's specified mean value and the random-number stream used for generating the parameter. In the FONSIM package, the exponential distribution is used for selecting the packet interarrival times and packet lengths. Specifically, a particular random observation, X, of the exponential distribution is determined from [26]

$$X = -\,\phi\,\ln[U(0,1)] \tag{4.1}$$

where ϕ is the mean of the exponential distribution. Figure 4.2 shows the inverse-transform approach for an exponential random variable. DUNIFM generates a discrete random variate which is uniformly distributed on the interval $[i,j]$, where i and j are integer-valued and i is less than j. In particular, the discrete uniform distribution is determined from [27]

$$X = i + \lfloor (j - i + 1)U(0,1) \rfloor \tag{4.2}$$

where $i \le X \le j$ and $\lfloor z \rfloor$ denotes the greatest integer that is less than or equal to any real number z. DUNIFM is the probability distribution used for selecting the destination nodes of all the transmitted packets.

UNIFRM generates a continuous random variate which is uniformly distributed on the inter-

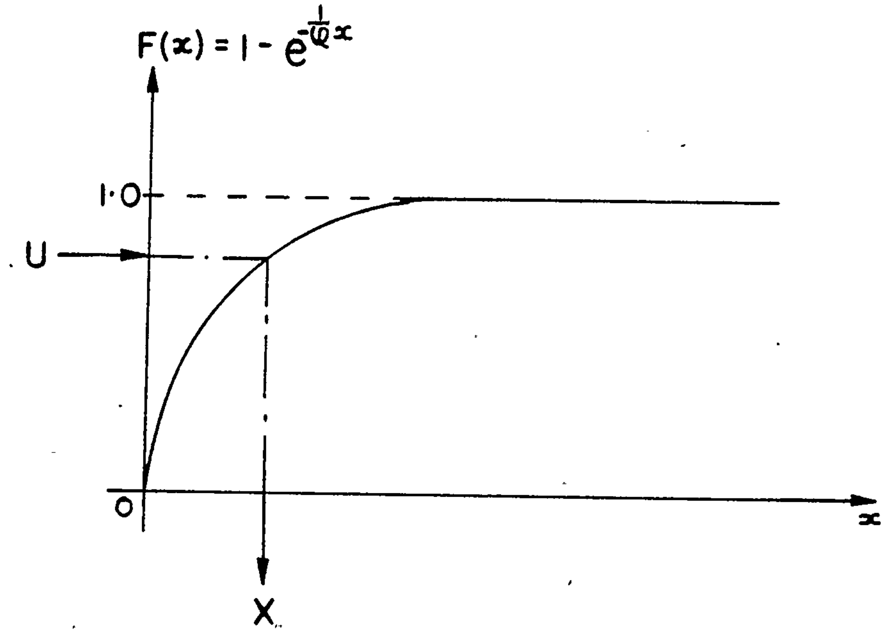

Fig. 4.2 The inverse-transform approach for an exponential random variable

val $[a,b]$, where a and b are real valued and a is less than b. The generation algorithm is defined by [27]

$$X = a + (b - a)U(0,1) \tag{4.3}$$

where $a<X<b$. For the uniform backoff algorithm, this function subprogram is the probability distribution applied in choosing the retransmission delays for the colliding packets.

(iii) Statistical Subroutines: In the FONSIM package, three subroutines are written for gathering and reporting statistics on the various network parameters computed during the course of a simulation run.

Subroutine SMPSTA computes the minimum, the maximum, the sample mean and the number of observations in a set of observations with respect to a variable that represents a network parameter. The statistical counter for the variable is updated each time a new value of the variable is computed during the course of the simulation run. In the FONSIM package, Subroutine SMPSTA is used for gathering statistics on the mean packet delay, the network throughput, the backlog clearing time and the average number of collisions experienced during a simulation run.

Subroutine TIMSTA computes the minimum, the maximum and the time-average of a set of observations on a variable. Each time a new value for the variable is computed during the simulation, the statistical counter for this variable is updated. TIMSTA serves as the statistical gathering subroutine for QUESTA.

QUESTA is the subroutine which reports the statistics on the nodal queue contents in the network. By calling QUESTA with a network node number as parameter, the minimum, maximum and time-average number of packets in that node is obtained. QUESTA is also used to determine the overall time-average number of packets in the network.

(iv) Output Subroutines: Subroutine REPORT calculates and prints out the final output parameters at the termination of each simulation run. The output parameters include the network path length, the network attenuation, the network dynamic range, the bandwidth capability, the network throughput, the average packet delay, the backlog clearing time, and the time average number of packets at each network node.

To assess the variability of the output results produced by the discrete-event simulation section of the FONSIM package, more than one simulation run is required. It is the practice in simulation studies to express the results in terms of confidence intervals placed on the mean values of the output parameters. The confidence interval for the mean of a parameter estimated by a sample of independent and identically distributed observations, for example, $Y = Y_1, Y_2, \cdots, Y_{N_s}$, is defined by the upper and lower interval limits [27] .

$$UI = \overline{Y}(N_s) + t_{N_s-1,1-\frac{\kappa}{2}} \sqrt{\frac{S^2(N_s)}{N_s}} \tag{4.4a}$$

$$LI = \overline{Y}(N_s) - t_{N_s-1,1-\frac{\kappa}{2}} \sqrt{\frac{S^2(N_s)}{N_s}} \tag{4.4b}$$

where

$$\overline{Y}(N_s) = \frac{\sum_{j=1}^{N_s} Y_j}{N_s}$$

is the sample mean and

$$S^2(N_s) = \frac{\sum_{j=1}^{N_s} [Y_j - \overline{Y}(N_s)]^2}{N_s - 1}$$

is the sample variance of the N_s observations. $t_{N_s-1,1-\frac{\kappa}{2}}$ is the upper $1-\frac{\kappa}{2}$ critical point for the t -distribution with $(N_s - 1)$ degrees of freedom where these critical points are available in the form of tables [28]. The confidence intervals thus obtained are referred to as the intervals with approximate 100(1− κ) percent and (N_s− 1) degrees of freedom. Subroutine CINTVL provides an approximate 95% confidence interval with 9 degrees of freedom for all the network traffic output parameters.

4.3.2. Level 2 Subroutines

All the subroutines used for performing queue (list) management and other commonly occurring discrete-event simulation activities are grouped into level 2. In the FONSIM package, each network node is represented by a list. Three additional lists are however required: the EVENT list in which all of the scheduled events are stored, the TOPPKT list which contains the top packets of all the network nodes and the CHANNEL list which represents the multiaccess optical fiber channel. In order to reduce the time required for processing these lists and also to reduce the computer storage locations, all the lists are stored using the linked storage allocation approach [29]. The function of level 2 subroutines are briefly summarized below :

INITLZ: initializes queue management variables such as successor and predecessor links together with the head and tail pointers for each list. INITLZ also sets the simulation clock time to zero and initializes the statistical counters required for gathering the network parameters.

FILPKT: inserts the attributes of a packet into the specified list and at the appropriate location. The packet can be filed either before the first packet or after the last packet in the specified list. Alternatively, the packet can also be filed so that the specified list is kept ranked in increasing or decreasing order on one particular attribute of the packet. In the FONSIM package, the EVENT list and TOPPKT list are kept ranked in increasing order on the event time attribute.

RMVPKT: removes a packet from the specified list

CNCPKT: cancels the first event with a specified type from the EVENT list

DLTPKT: deletes all the scheduled events of a specified type from the EVENT list

NXTPKT: determines the event type of the next event to occur and updates the simulation clock. NXTPKT picks the earliest event to occur from either the EVENT list or the TOPPKT list.

MONITR: prints out the contents of all the lists and the statistical counters. This subroutine is very useful for obtaining a trace of the simulation outputs.

CPYPKT: prints out the attributes of a packet which is located at any position in a specified list.

4.3.3. Level 3 Subroutines

It has been mentioned that the FONSIM package incorporates a separate module for each performance measure, this allowing each performance parameter to be considered separately, and furthermore, it helps in the program debugging process. For the path length, network attenuation, network dynamic range and bandwidth capability criteria, the algorithm and expressions presented in Chapter Three form the basis for the subroutines developed to evaluate these parameters. The network traffic characteristics are determined by the discrete-event simulation approach.

Subroutine PATH computes the path length of any selected network topology using the algorithm described in Chapter Three. The network attenuation (maximum transmission loss) is determined by the subroutine TRXLOS and this transmission loss computation is preceded by a call to subroutine RCVR, whose function is to compute the receiver sensitivity. Subroutine TRXLOS also determines the maximum attenuation coefficient of the fiber required for the network interconnections. Subroutine DYRNGE first computes the maximum and minimum transmission losses from which the network dynamic range is determined for the selected topology. Two schemes are employed in the evaluation of the bandwidth of a chosen network topology and both schemes are implemented by the BNDWDT subroutine. The first scheme gives the dispersion limited bandwidth which is computed from the specified fiber bandwidth-length product and the distance between the two furthest nodes in the network. The second scheme gives the attenuation limited bandwidth obtained from Equation (3.22). In the second scheme, $\bar{P}$ is the difference between the coupled power into the fiber and the sum of all the losses incurred between a transmitting node and the furthest receiving node. The overall network bandwidth is the lower value of the bandwidths computed from the two schemes.

The network traffic characteristics are determined by subroutine TRAFIC which is a discrete-event simulation program using the next event time advance technique to run the simulation clock. As mentioned in Chapter Three, there are three events which are incorporated into TRAFIC: packet arrival into the network, collision checking on the multiaccess optical fiber channel, and packet departure from the network and each of these events is processed by a separate subroutine. The simulation models developed for TRAFIC and also the three event-handling subroutines are shown in Figures 4.3(a,b,c,d). Figure 4.3a depicts the operational flowchart of TRAFIC. At the start of a simulation run, subroutine INITLZ is called to initialize certain variables and statistical counters. A packet arrival at each of the network nodes is scheduled and placed in the EVENT list. The earliest event to occur during the course of a simulation run is then selected by subroutine NXTPKT from either the EVENT list or the TOPPKT list and depending upon the type of this earliest event, the appropriate subroutine to process the event is called. Arrival events are processed by PKTARV, collision checking events by COLCHK and departing events by PKTDEP. After every event, the program checks whether or not enough packets have been transmitted or sufficient simulation time has elapsed and if so, the simulation is terminated, otherwise the next sequential event is picked and executed. At the end of a simulation run, subroutine REPORT is called to print out the results for the just completed run and additional replications are performed until the specified number of simulation runs has been completed. Subroutine TRAFIC finally computes the confidence intervals of the output parameters by calling subroutine CINTVL after which it passes control to the main program. The description of the event-handling subroutines is now given:

Subroutine PKTARV: Figure 4.3b shows the operational flowchart of PKTARV. When PKTARV is called, it first gathers the attributes of the arriving packet. Each packet to be transmitted has ten attributes:

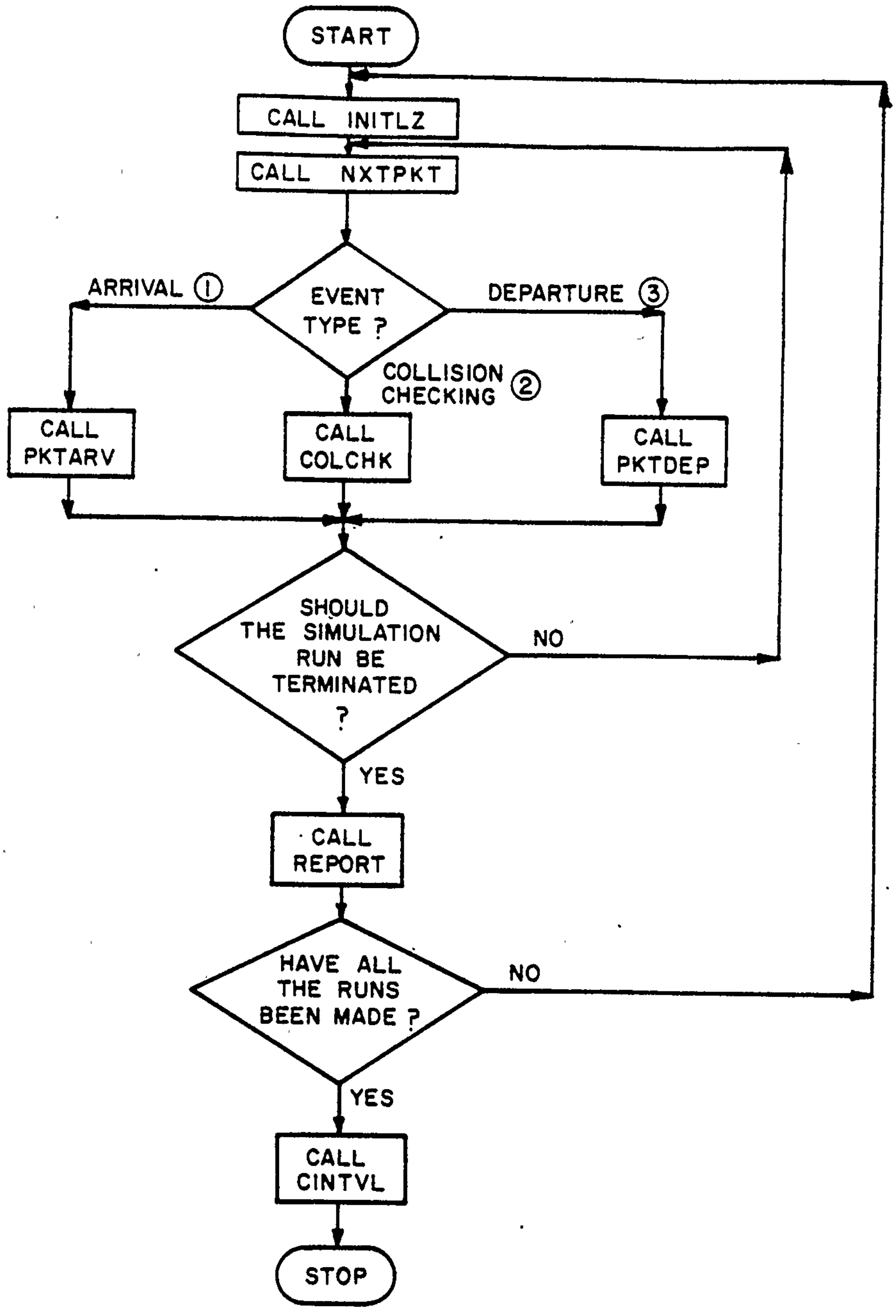

Fig. 4.3 (a) Operational flowchart of TRAFIC

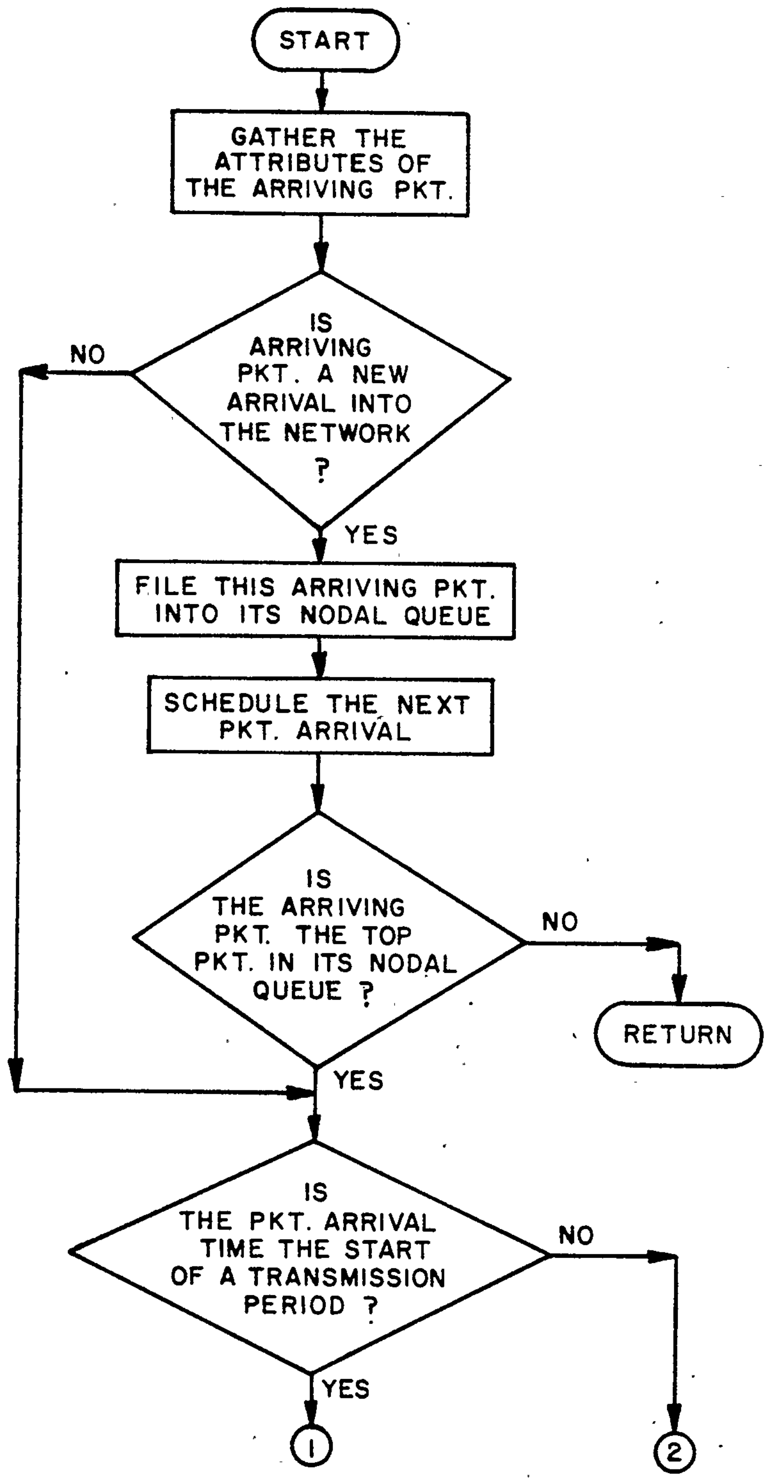

Fig. 4.3 (b) Operational flowchart of PKTARV

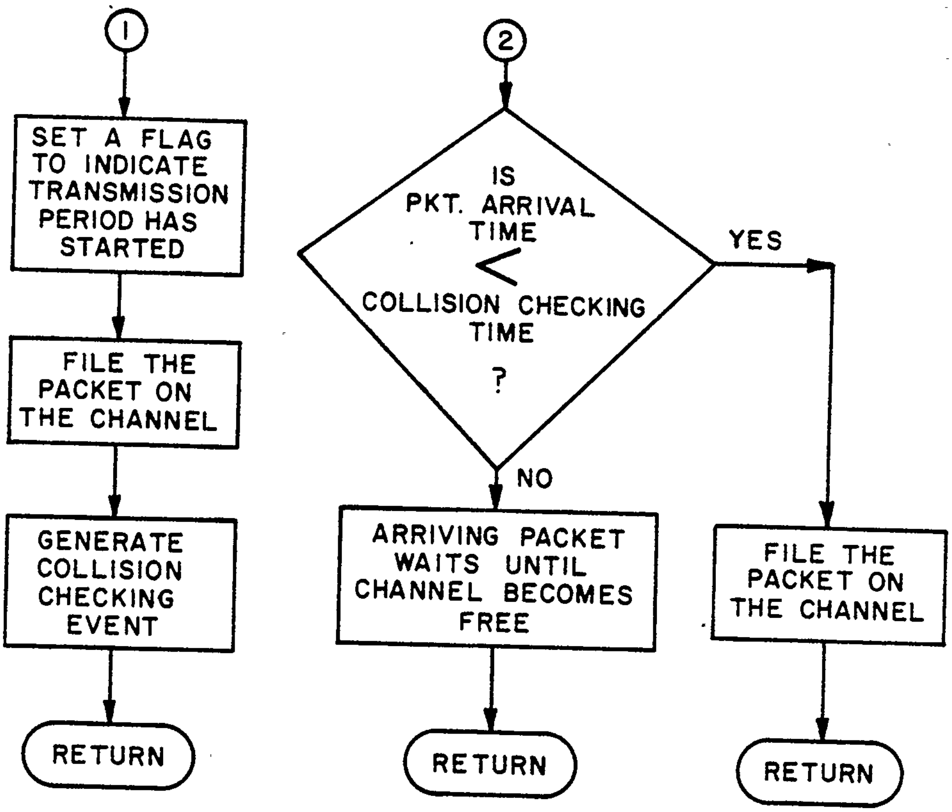

Fig. 4.3 (b) (continued)

(i) Packet arrival time into the network

(ii) Packet event type

(iii) Packet Status - whether new or rescheduled

(iv) Packet source node number

(v) Packet destination node number

(vi) Packet length

(vii) Distance between the source and the destination nodes

(viii) Number of packet transmission attempts

(ix) Packet identification number

(x) Global list number where the packet is stored

Based on the above attributes, a check is made as to whether the arriving packet is completely new or if it is an old packet which is being retransmitted. As the first-in, first-out queueing discipline is employed at each network node, a new arriving packet is filed after the last packet in the transmit queue of its source node and the next packet arrival to this node is then scheduled and placed in the EVENT list. A further check on the arriving packet is made as to whether it is at the top of its nodal transmit queue and if not, the subroutine execution terminates and control passes to the TRAFIC program. If the arriving packet is new and it is at the top of its nodal queue or if the arriving packet is an old packet, a check is made on whether a transmission period is already in progress. If a transmission period is not in progress, the arriving packet initiates a new transmission period and sets a flag to indicate to other subsequent arriving packets of the commencement of a transmission period. A collision checking event is also scheduled to occur at the expiration of the round-trip propagation delay of the packet that has initiated a transmission period and control is then returned to the TRAFIC program. Due to the multiaccess nature of the optical fiber channel, any packet arriving after the start of a transmission period but before the collision checking event also accesses the channel. Any packet which arrives after the occurrence of the collision checking event (within the same transmission period) simply waits in its respective nodal queue until the channel becomes free. It is clear from these statements that the transmission of more than one packet on the channel before the occurrence of the collision checking event results in collision, also, more than one packet waiting for the channel to be free guarantees a collision in the next transmission period.

Subroutine COLCHK: This subroutine whose flowchart is shown in Figure 4.3c simply determines the total number of packets being transmitted on the channel. If there is only one packet on the channel, no collision occurs and the packet holds the channel solely until all its bits are transmitted. A departure event for the packet is then scheduled and inserted in the EVENT list after which control is returned to the TRAFIC program. Any packet arriving between the time when the channel is seized and the packet departure time waits (1-persistent CSMA/CD) until the channel becomes free. On the other hand, more than one packet on the channel indicates collision occurrence. A jamming signal is sent to all of the network nodes so that they are made aware of the collision occurrence and also to inhibit further transmission. All the colliding packets are then rescheduled with the retransmission delays selected from a specified backoff algorithm of the CSMA/CD protocol and the transmission flag is set to indicate the end of an unsuccessful transmission period and control is returned to TRAFIC.

Subroutine PKTDEP: This subroutine (Figure 4.3d) processes all the successfully transmitted packets which are departing from the network. Statistics on output parameters are gathered by calling subroutine SMPSTA. The output parameters include the total number of successfully transmitted packets - this is used for computing the network throughput, the packet transmission time, and the

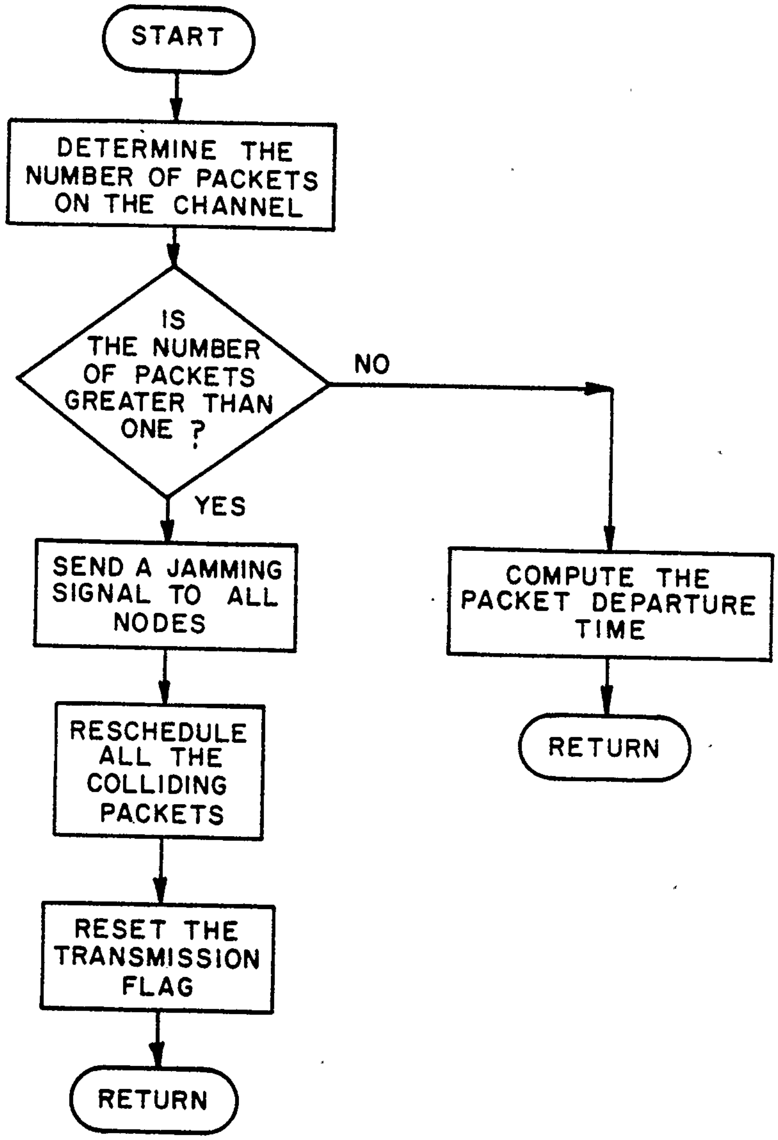

Fig. 4.3 (c) Operational flowchart of COLCHK

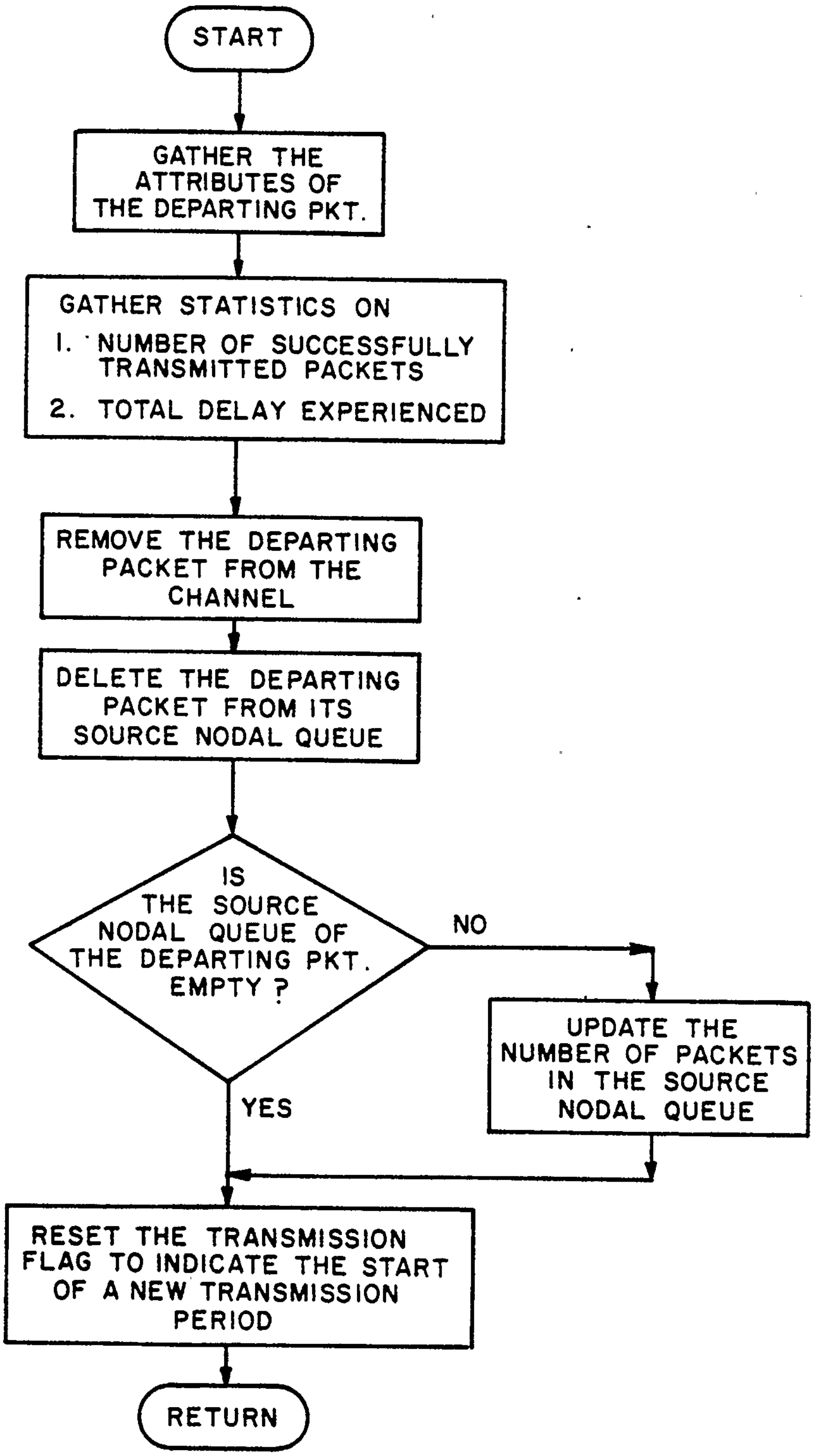

Fig. 4.3 (d) Operational flowchart of PKTDEP

total packet delay. Information is also gathered as to whether a departing packet has experienced any collisions and the number of transmission attempts necessary for successful transmission. The departing packet is then deleted from the channel and from its source nodal queue after which PKTDEP checks whether there is any packet awaiting transmission in the source nodal queue. If there is any packet awaiting transmission, a flag is set to signal the end of the current transmission period and the new top packet in this source nodal queue becomes ready for transmission in the next transmission period. If the source nodal queue of the departing packet is empty, the transmission flag is immediately set to indicate the end of a successful transmission period and control is returned to the TRAFIC program.

4.4. FONSIM Verification and Validation

Verification of a simulation model and validation of the predicted results are two essentials of all simulation work. Verification is applied to ensure that the simulation model (computer program) performs as intended. In this work, the discrete-event simulation section of the FONSIM package is verified by the tracing technique. The performance evaluation modules which are based on analytical expressions are individually checked by inputting known data and comparing the subroutine outputs to the results calculated manually. Validation, on the other hand, establishes that the simulation model output results "closely" resemble the output results which will be expected from the real system or from an exact mathematical analysis of the system behavior.

Two approaches are employed to build confidence into the results produced by the FONSIM package, especially in the results from the discrete-event simulation section. The first approach involves the comparison of analytical and simulation results for a simpler system which is similar in some extent to the POFLANs' under study. In the modeling of communication networks in general, it is usual to model each of the network nodes by the single-server queueing system shown in Figure 4.4 to which analytical results are readily available. By making the assumptions that packet arrivals at each node follow a Poisson process and the transmission times of these packets are exponentially distributed, (same as assumptions (i) and (ii) in Section 3.2.5), then the performance

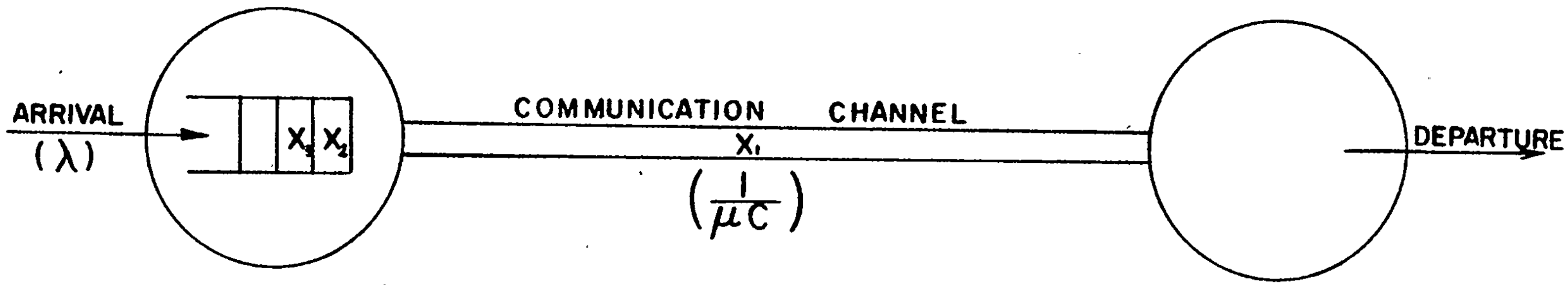

Fig. 4.4 M/M/1 Queueing System

measures for this $M/M/1$ queueing system are given by [30]

$$L = \frac{\rho}{1-\rho} \tag{4.5a}$$

$$L_q = \frac{\rho^2}{1-\rho} \tag{4.5b}$$

$$W = \frac{1}{1-\rho} \left(\frac{1}{\mu C}\right) \tag{4.5c}$$

$$W_q = \frac{\rho}{1-\rho} \left(\frac{1}{\mu C}\right) \tag{4.5d}$$

The factor $(\frac{1}{\mu C})$ has a unit of seconds per packet while the derivation of Equations (4.5(a,b,c,d)) are given in the Appendix.

The performance measures calculated using Equations (4.5(a,b,c,d)) are compared with those obtained from the discrete-event simulation approach. The simulation model constructed for this $M/M/1$ system is a simplified version of the discrete-event simulation section of the FONSIM package. The comparison of the simulation and analytical results regarding the average number of packets in the $M/M/1$ system and in its nodal queue is shown in Figure 4.5 and the two results are in close agreement. Figure 4.6 shows that the simulation and analytical results with respect to the average packet delay compare very favorably.

In the second approach, the available experimental results of an existing network, the Ethernet, reported by Shoch and Hupp [31] are compared with the results obtained from the FONSIM package. The equivalent fiber-optic Ethernet network is simulated with the selected parameters shown in Table 4.2 which are identical to those used in Ethernet. The network throughput-offered load results shown in Figure 4.7 depict the comparison of the experimental results with those obtained using the simulation approach.

Under light to moderate offered load on the network, the simulation results fit with the experimental results whereas under high network loads, the simulation results deviate from the experimental

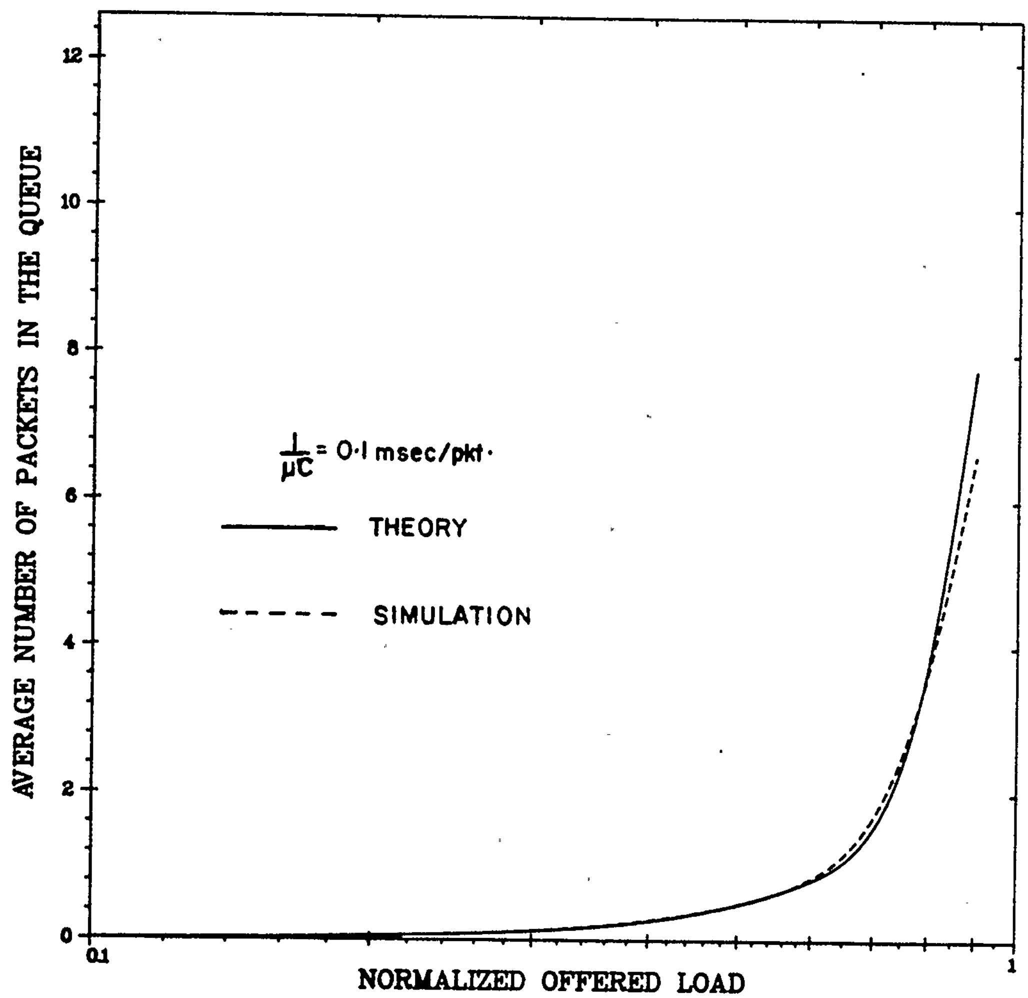

Fig. 4.5 (a) Average Number of Packets in the Nodal Queue Versus Offered load

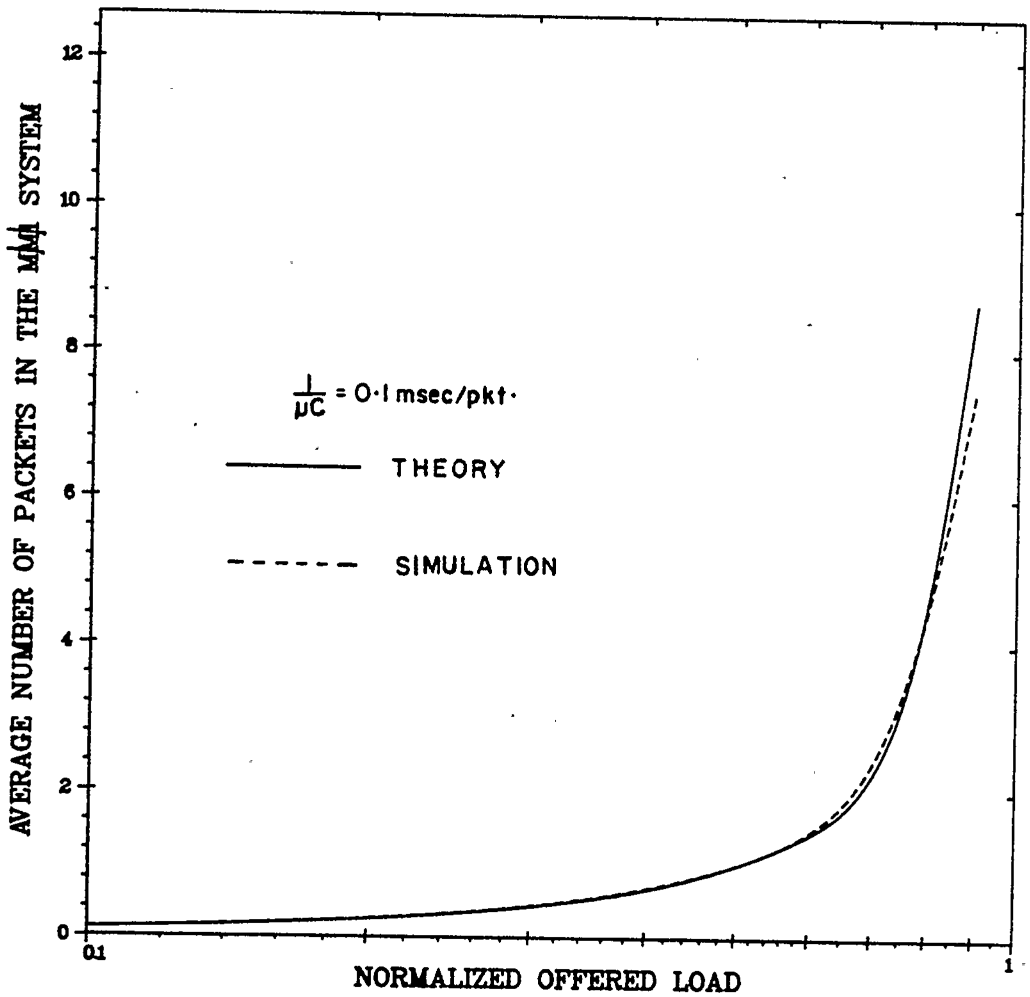

Fig. 4.5 (b) Average Number of packets in the M/M/1 System Versus Offered load

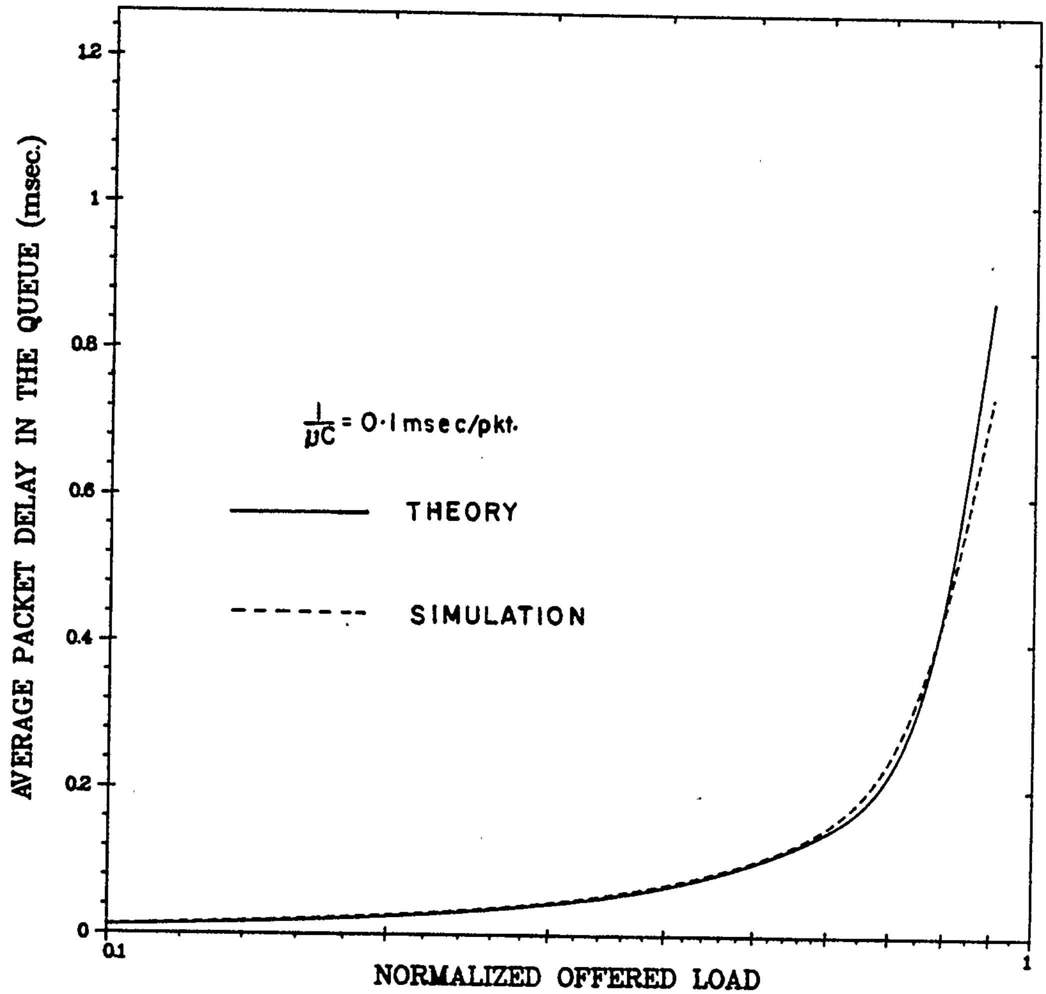

Fig. 4.6 (a) Average Packet Delay in the Nodal Queue Versus Offered load

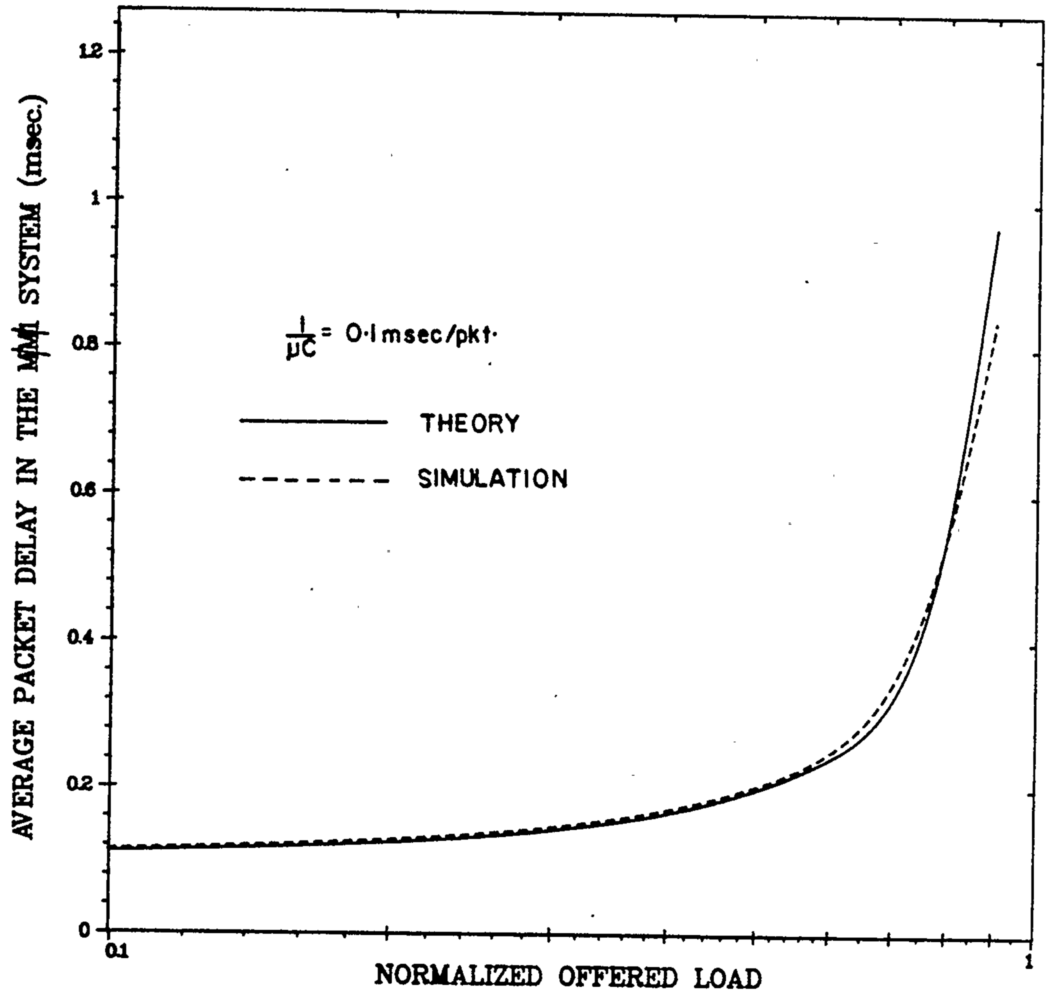

Fig. 4.6 (b) Average Packet Delay in the M/M/1 System Versus Offered load

Bus Bandwidth	2.94 Mb/s
Bus Length	0.55 km
Backoff Algorithm	BEB, truncated at 2^8
Slot time	38 ns
$\frac{1}{\mu}$	1024 bits
N	6
Jam Time	3 μs

Table 4.2 Ethernet Parameters

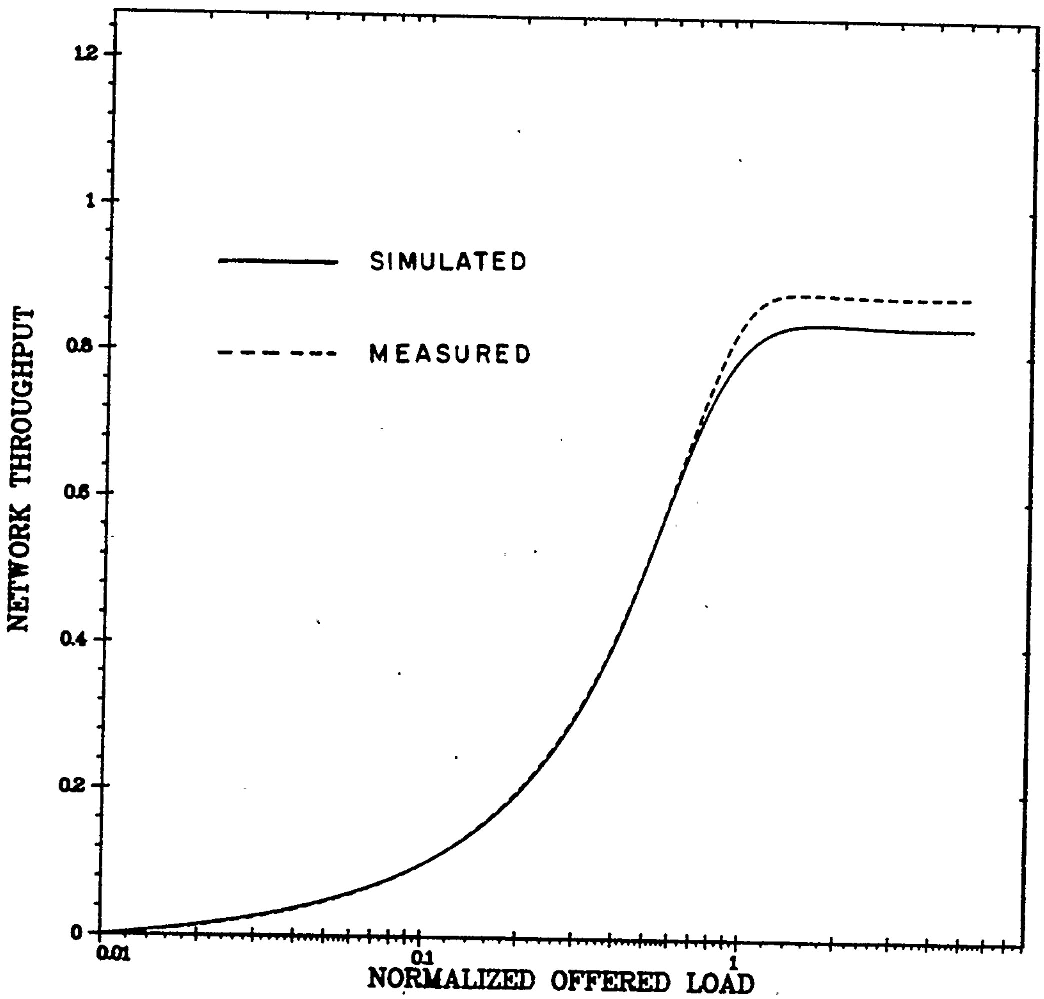

Fig. 4.7 Comparison of Experimental and simulated values of Ethernet Throughput - Offered Load Characteristics

results by a margin of approximately 4.5%. It is seen from Figure 4.7 that under high loads the simulated results are somewhat pessimistic, this being due to the worst case condition simulated for the CSMA/CD access protocol. It is important to note that the deviation is however very small and taking cognizance of the fact that any simulation model is only an approximation to the real system, the simulation results obtained from the FONSIM package are considered most acceptable.

4.5. Application of the FONSIM Package

The usefulness of the FONSIM package is illustrated by its application in the performance evaluation of two passive optical fiber local area network examples. The first example is a POFLAN of an arbitrary size which can be installed within a building while the second example is a network which consists of 6 nodes and all the possible physical connecting paths between any two nodes (Figure 4.8). Table 4.3 depicts the associated distance matrix (in kilometers) for the 6-node network. This example illustrates a POFLAN design that is typical for a University campus or a city where different buildings/departments or office branches are to be interconnected.

4.5.1. Simulation Experiments

Several simulation experiments were performed in order to demonstrate the realization of the previously stated capabilities of the FONSIM package with these experiments being divided into two categories. Category One focused mainly on the first network example while the second category dealt with the 6-node network.

The objectives of these experiments are outlined as follows:

CATEGORY I EXPERIMENTS

EXPERIMENT 1: The objective of the experiment is to determine the total number of network nodes which can be supported by each of the POFLAN topologies. The varying parameter is the operating bit rate while the light source output power, the fiber attenuation coefficient and the maximum distance between the two furthest nodes in each POFLAN topology are fixed.

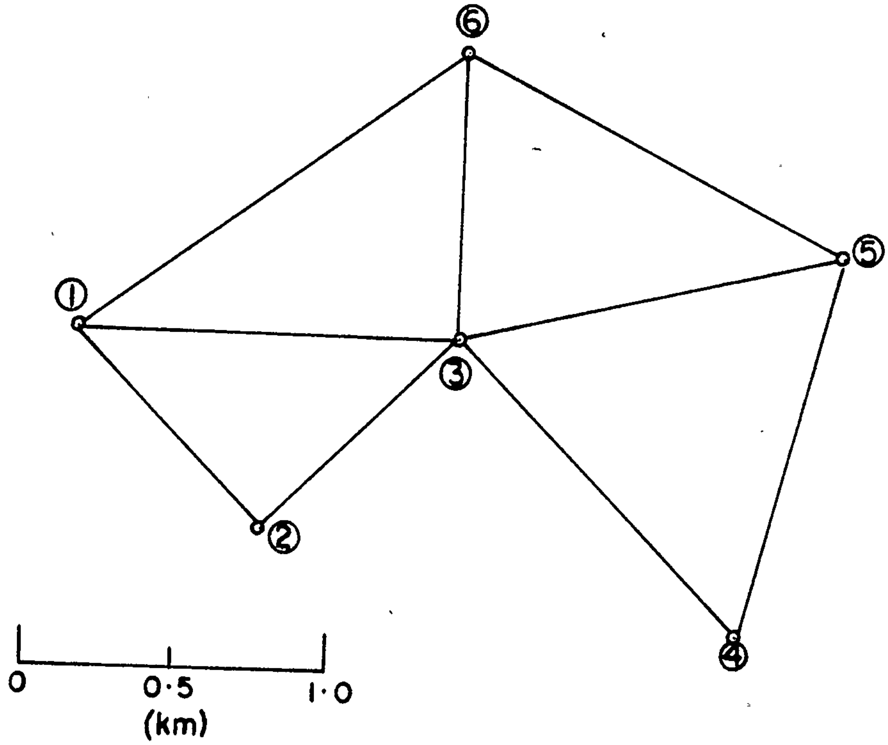

Fig. 4.8 Configuration of the 6-node Network example

$$\begin{array}{c|c}
 & \begin{array}{cccccc} 1 & 2 & 3 & 4 & 5 & 6 \end{array} \\
\begin{array}{c} 1 \\ 2 \\ 3 \\ 4 \\ 5 \\ 6 \end{array} & \begin{bmatrix} 0.0 & 0.9 & 1.25 & 0.0 & 0.0 & 1.6 \\ 0.9 & 0.0 & 0.9 & 0.0 & 0.0 & 0.0 \\ 1.25 & 0.9 & 0.0 & 1.35 & 1.3 & 0.95 \\ 0.0 & 0.0 & 1.35 & 0.0 & 1.3 & 0.0 \\ 0.0 & 0.0 & 1.3 & 1.3 & 0.0 & 1.45 \\ 1.6 & 0.0 & 0.95 & 0.0 & 1.45 & 0.0 \end{bmatrix}
\end{array}$$

0.0 $\Longrightarrow$ No direct connection from NODE i to NODE j

Table 4.3 Distance Matrix (in km) of the 6-node Network Example

EXPERIMENT 2: The aims of this experiment are twofold: the first is concerned with the evaluation of the minimum and maximum transmission losses for a varying number of nodes supported by each POFLAN topology, whilst the second objective deals with the dynamic range required by each POFLAN topology as a function of the number of nodes supported, and in either case, the fiber attenuation coefficient remains constant.

EXPERIMENT 3: In this experiment, the maximum attenuation coefficient of the fiber required for network interconnections is computed with respect to different operating bit rates for a fixed network size. The variation of the fiber attenuation coefficient with varying network sizes under a constant operating bit rate is also determined.

EXPERIMENT 4: The objective of this experiment deals with the investigation of the maximum network bandwidth capability as a function of the maximum link distance for each POFLAN topology with the network size, the fiber attenuation coefficient, the bandwidth-length dependence factor and the fiber bandwidth-length product all being constant.

CATEGORY II EXPERIMENTS

EXPERIMENT 5: The path length, the transmission loss, the dynamic range requirement and the bandwidth capability for each of the implemented POFLAN topologies of the 6-node network are computed with the purpose of selecting the optimum topology in terms of each of these performance measures.

EXPERIMENT 6: The objective of this experiment is to investigate the network throughput versus offered load for each POFLAN topology where this is carried out under the following operating conditions:

(i) Varying the operating bit rate with the mean packet length constant.

(ii) Varying the mean packet length with a constant operating bit rate

EXPERIMENT 7: The variation of the average packet delay with the applied load on the network is investigated, this characteristic being determined for the same conditions specified in Experiment 6.

EXPERIMENT 8: The clearing time of the backlogged packets in all the nodal queues are computed for different traffic conditions where this computation is also based on the two conditions stated in Experiment 6.

EXPERIMENT 9: In this experiment, the effects of the backoff algorithms employed for selecting the retransmission delays of the colliding packets on the throughput-delay characteristics are investigated. The performance of two rescheduling algorithms are compared: the IEEE BEB algorithm (defined in Chapter Three) and the uniform backoff algorithm in which the retransmission delays are selected from a uniform probability distribution with a specified mean retransmission delay.

4.5.2. Selected Network Parameters

Tables 4.4(a-d) show the network input parameters which are selected for the simulation experiments where most of these are typical data extracted from data sheets of currently available opto-electronic devices while some are obtained from experts in industry through private communication [15,32-34]. Table 4.4a shows the selected network parameter values required for network design, Table 4.4b depicts the data for the light source, Table 4.4c contains the optical fiber parameters while Table 4.4d shows the optical detector and amplifier parameters.

4.5.3. Simulation Results and Discussion

The simulation results are presented in a variety of forms so as to illustrate the interesting behavior of the POFLAN topologies where these results are shown in Figure 4.9 to Figure 4.16 and in Table 4.5. In the following, an in-depth discussion on these results is given under appropriate headings.

α_c	0.7943
β	0.7943
σ_h	0.2
BER	10^{-9}
L_M	4 dB
B	1 Mb/s , 10 Mb/s

Table 4.4a Selected Network Parameter Values

λ_s	0.85 μm
P_o	1 mW
η_c	0.1
ε	0.12

Table 4.4b Selected Typical LED Data

BWL	100 MHz - km
α	3 dB/km
ξ	0.7 , 1.0
Fiber Crosssection	85/125 μm
Numerical Aperture	0.26

Table 4.4c Selected Typical Fiber Parameters

λ_s	0.85 μm
η_e	0.7
C_{phd}	0.5 pF
x	0.5
I_{du}	1nA
I_{dm}	0.001 nA
Γ	0.7
g_m	5 mS
$C_{gs} + C_{gd}$	3.5 pF
$R_F - B$	750 K Ω - Mb/s

Table 4.4d Selected typical SiAPD and TZ amplifer parameters

4.5.3.1. Network Size

The variation of the network size with operating bit rate for the STAR, LOOP and LINEAR BUS topologies is shown in Figure 4.9a where it is observed that the STAR topology (STARNET) is capable of supporting many more nodes than either the LOOP topology (LOOPNET) or the LINEAR BUS topology (BUSNET). For the network parameters used in this example, it is seen that while the STARNET is capable of supporting nodes in the range of hundreds to thousands, the LOOPNET or BUSNET can support less than ten network nodes. An explanation for this behavior is partly due to the logarithmic dependence of the maximum transmission loss of the STARNET on the number of nodes supported, N, whereas the maximum transmission loss of the LOOPNET and BUSNET is linearly dependent on N. Another explanation which can be adduced for this behavior is that the insertion and coupling losses of the Star coupler are small and independent of N whereas the coupling losses of the access couplers used in the LOOPNET and BUSNET implementations are functions of N. It is also noted from the transmission loss analysis presented in Chapter Two that the coupling losses form the dominant component of the maximum transmission loss for the BUSNET and LOOPNET. In this particular example where the fiber loss of the STARNET exceeds the corresponding values for the LOOPNET and BUSNET, the STARNET still shows a superior performance and it is therefore concluded that the coupling losses effectively limit the number of nodes which can be supported by the BUSNET and LOOPNET. The other important observation from Figure 4.9a is the sensitivity of the network size as a function of the operating bit rate. The number of nodes supported by all the topologies decreases with increasing operating bit rate and it is also noted that the STARNET has the fastest rate of decrease compared to the LOOPNET and BUSNET. In Figures 4.9(b,c,d) are shown the network size-operating bit rate characteristics for the STARNET, LOOPNET and BUSNET respectively where the effects of the optical receiver degradation factors are taken into consideration and it is seen from these figures that the number of nodes supported by all the network topologies is reduced as a result of the lower power budget. Even with the degradation factors included, the STARNET still supports a higher number of nodes than the other topologies.

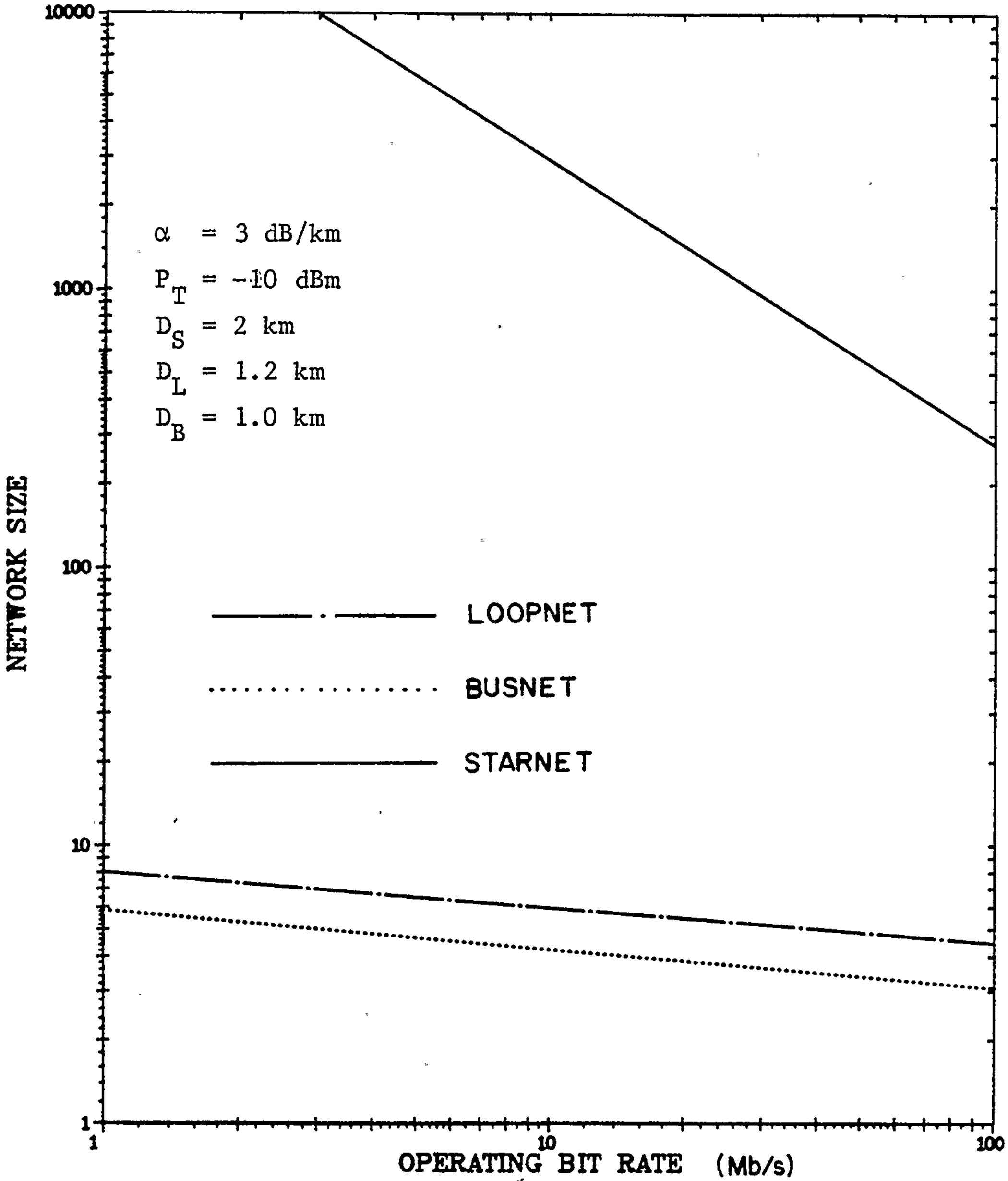

Fig. 4.9 (a) Network size Versus Operating bit rate

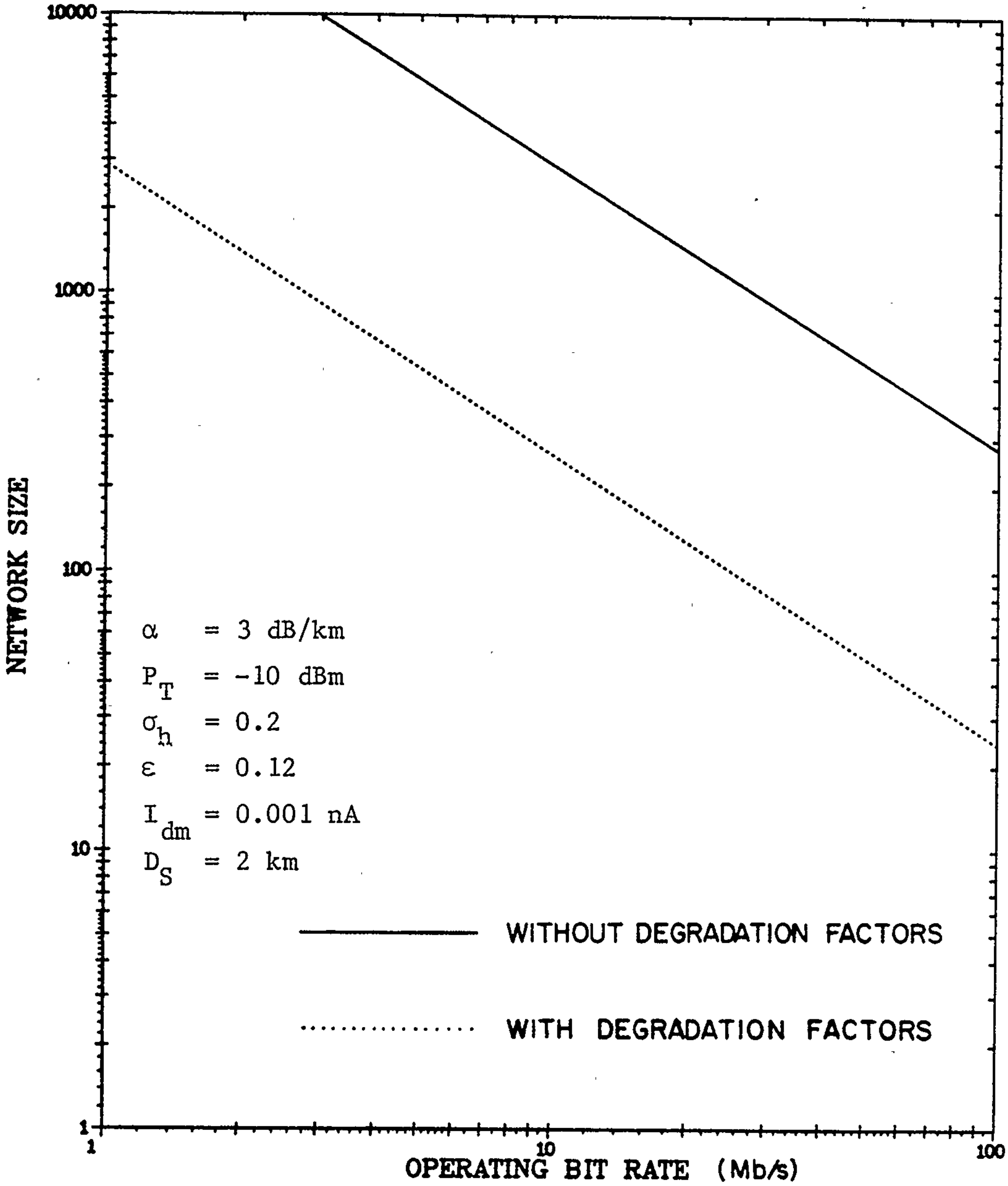

Fig. 4.9 (b) Effect of degradation factors on Network size for STARNET

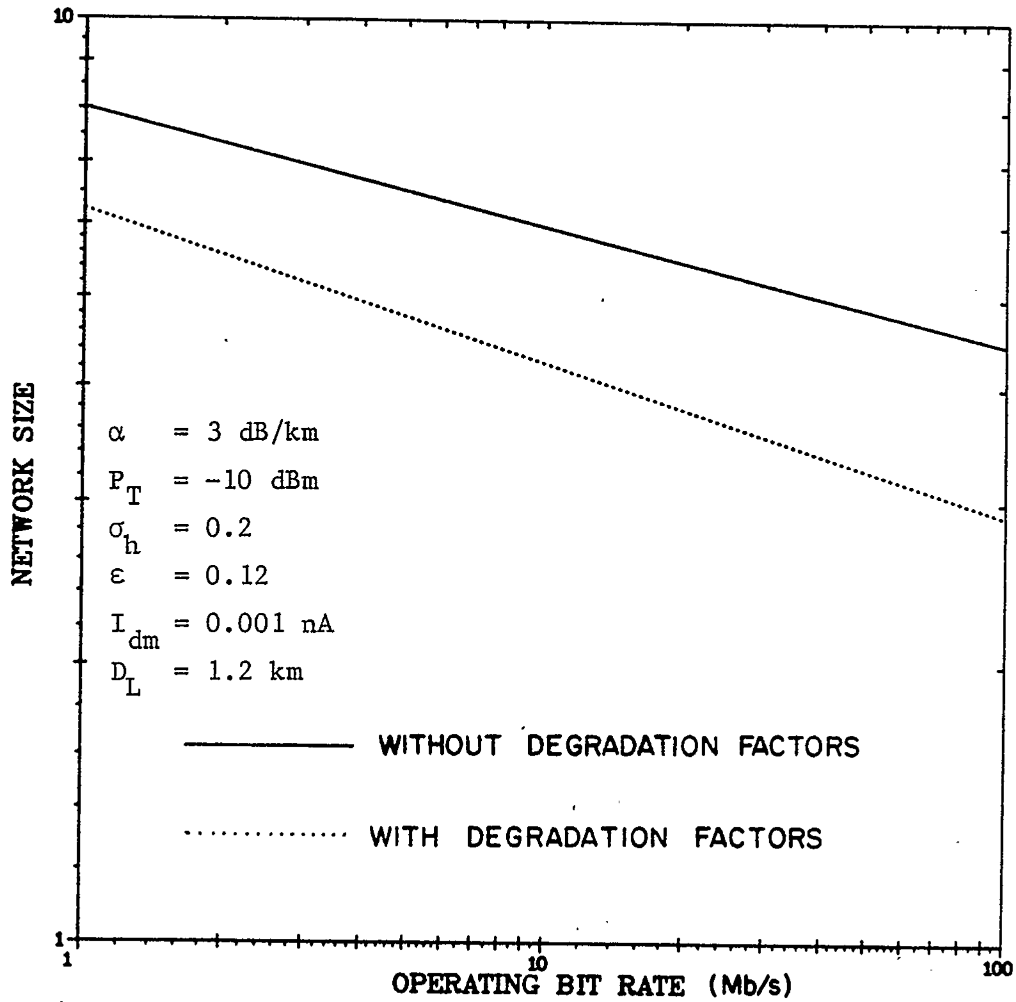

Fig. 4.9 (c) Effect of degradation factors on Network size for LOOPNET

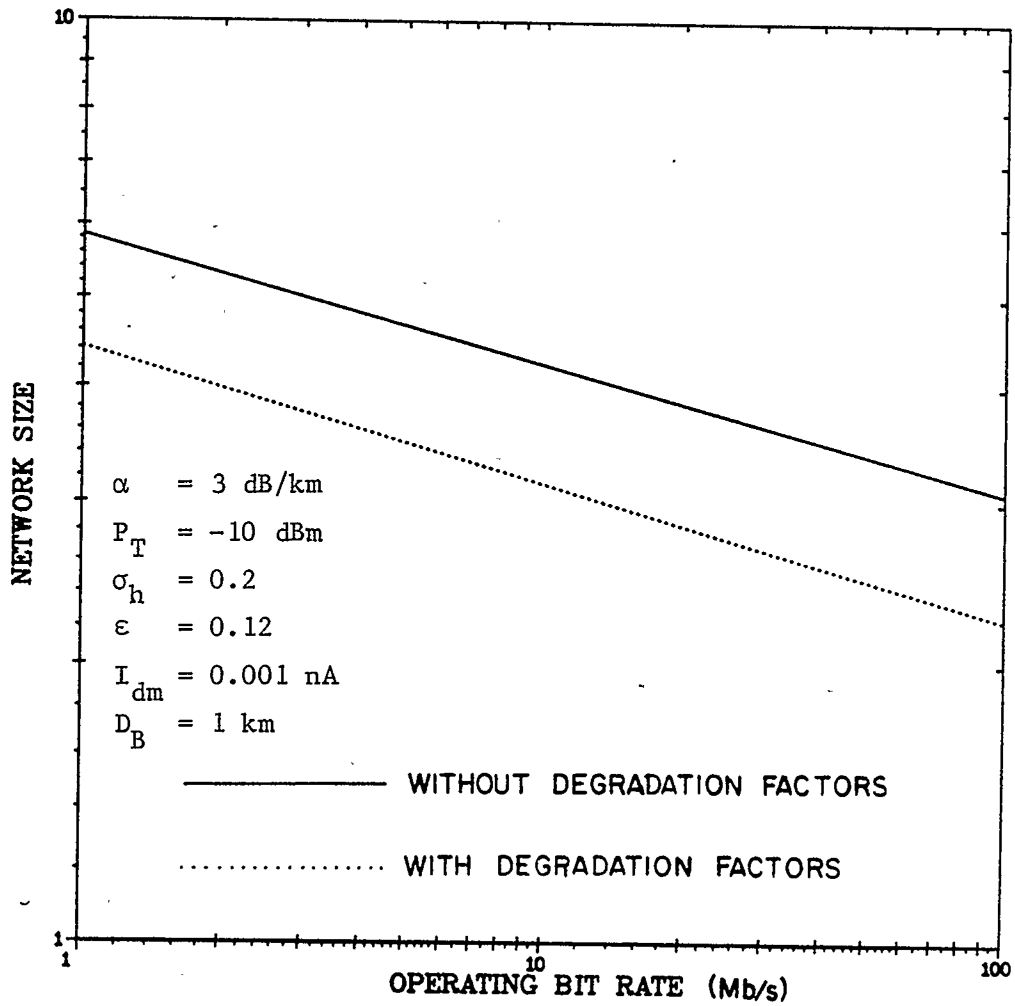

Fig. 4.9 (d) Effect of degradation factors on Network size for BUSNET

4.5.3.2. Transmission Loss and Dynamic Range

The variation of the minimum and maximum transmission losses with respect to the network size are depicted in Figure 4.10a and Figure 4.10b respectively. In Figure 4.10a, the STARNET has the least minimum transmission loss while the BUSNET has the highest value. Figure 4.10b depicts the linear relationship between the maximum transmission loss and the network size for the LOOPNET and BUSNET while the maximum transmission loss for the STARNET varies logarithmically with the network size, it also being obvious from this figure that the STARNET has the least maximum transmission loss for all the network sizes considered.

The network dynamic range requirements for the three topologies are illustrated in Figure 4.10c. It is clear that the STARNET requires the processing of an approximately constant dynamic range of 5 *dB* at all the nodal receivers in the network while for both the LOOPNET and BUSNET, a high dynamic range which linearly increases with N must be processed. The implication of this is the greater constraint placed on the receiver design to be employed in the BUSNET and LOOPNET, that is, each time the network size is increased, the receiver may have to be readjusted to accommodate the increase in the number of network nodes. The conclusion that can be drawn from Figure 4.10c is the limitation imposed on the number of network nodes which can be supported by the BUSNET and LOOPNET because of the high transmission loss and high dynamic range requirements. The low transmission loss and low dynamic range requirement of the STARNET makes it preferable to the other two topologies.

4.5.3.3. Maximum Fiber Attenuation Coefficient

The curves depicting the variation of the maximum fiber attenuation coefficient (taking into account the receiver degradation factors) with the operating bit rate for 5-node LOOP and STAR topologies are shown in Figure 4.11a. (The characteristic for the BUSNET is not shown because this topology fails under the chosen conditions, in fact Figure 4.11e shows that the BUSNET will be practicable for $N = 5$ only if the maximum fiber attenuation of 1 *dB/km* is used). At a specified

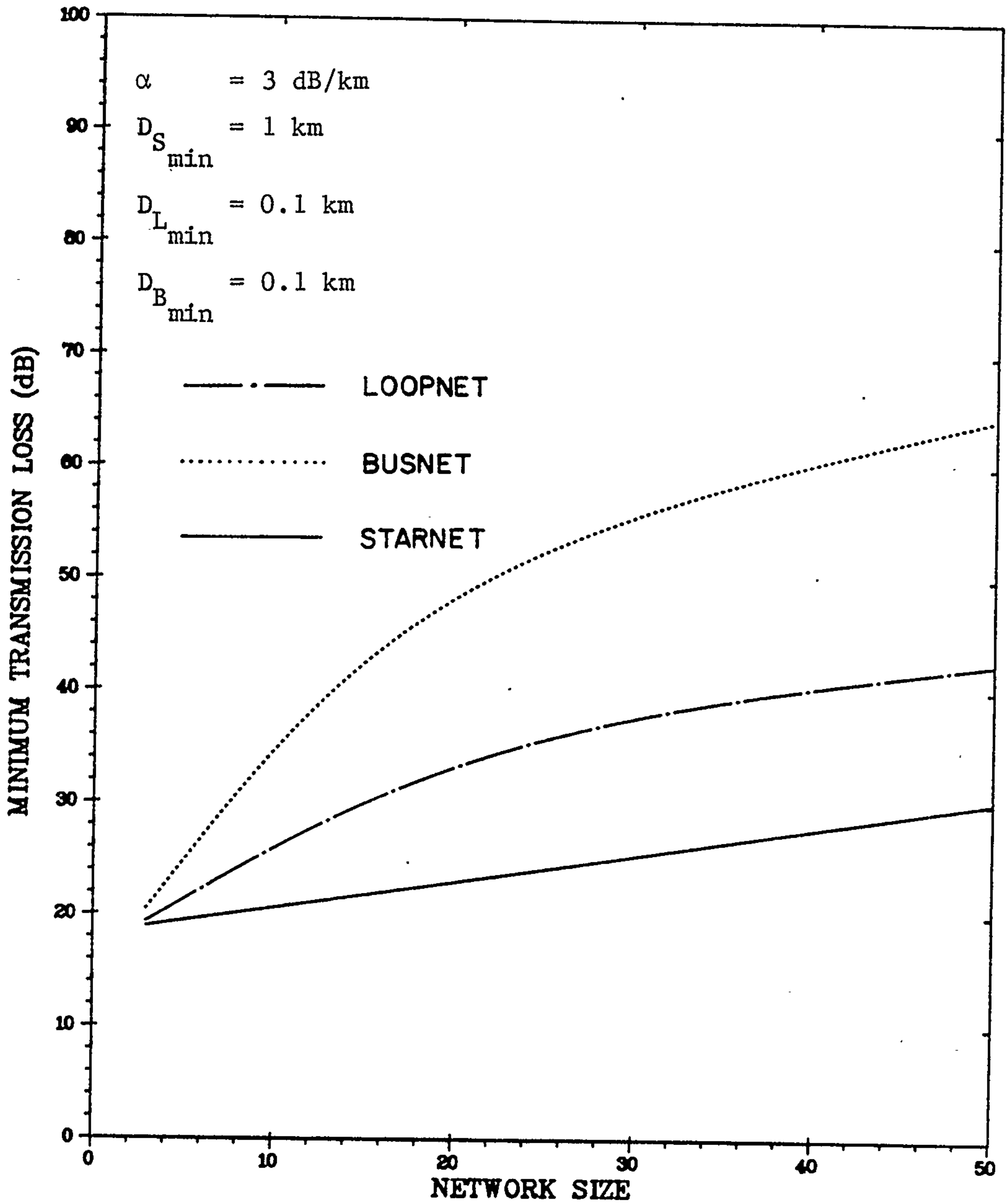

Fig. 4.10 (a) Minimum Transmission Loss Versus Network Size

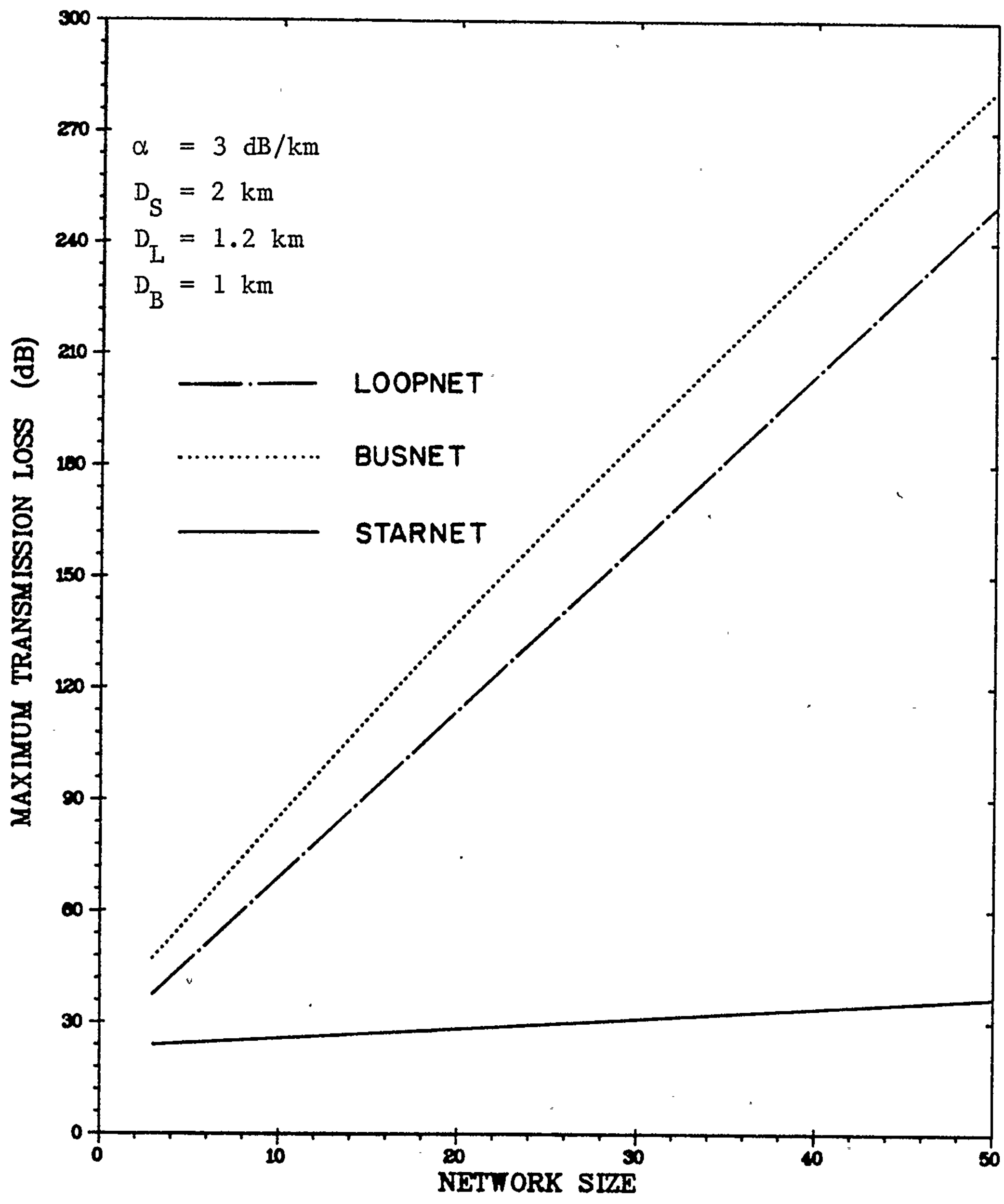

Fig. 4.10 (b) Maximum Transmission Loss Versus Network Size

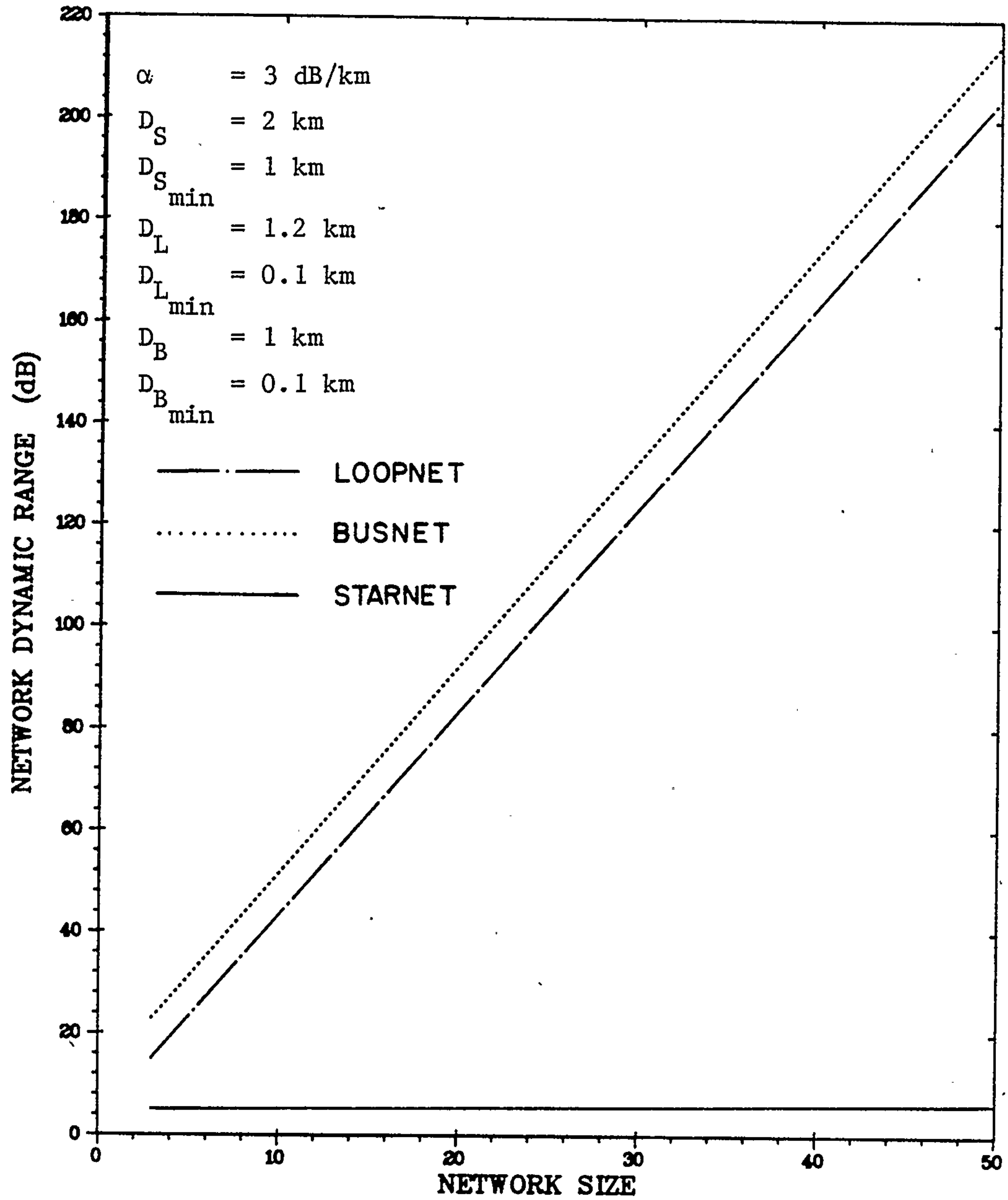

Fig. 4.10 (c) Network Dynamic Range Versus Network size

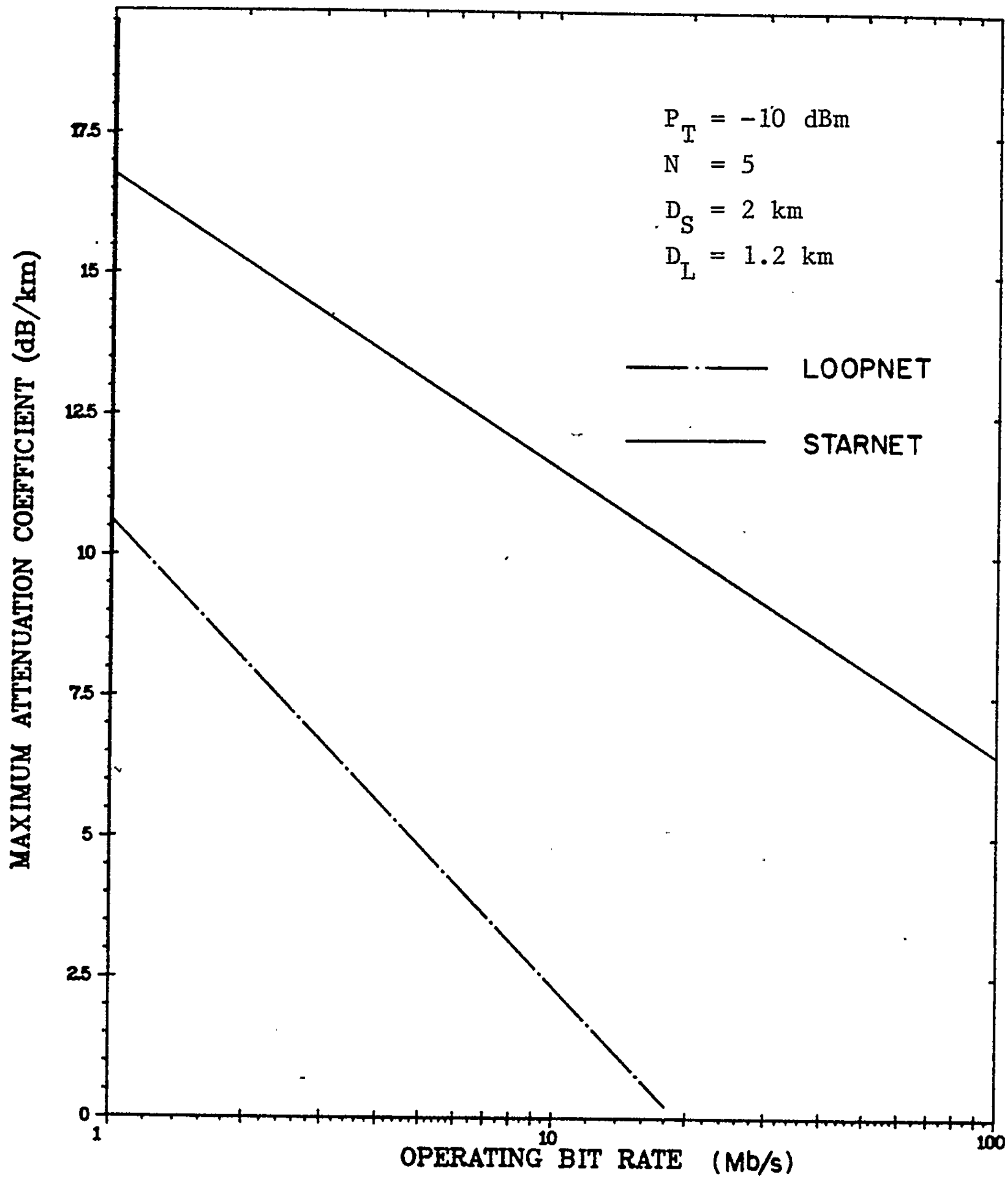

Fig. 4.11 (a) Maximum Attenuation Coefficient Versus Operating Bit rate

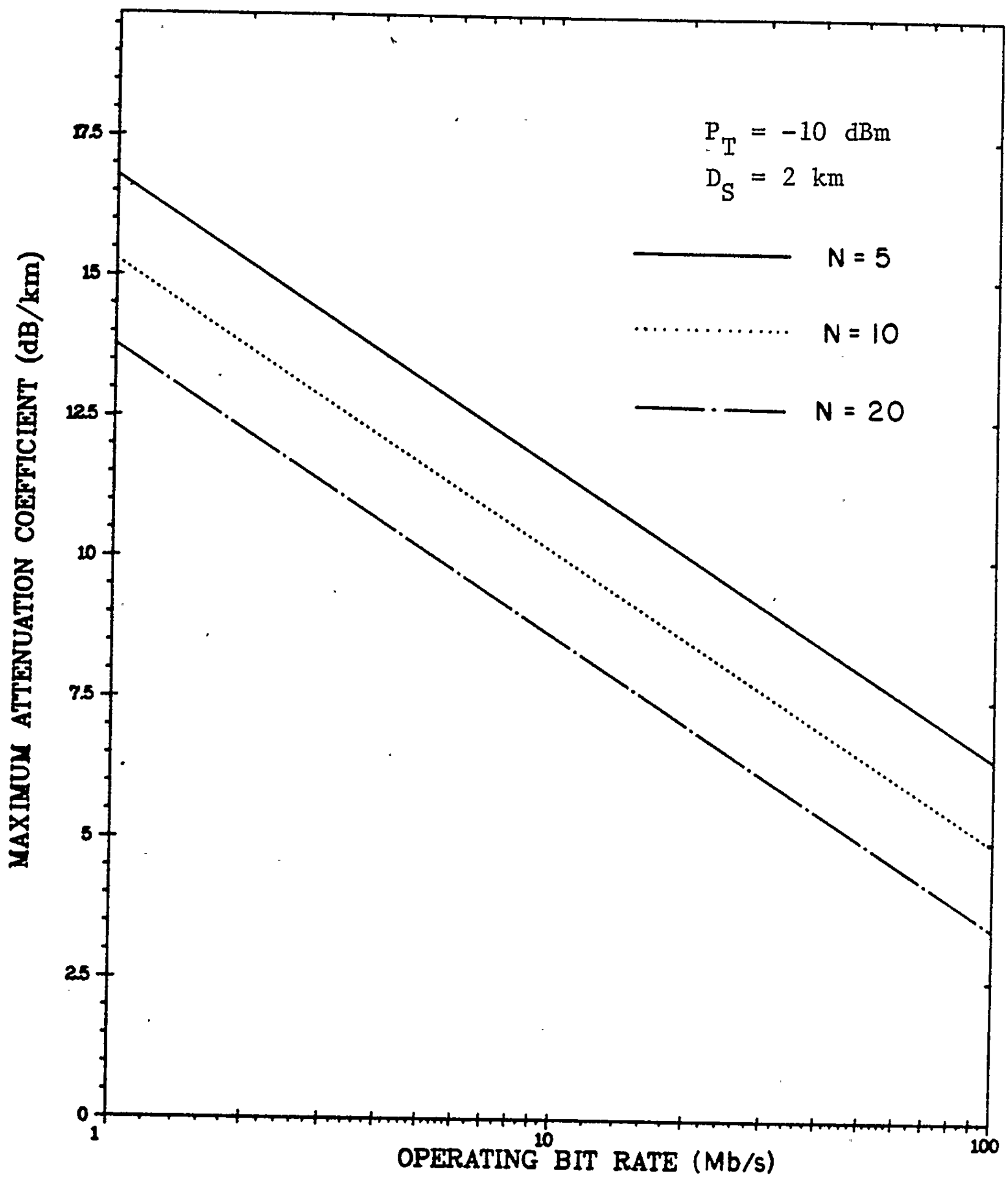

Fig. 4.11 (b) Variation of the Maximum Attenuation Coefficient with Operating Bit Rate for STARNET

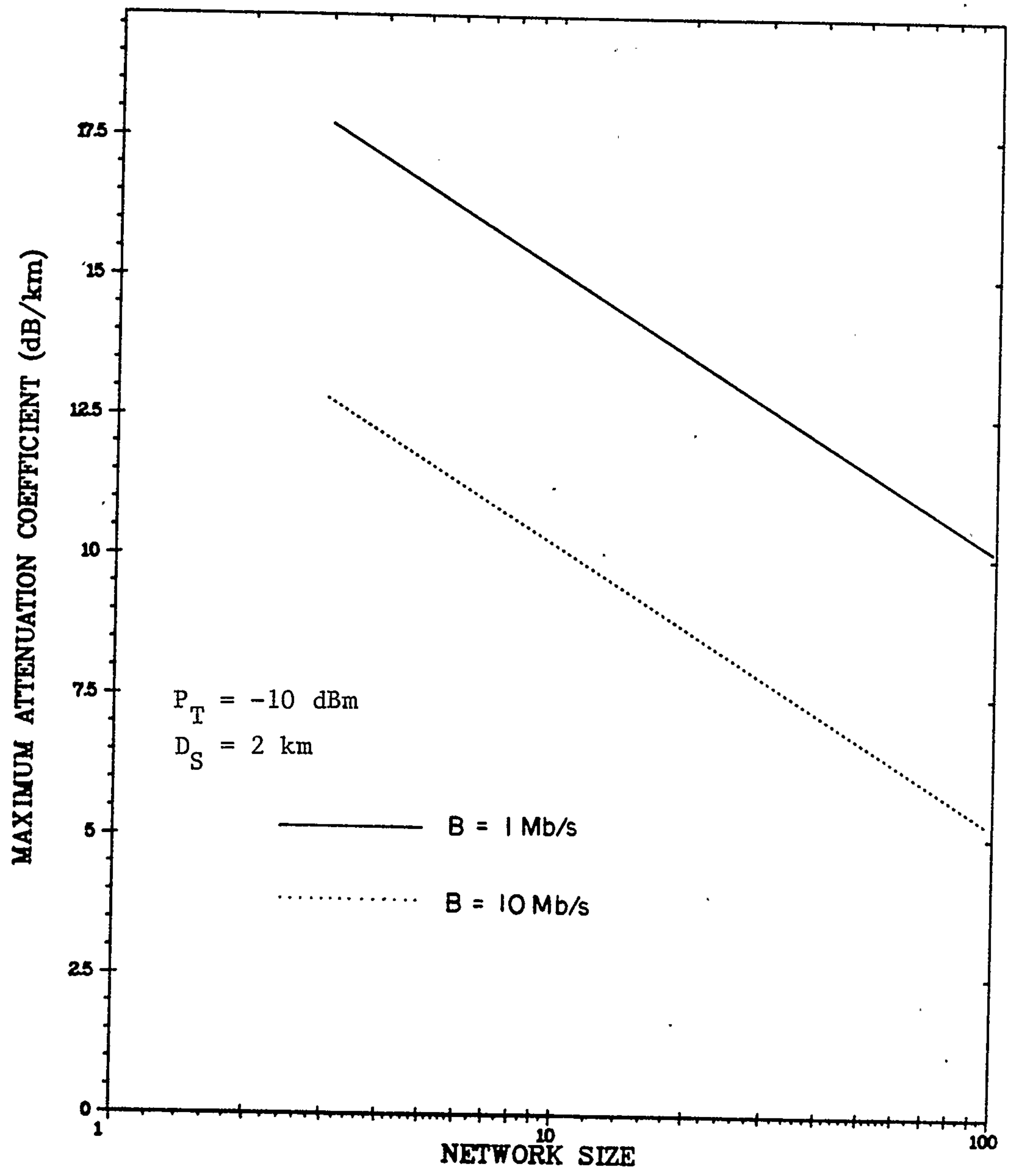

Fig. 4.11 (c) Variation of the Maximum Attenuation Coefficient with Network size for STARNET

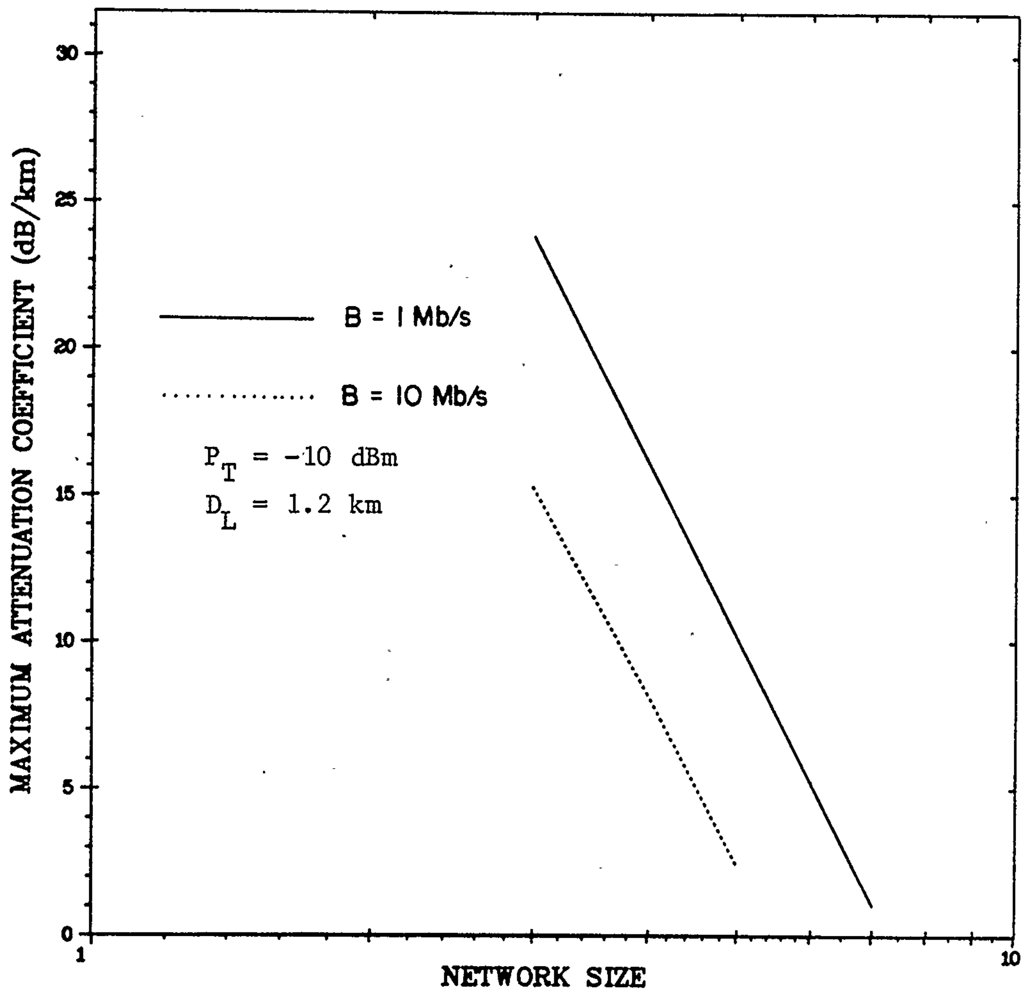

Fig. 4.11 (d) Variation of the Maximum Attenuation Coefficient with Network size for LOOPNET

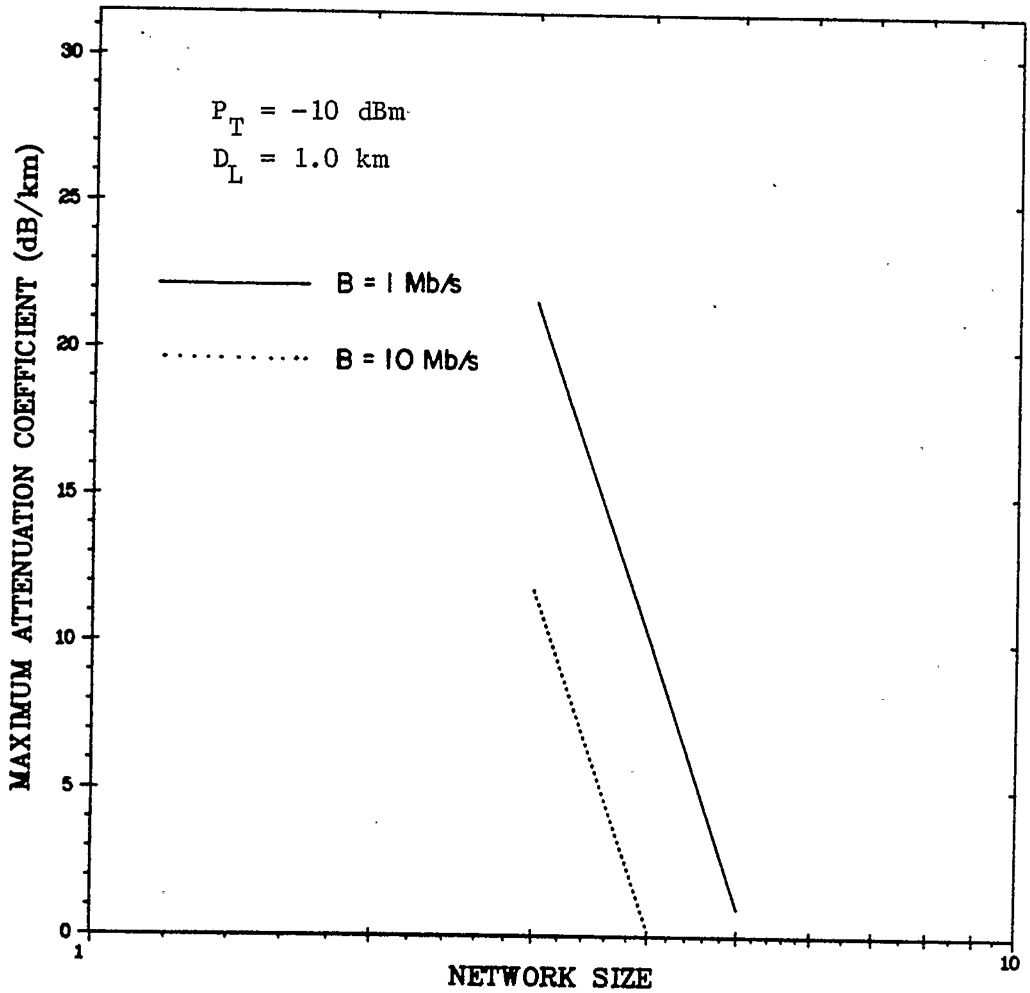

Fig. 4.11 (e) Variation of the Maximum Attenuation Coefficient with Network size for BUSNET

value of the operating bit rate, any fiber which has a loss coefficient from zero up to the corresponding point on the curve for a given network topology can be chosen for network interconnection. For the two topologies shown, the range of possible selection for the fiber attenuation coefficient decreases with increasing operating bit rate, this being due to the reduction in the receiver sensitivity as the bit rate increases, which in effect reduces the network power budget. It is also observed that in the operating bit range from 1 *Mbit/sec* to approximately 10 *Mbits/sec*, the LOOPNET requires higher quality fibers than the STARNET. The explanation for this is due to the fact that the power difference between P_B and $(L_{\max}^{TRX} + L_M)$ (from Equation (3.4)) for the LOOPNET over this operating bit range is smaller than the corresponding value for the STARNET. The results of two additional investigations reveal that at a fixed operating bit rate, higher quality fibers are required for network interconnections as the network size increases (Figure 4.11b). For a fixed network size, higher quality fibers are also required as the operating bit rate is increased (Figure 4.11c for the STARNET, Figure 4.11d for the LOOPNET and Figure 4.11e for the BUSNET).

4.5.3.4. Network Bandwidth Capability

Figures 4.12(a-f) show several families of curves which illustrate the variation of the network bandwidth capability with the distance between the two furthest nodes in a given network topology. Each curve is the resultant of two superimposed curves: one curve is drawn on the basis that the fiber bandwidth-length product is length dependent while the other is drawn based on the fact that the receiver sensitivity is a function of bandwidth. The criterion for choosing the network bandwidth capability is founded on a consideration of all combinations of bandwidth and distance that lie between the appropriate limiting curves and the axes of the coordinate system and the greater this bandwidth-length area, the larger the bandwidth capability of the network. From Figures 4.12(a-f), the following conclusions can be drawn:

(i) the STARNET has a larger bandwidth capability than either the LOOPNET or BUSNET (Figure 4.12a)

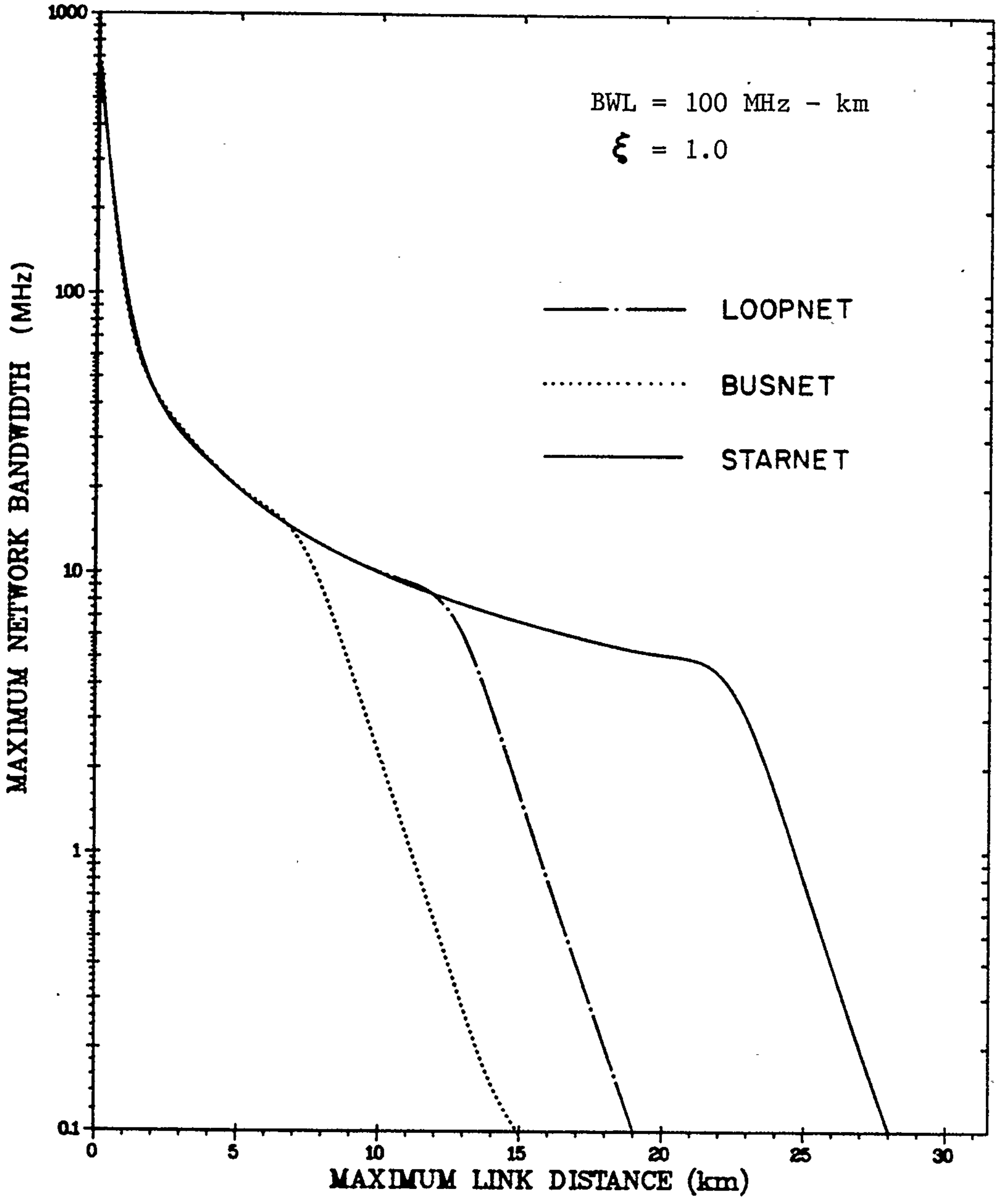

Fig. 4.12 (a) Maximum Network Bandwidth Versus Maximum Link Distance for α = 3 dB/km and N = 6

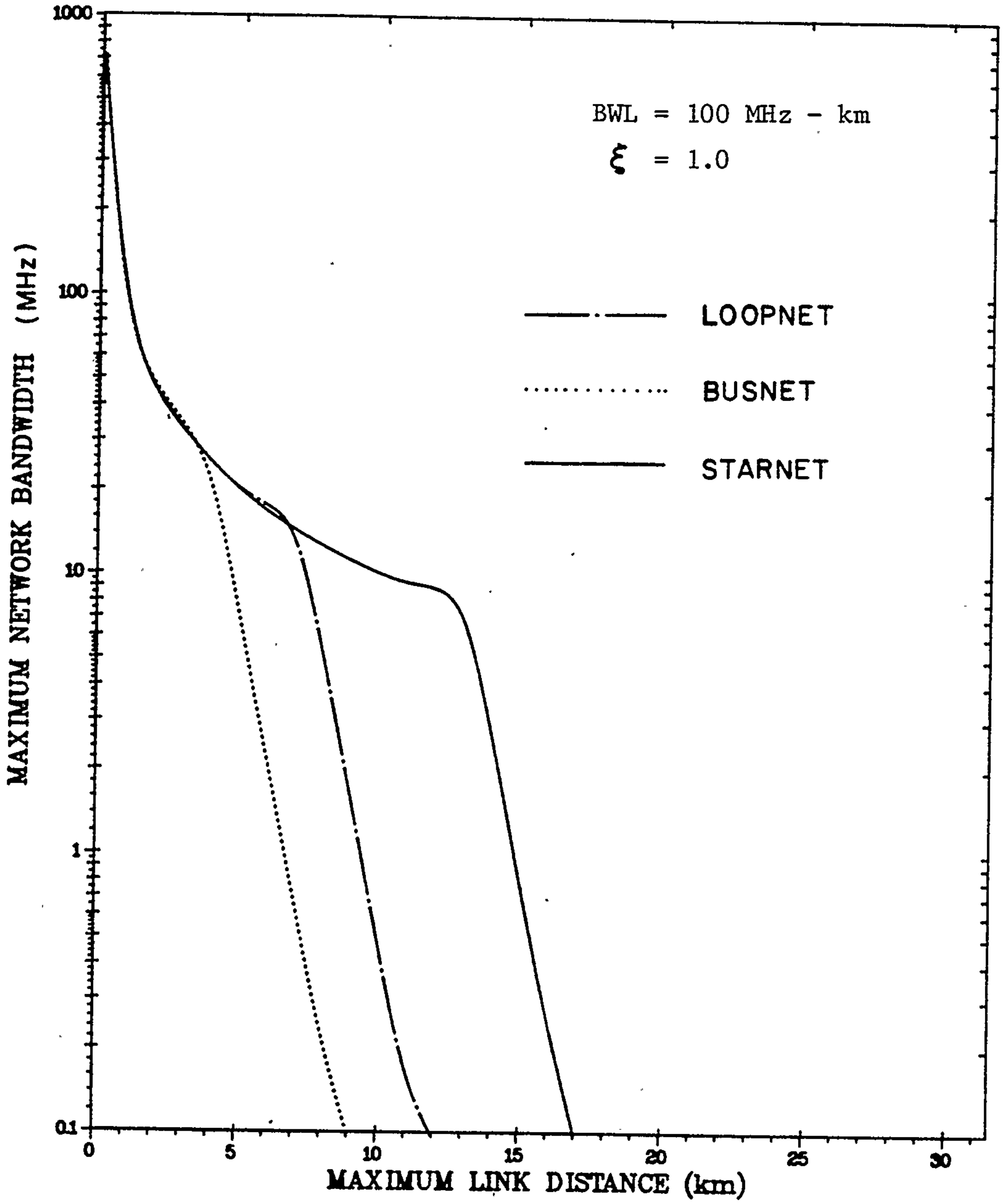

Fig. 4.12 (b) Maximum Network Bandwidth Versus Maximum Link Distance for α = 5 dB/km and N = 6

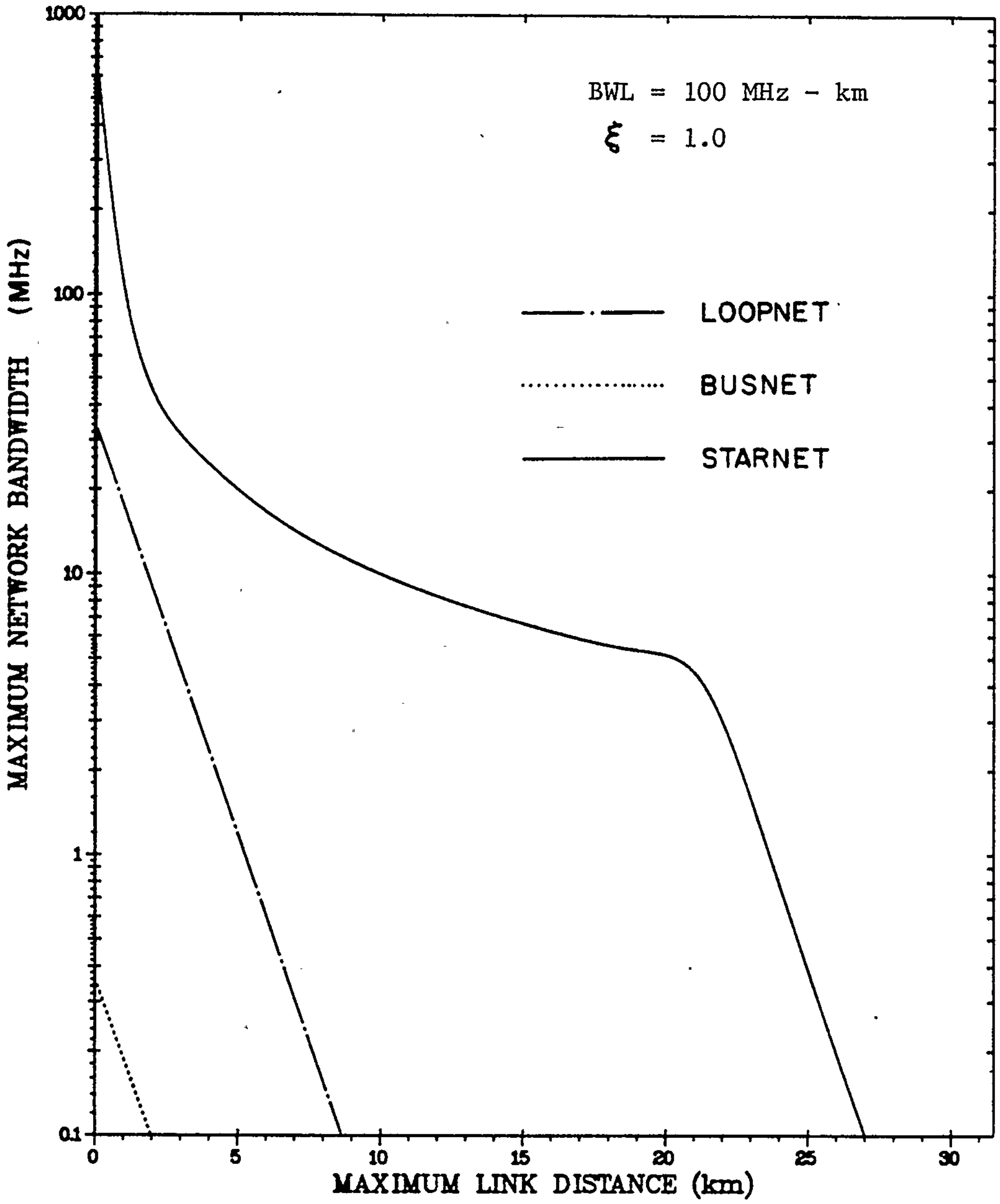

Fig. 4.12 (c) Maximum Network Bandwidth Versus Maximum Link Distance for α = 3 dB/km and N = 12

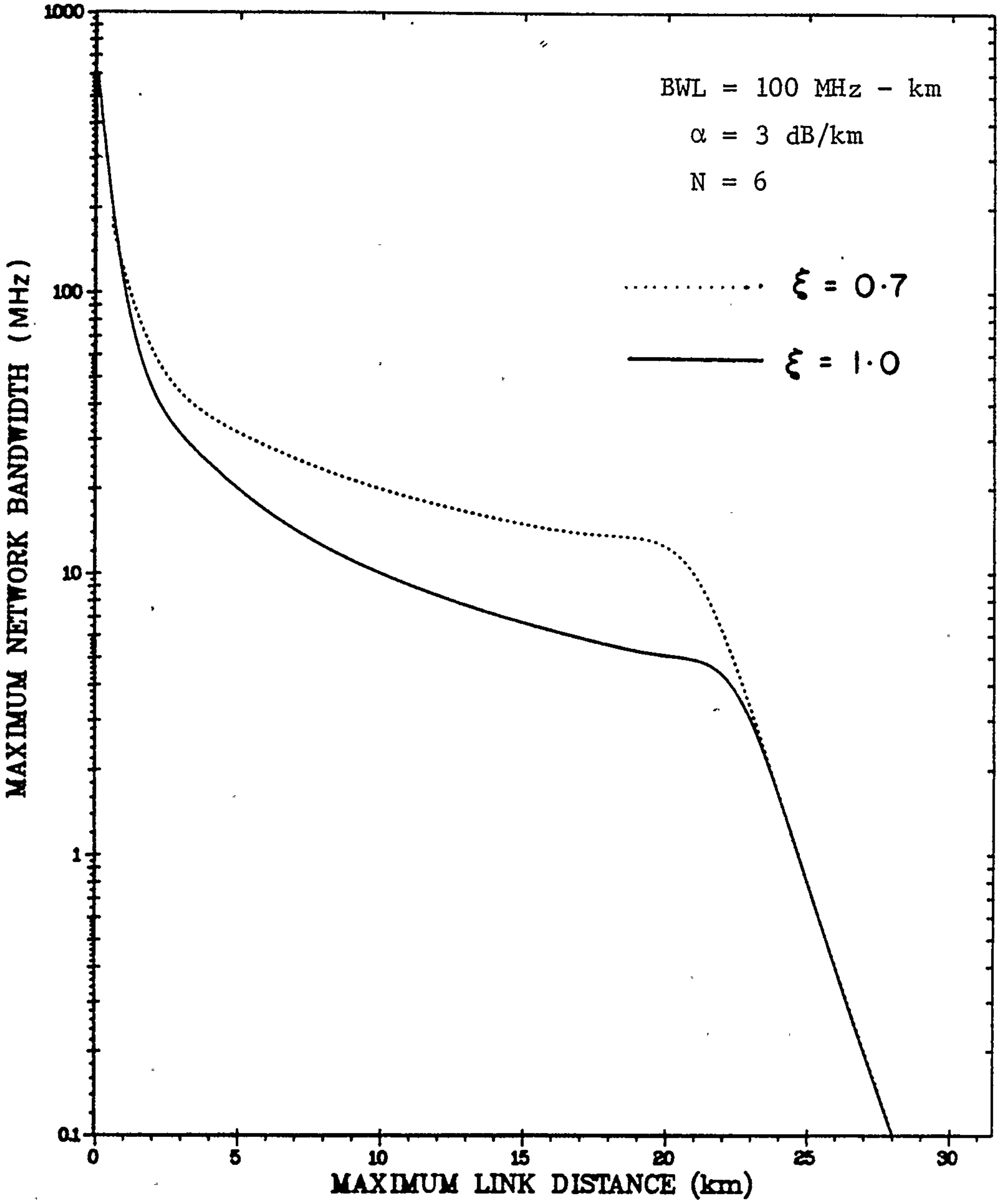

Fig. 4.12 (d) Effect of Bandwidth Length dependence factor on Maximum Network Bandwidth for STARNET

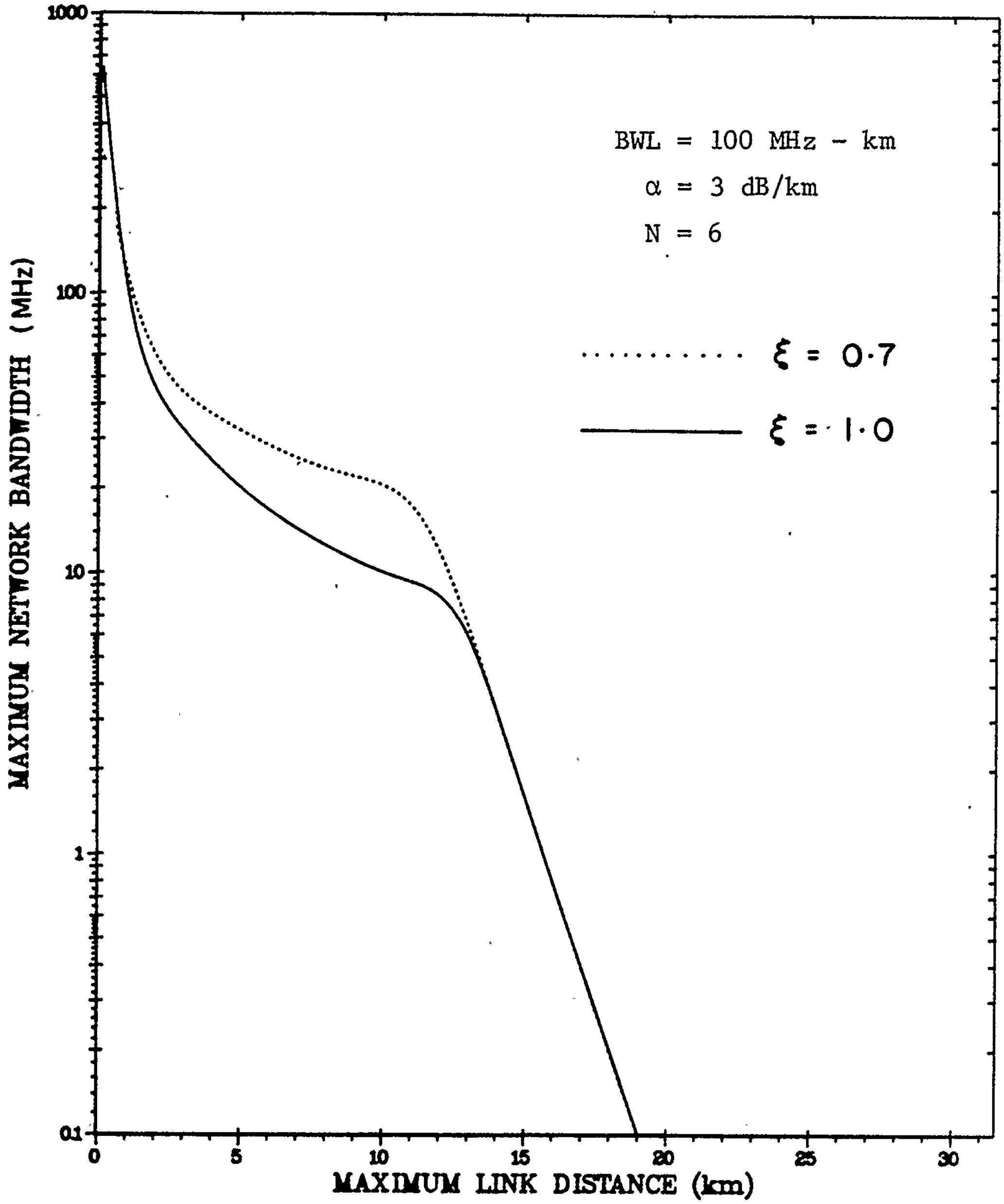

Fig. 4.12 (e) Effect of Bandwidth Length dependence factor on Maximum Network Bandwidth for LOOPNET

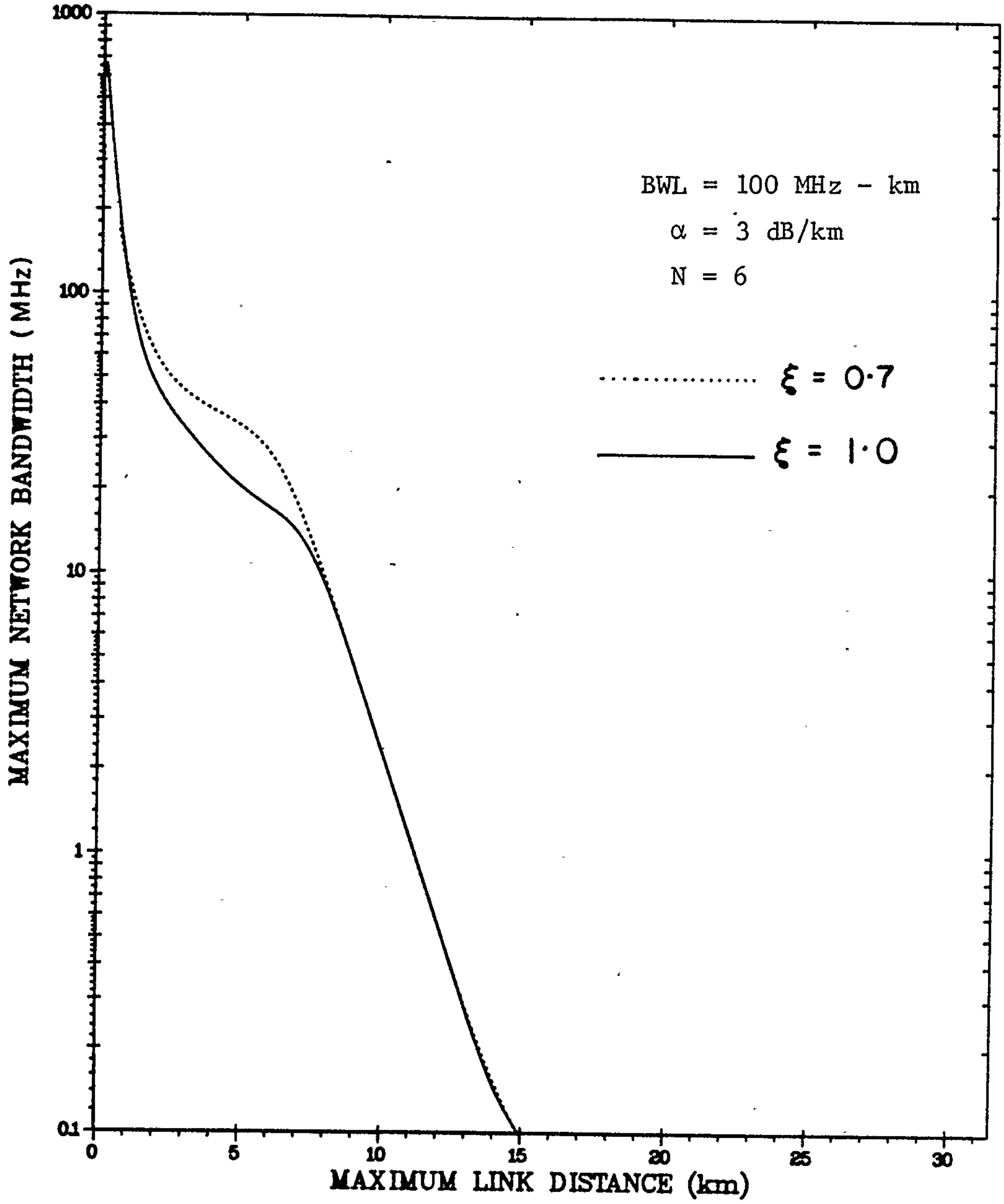

Fig. 4.12 (f) Effect of Bandwidth Length dependence factor on Maximum Network Bandwidth for BUSNET

(ii) increasing the fiber attenuation coefficient while the network size remains constant results in the reduction of bandwidth capability (Figure 4.12b). The same trend is obtained for the case when the attenuation coefficient is constant while the network size is increased (Figure 4.12c)

(iii) the effect of reducing the bandwidth length dependence factor also causes an increase in the bandwidth capability (Figures 4.12(d-f)).

4.5.3.5. Basic Performance Parameters for the 6-node Network

The computed path lengths for the network topologies are shown in Table 4.5 and it is seen that the STARNET requires the greatest fiber length and BUSNET the least.

The calculated ideal optical receiver sensitivity (using a SiAPD detector and a TZ amplifier front-end) is -72.7 *dBm* at an operating bit rate of 1 *Mb/sec*. With a high power LED source coupling −4 *dBm* of optical power into the fiber, the system power budget is therefore 68.7 *dB*. By making use of the specified parameters in Tables 4.4(a-d) and also using a fiber with a loss coefficient of 1.5 *dB/km* for network interconnection, the network loss (transmission loss) and the dynamic range computed for each POFLAN topology are as shown in Table 4.5. It is obvious from Table 4.5 that all the network topologies satisfy the attenuation criterion, the STARNET suffering the lowest transmission loss and the BUSNET the highest.

In terms of the network dynamic range requirement, it is clear that the STARNET is superior to the other network topologies while the BUSNET requires the highest dynamic range.

The STARNET also exhibits a superior performance over the other network topologies with respect to the bandwidth capability criterion. It is important to mention in passing that the optical bandwidths evaluated for all the network topologies are dispersion limited, that is, they are computed from the manufacturer specified fiber bandwidth-length product (100 *MHz− km*) and the maximum link distance of each network topology (2.6 *km* for the STARNET, 6.6 *km* for the LOOPNET and 5.9 *km* for the BUSNET). The bandwidth capability of the BUSNET is higher than

TOPOLOGY	NETWORK PATH (km)	NETWORK LOSS (dB)	DYNAMIC RANGE (dB)	BANDWIDTH (MHz)
LOOPNET	7.5	55.6	32.3	15.2
BUSNET	5.9	68.0	39.6	16.9
STARNET	11.5	21.8	4.6	37.7

Table 4.5 Basic Performance Parameters for the 6-node Network example.

that for the LOOPNET because the maximum link distance in the BUSNET is lower than the corresponding value in the LOOPNET.

4.5.3.6. Network Throughput

The normalized network throughput is determined by the number of successful transmissions (during a simulation run) multiplied by the average packet transmission time (in milliseconds), divided by the simulation run time (also in milliseconds). The variation of the network throughput with the normalized offered load is shown in Figure 4.13a and it is evident from this figure that the network throughput is virtually identical for all the network topologies under low traffic conditions (from 1 to about 50%) where in this range the network throughput is approximately equal to the offered load (ideal situation). Under heavy traffic, the topologies exhibit differing performances and it is seen from Figure 4.13a that the STARNET has the highest throughput (approximately 96%) while the BUSNET and LOOPNET can be operated at about 90% of the optical channel capacity. The disparity in performance is explained by the propagation delay associated with each network topology and in this example, the computed round-trip propagation delays of the 6-node STARNET, BUSNET and LOOPNET are 26 μsec, 59 μsec, and 66 μsec respectively. Clearly, under the same loading condition for all topologies, the STARNET has the smallest collision detection window thus making collisions detectable more quickly and thereby reducing the wasted time spent transmitting the colliding packets, thus leading to higher network throughput. An alternative explanation follows from the theoretical analysis of the 1-persistent CSMA/CD protocol. Stalling has shown that the network throughput of a LAN operating under the CSMA/CD protocol is inversely proportional to the normalized propagation delay parameter [22]. This statement implies that a low value of end-to-end propagation delay or high mean packet transmission time will result in high network throughput. The curves shown in Figure 4.13a also indicate that under heavy network traffic, (>100%), the maximum throughput attained by all the network topologies deviate from the ideal throughput value of unity, this deterioration being expected since under the high loading conditions, there is an increased number of collisions. The advantage of the 1-persistent CSMA/CD

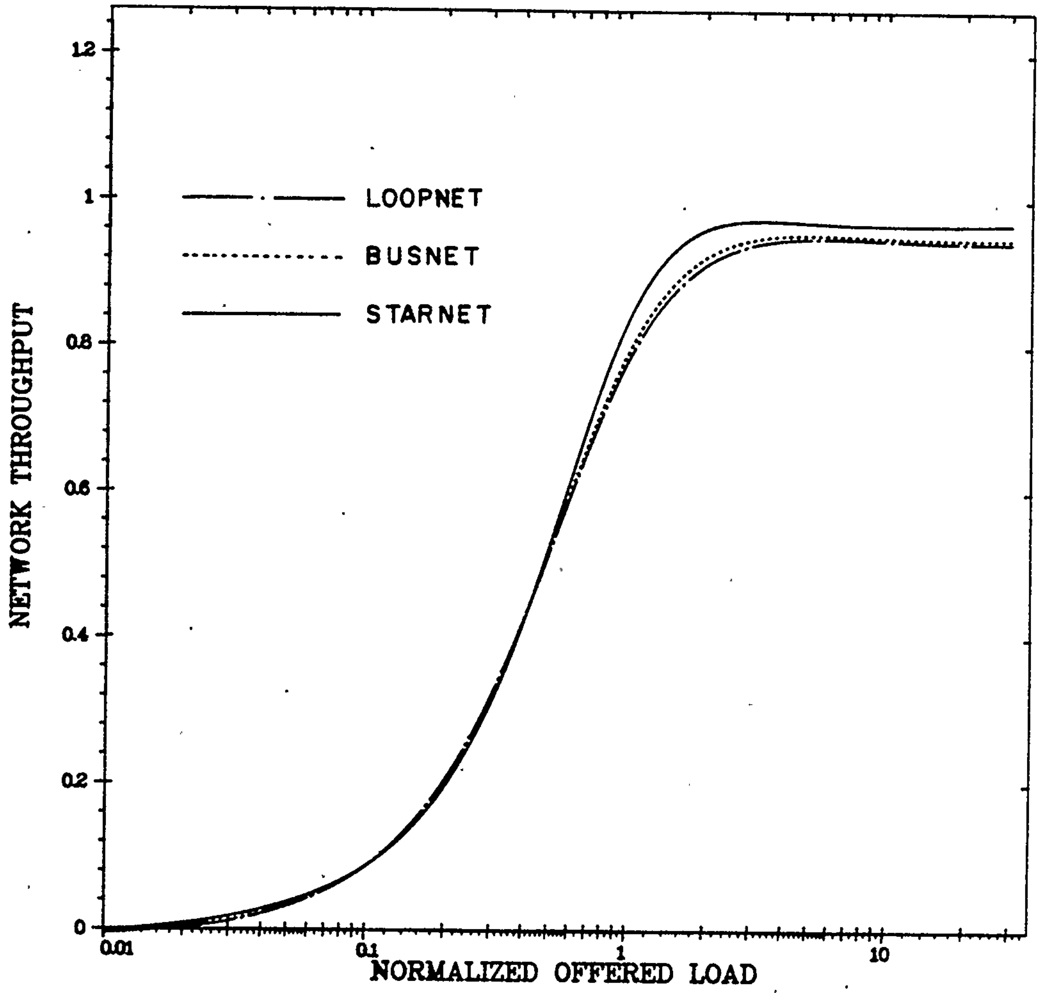

Fig. 4.13 (a) Network Throughput Versus Offered Load for B = 1 Mb/s, $\frac{1}{\mu}$ = 2000 bits

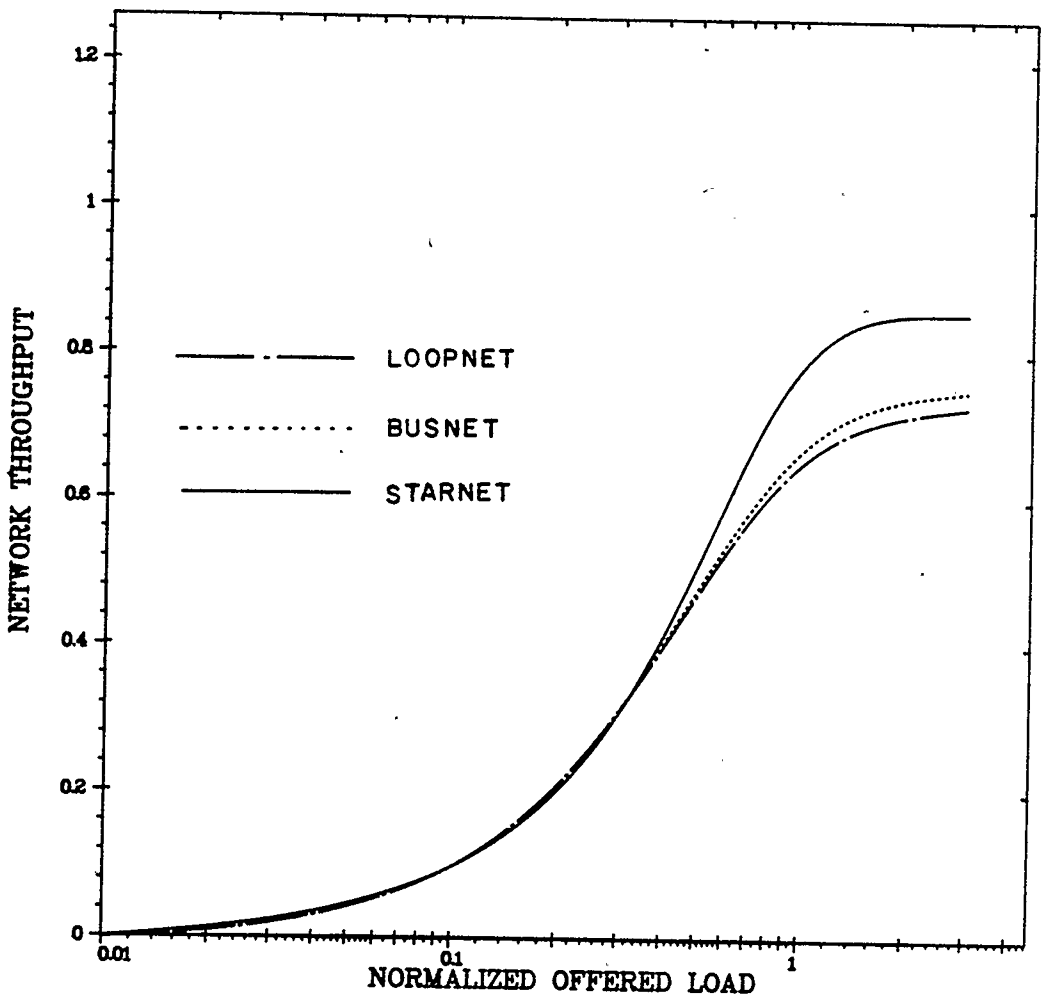

Fig. 4.13 (b) Network Throughput Versus Offered Load for $B = 10$ Mb/s, $\frac{1}{\mu} = 2000$ bits

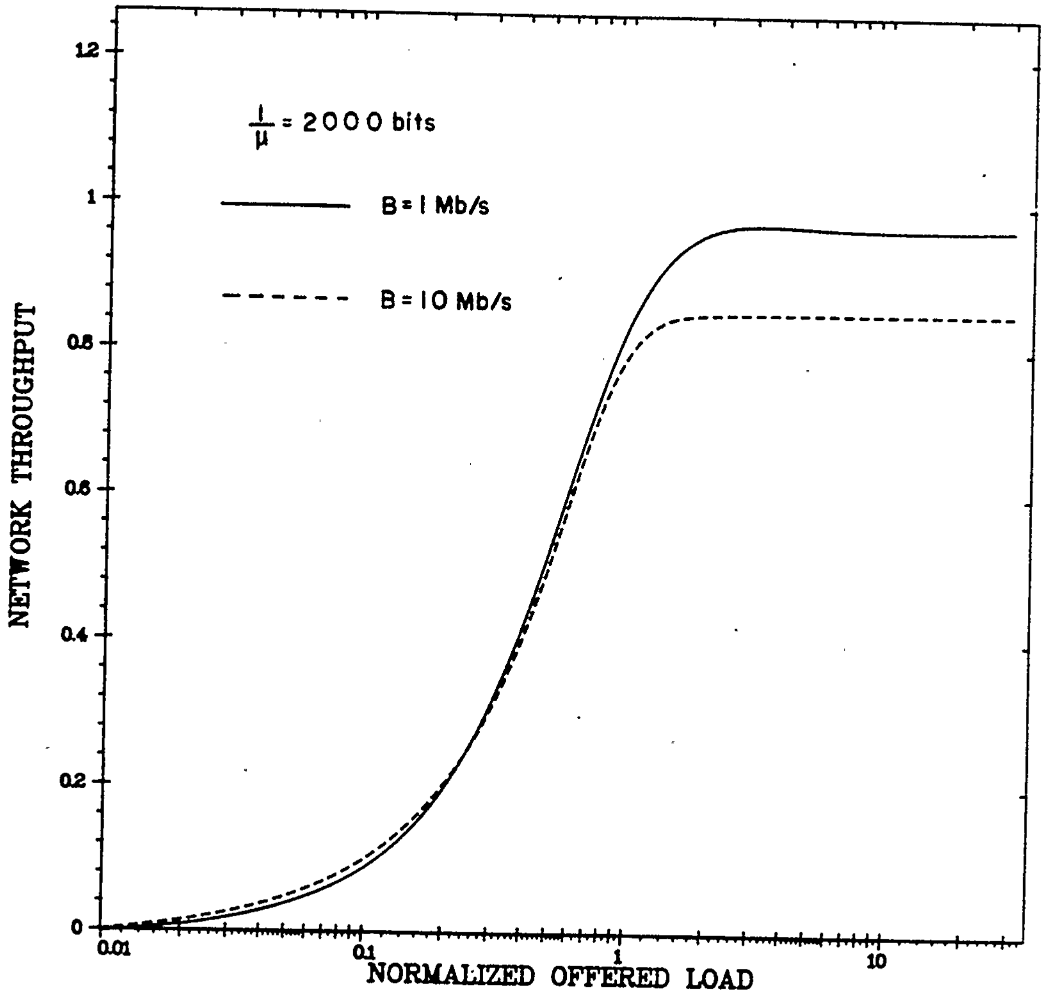

Fig. 4.13 (c) Effect of varying the channel capacity on Network Throughput for STARNET

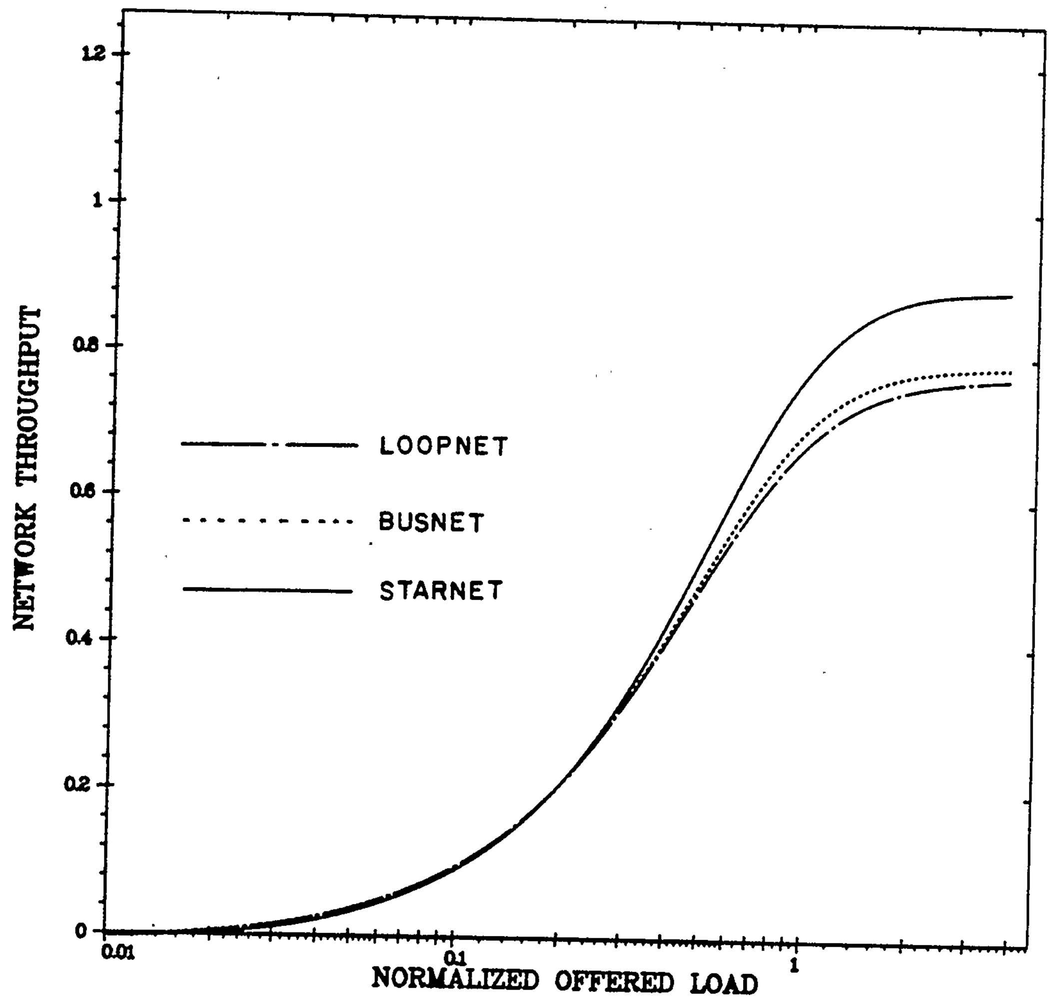

Fig. 4.13 (d) Network Throughput Versus Offered Load for B = 10 Mb/s, $\frac{1}{\mu}$ = 256 bits

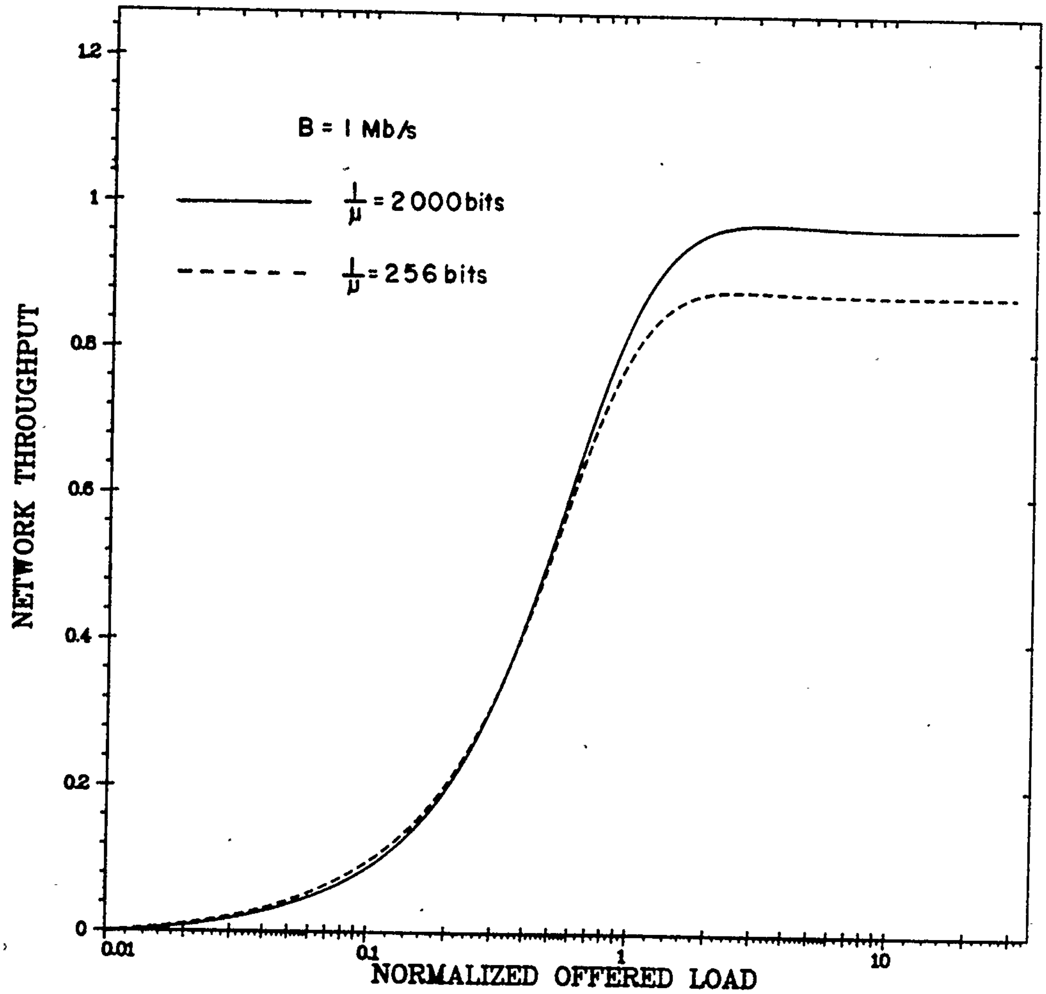

Fig. 4.13 (e) Effect of varying the mean packet length on Network Throughput for STARNET

protocol using the binary exponential backoff is that the topologies maintain an approximately constant throughput over a wide range of high traffic. Although not shown, (due to the large computer storage requirements and high processing run times for high traffic simulations), it is known that under exceptionally high traffic, the network throughput will drop to zero.

The variation of the network throughput with an increase in channel capacity (mean packet length being constant) demonstrates that under low network traffic, the change in network throughput for the different topologies is insignificant whereas under high traffic, there is seen to be a marked difference (Figure 4.13b). It is also evident from this figure that at a channel capacity of 10 *Mbit/sec*, the STARNET can achieve a maximum throughput of about 88% while the BUSNET and LOOPNET attain maximum throughputs of 74 and 76% respectively. From the theoretical explanation given above, the increase in the channel capacity results in a decrease in the mean packet transmission time which increases the normalized delay parameter and thus leads to a decrease in the network throughput. The network throughput for different channel capacities for the STARNET is shown in Figure 4.13c.

The result of a further investigation shows that the effect of lowering the mean packet length (at constant channel capacity) also yields a declining network throughput under high traffic (Figure 4.13d), this resulting from the decrease in the mean packet transmission time. A comparison of the network throughput for the STARNET for mean packet lengths of 2000 bits and 256 bits is shown in Figure 4.13e.

4.5.3.7. Average Packet Delay

The average packet delay consists of the queueing delay, the retransmission delay and the transmission time of the transmitted packets. From Figure 4.14a, it is seen that under low to medium traffic, the mean packet delay is approximately equal to the mean packet transmission time of 2 milliseconds, this being a result of the small queueing delay as most of the packets are transmitted as soon as they arrive into the network, and in addition, the retransmission delay is minimum because of the very small number of collisions since most of the packets are successfully transmitted in their first transmission attempt. Beyond the offered load of 50%, the mean packet delay is seen to increase very rapidly for all the topologies and two reasons can be adduced for this: first, the packet queueing delay that results from an increased number of collisions under heavy load conditions is rapidly increasing; second and also important is the increase in the retransmission delay due to the increased number of collisions. As mentioned in Chapter Three, the retransmission delay selected using the IEEE BEB algorithm is a function of the number of collisions experienced by the colliding packets and hence, as the number of collisions increases, the retransmission delay increases. It is observed from a tracing of the simulation outputs that a number of the network nodes are blocked out for some time (due to high retransmission delay) while other nodes capture the optical channel during this interval. It is evident from Figure 4.14a that all the network topologies have the same mean packet delay under low to medium traffic, however, under heavy traffic conditions, the packets transmitted in the STARNET experience the least delay while those that are transmitted on the LOOPNET have the greatest delay. The obvious reason for this difference is the propagation delays of these topologies. As previously discussed, the retransmission delay computed using the IEEE BEB algorithm is an integral multiple of the propagation delay, therefore, under high load when collisions become excessive, the rescheduled packets in the STARNET will experience the least retransmission delay because of its small propagation delay.

Increasing the channel capacity from 1 *Mbit/sec* to 10 *Mbits/sec* (at constant mean packet length) results in a high mean packet delay under heavy traffic conditions (Figure 4.14b) thus at a bit rate of 10 *Mbits/sec* and a mean packet length of 2000 *bits*, the mean packet transmission time is 0.2 *milliseconds*. This value of the mean transmission time under high traffic increases the frequency of transmissions which leads to an increased number of collisions. The consequent need for retransmissions thus causes the mean packet transfer delay to grow and it is seen from Figure 4.14c that the mean packet delay experienced by packets which are transmitted in the STARNET

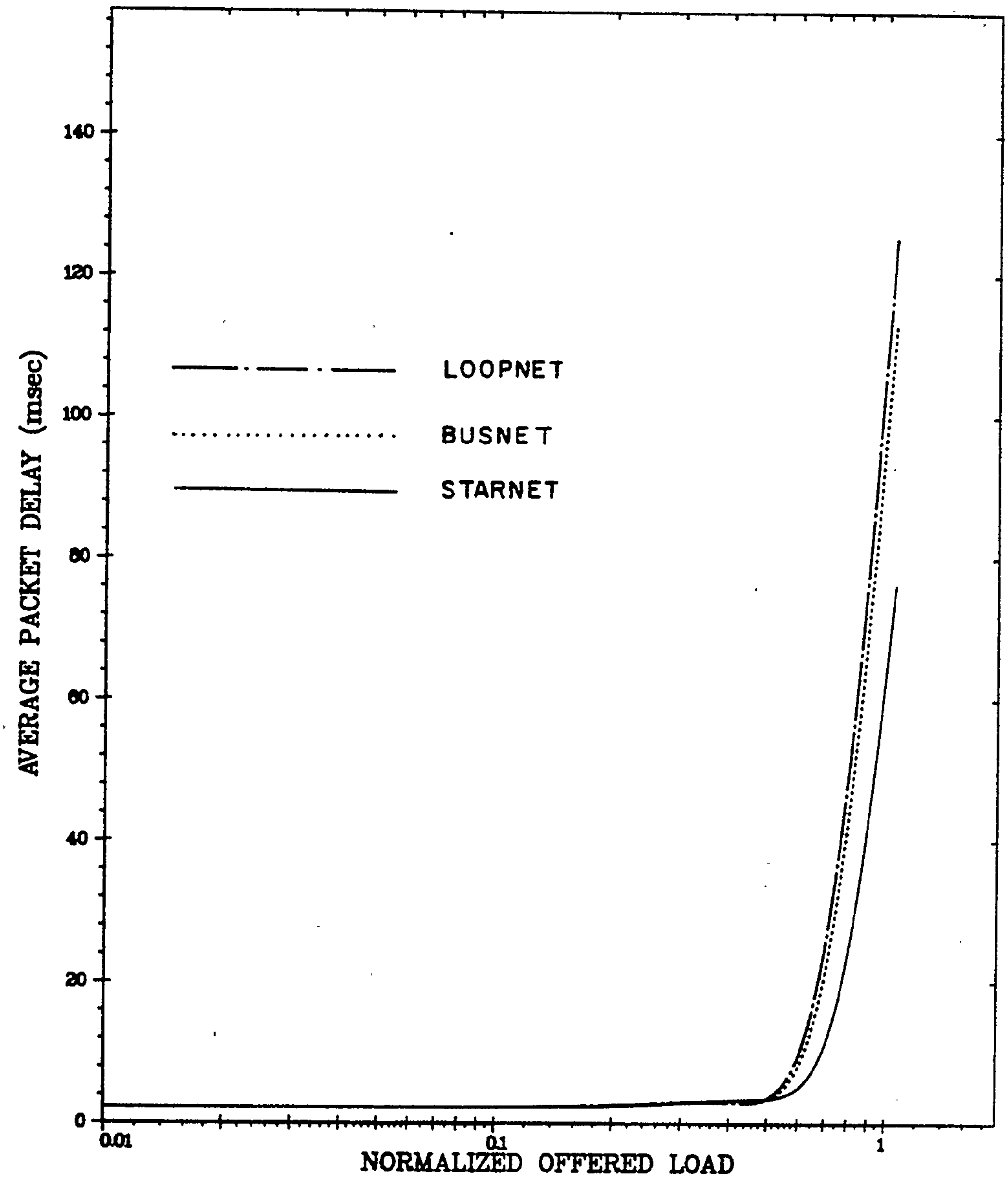

Fig. 4.14 (a) Average Packet Delay Versus Offered Load for B = 1 Mb/s, $\frac{1}{\mu}$ = 2000 bits

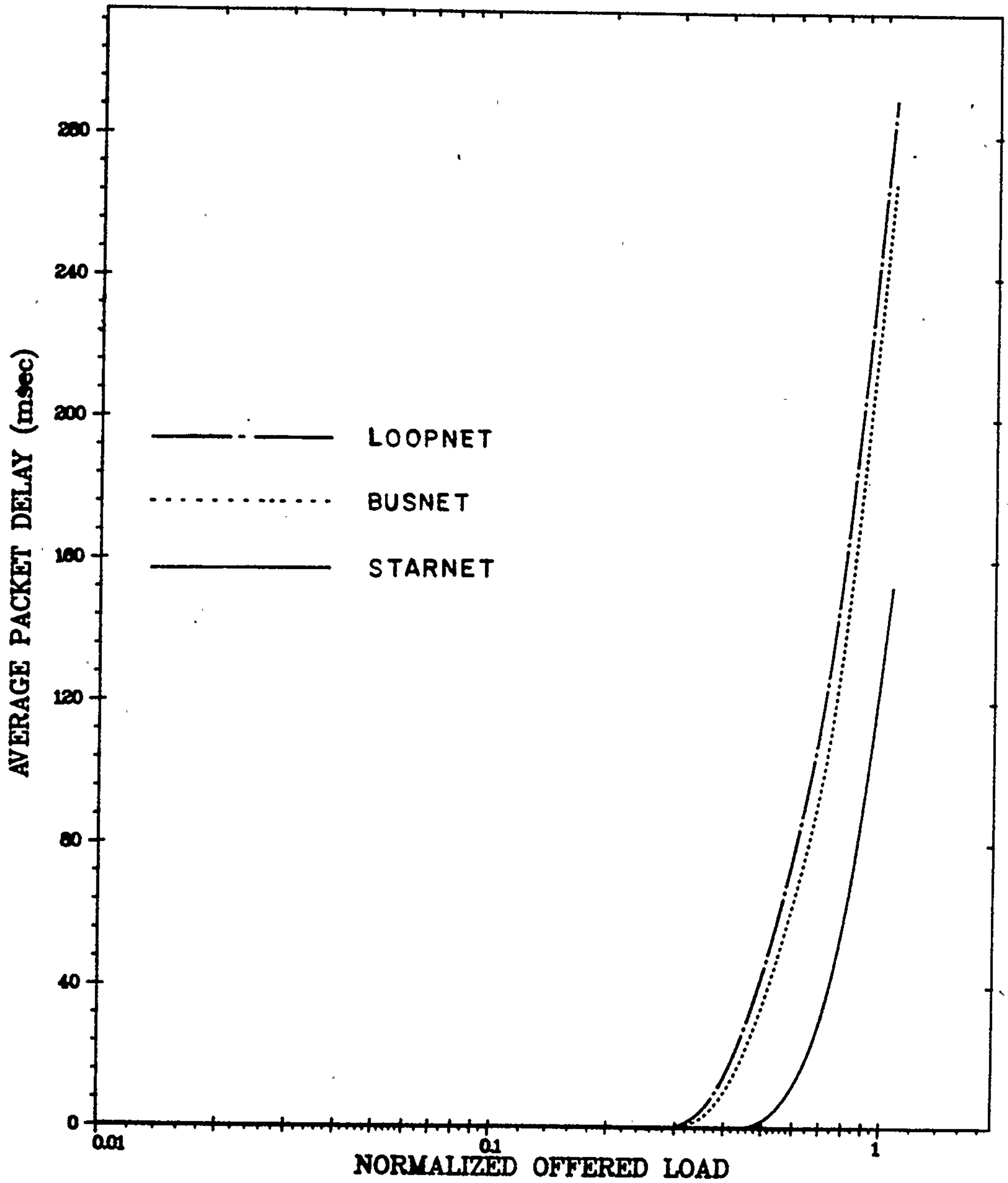

Fig. 4.14 (b) Average Packet Delay Versus Offered Load for B = 10 Mb/s, $\frac{1}{\mu}$ = 2000 bits

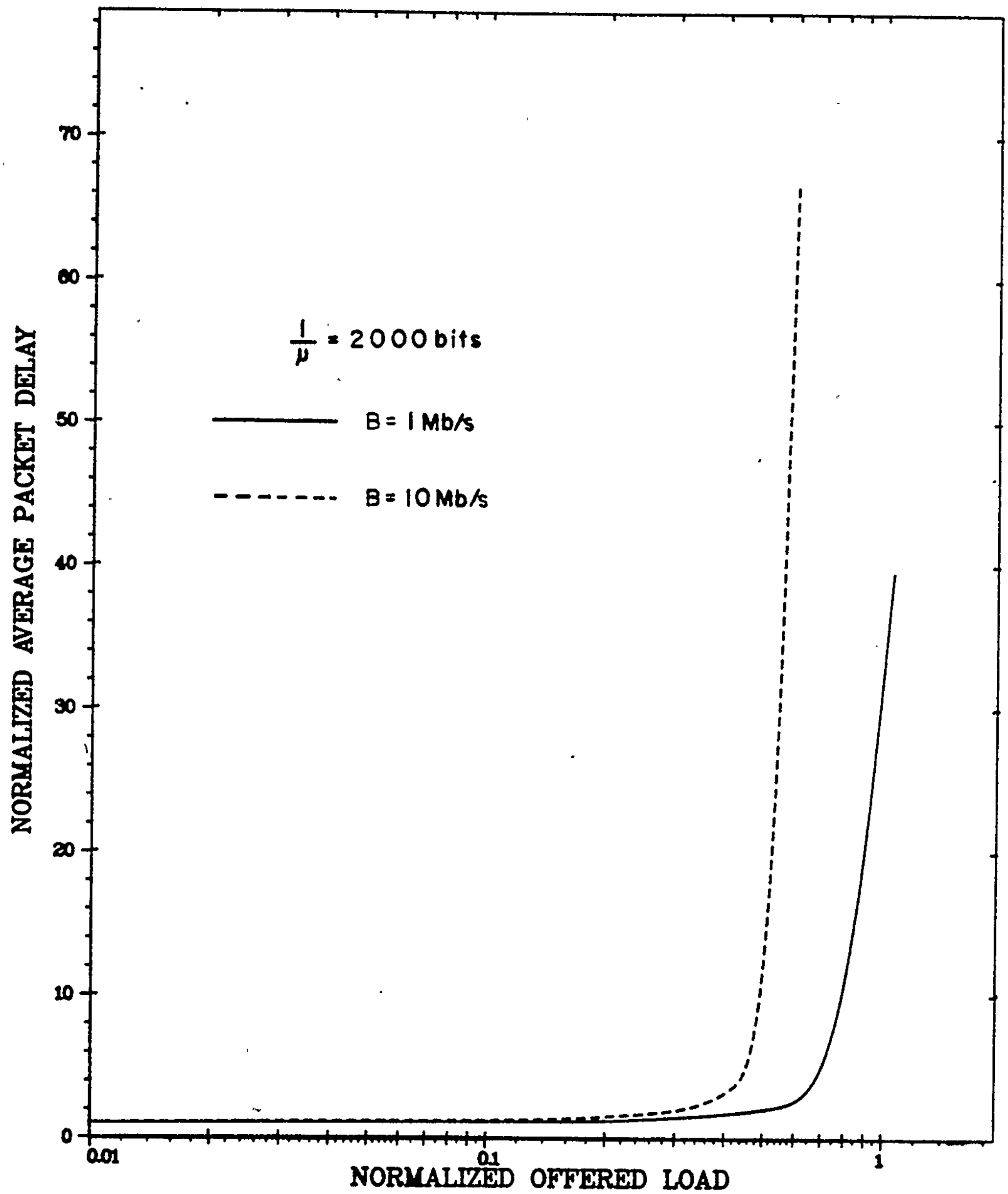

Fig. 4.14 (c) Effect of varying the channel capacity on average normalized packet delay for STARNET

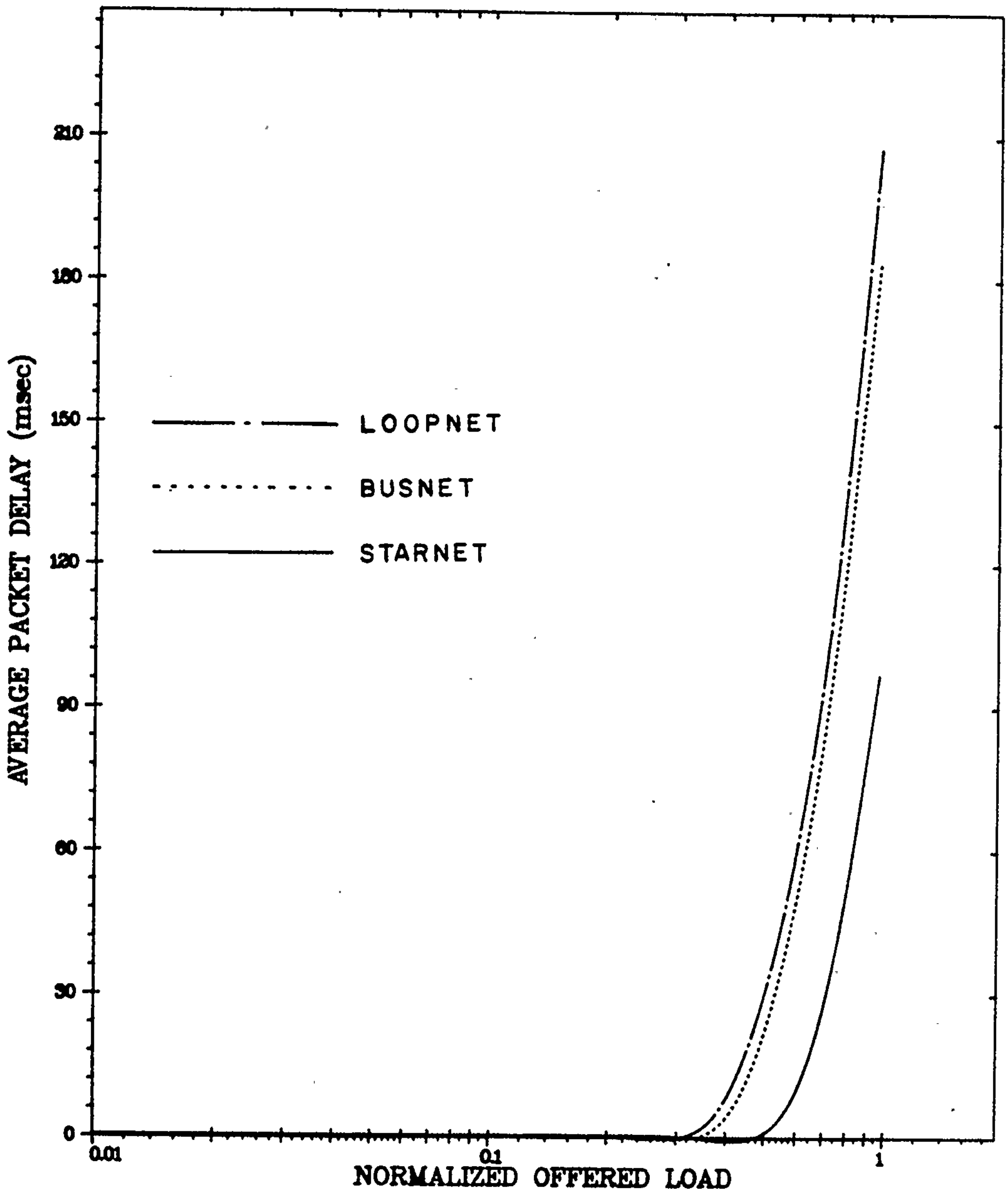

Fig. 4.14 (d) Average Packet Delay Versus offered load for B = 1 Mb/s, $\frac{1}{\mu}$ = 256 bits

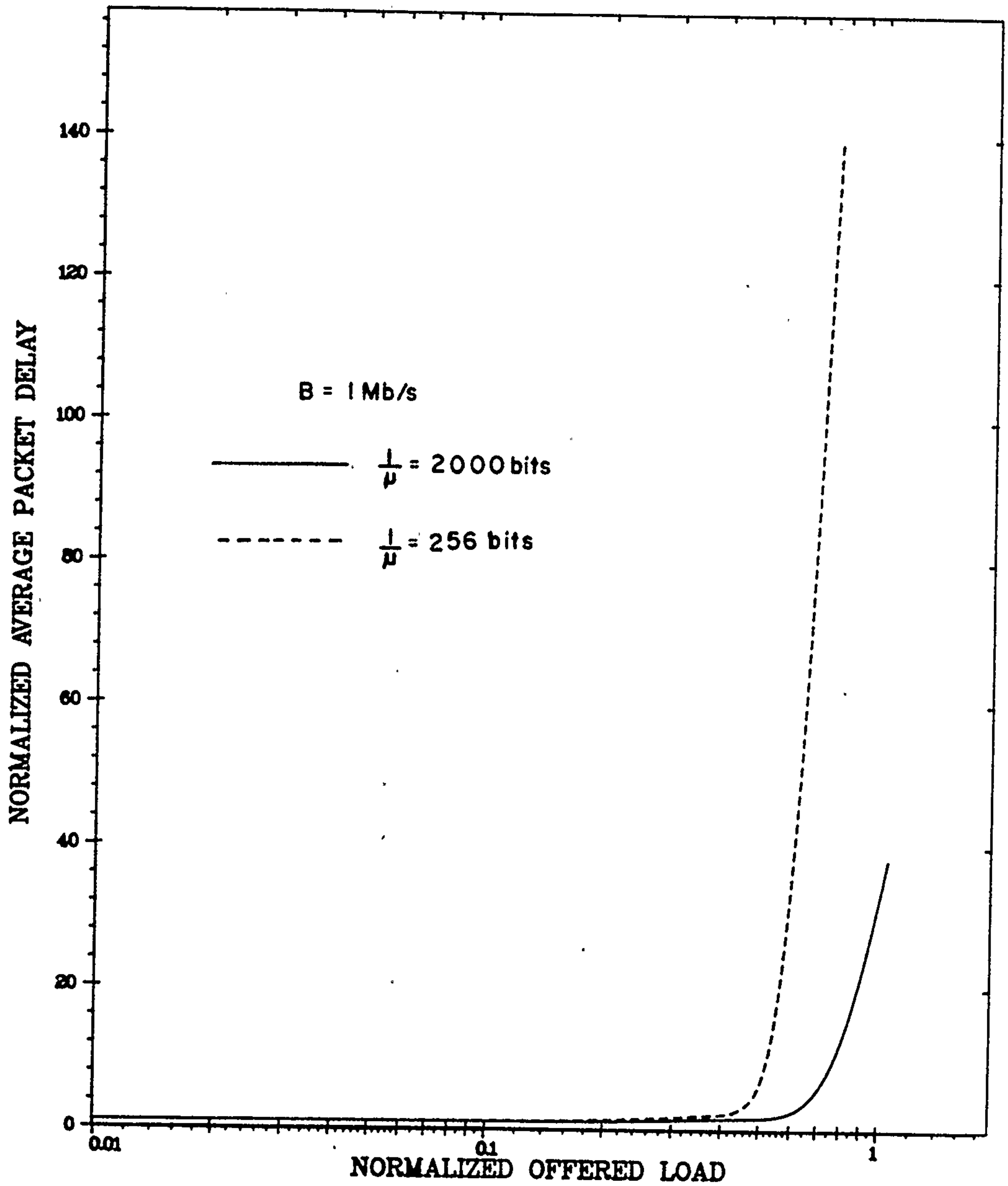

Fig. 4.14 (e) Effect of varying the mean packet length on Normalized Average Packet Delay for STARNET

increases very rapidly from an offered load of about 40% when the channel capacity is 10 *Mbits/sec* compared to 65% when the channel capacity is 1 *Mbit/sec*. Figures 4.14(d-e) show that for a small mean packet length under heavy traffic conditions (at constant channel capacity), a high mean packet delay is obtained since more frequent transmissions due to the smaller packet lengths result in a greater number of collisions thereby causing an increase in the mean packet delay.

Remarks on Network Throughput and Mean Packet Delay

A comparison of Figures 4.13(a-e) with Figures 4.14(a-e) leads to the following remarks: Under low traffic, it is observed that the network throughput follows the ideal behavior and that the mean packet delay is very low, however, under heavy traffic conditions, it is seen that the network throughput deviates from the ideal behavior, and in addition, the mean packet delay becomes excessive. From the network designer's point of view, it is desirable to operate a network in the high throughput range but the results indicate that this range of operation may not be acceptable to the network user because of the excessive delay. A tradeoff between the amount of throughput which can be attained and the allowable mean packet delay must therefore be made. The bottom line is that, for a particular customer application or service requirement, an appropriate choice of an operating offered load which will maximize the throughput and maintain an acceptable packet delay must be chosen.

4.5.3.8. The Effects of Different Backoff Algorithms

Aside from the effect of the normalized propagation delay parameter on the throughput-delay characteristics, another factor which affects networks using the CSMA/CD protocol is the type of backoff algorithm employed for rescheduling the colliding packets. In the simulation examples presented, the IEEE BEB algorithm has been used. This algorithm has the advantage of reducing the total number of collisions and this is achieved primarily by rescheduling all of the colliding packets on the basis of the number of collisions which has previously been encountered by the individual colliding packets. It is evident from the tracing of the simulation outputs that this algorithm introduces a problem in which the packet transmissions from some of the network nodes are blocked as a result of high retransmission delays while some other more fortunate nodes continue to be able to transmit their packets. One solution to the problem requires an algorithm which is not necessarily based on the number of previously experienced collisions. Kleinrock and Tobagi have suggested the selection of the retransmission delay from a uniform probability distribution where the mean retransmission delay is chosen to be very much greater than the mean packet transmission time [35]. The performances of the IEEE BEB algorithm and the uniform backoff algorithm (with a mean retransmission delay of 10 *milliseconds*) are investigated where the network throughput and average packet delay versus offered load characteristics are shown in Figure 4.15a and Figure 4.15b respectively. It is seen that the uniform backoff algorithm yields a lower maximum throughput (66%) compared to about 96% throughput attained by the use of the IEEE BEB algorithm. With the uniform backoff algorithm, there is increased number of collisions especially under very high traffic which in effect lowers the network throughput, however, as observed in the tracing of simulation outputs, the problem of nodal blocking is insignificant. It is also evident from further testruns that the maximum throughput attained using the uniform backoff algorithm can be increased if a higher mean retransmission delay is chosen, but then the mean packet delay becomes excessive. Figure 4.15b shows the superiority of the IEEE BEB algorithm over the uniform backoff algorithm in terms of the mean packet delay.

4.5.3.9. Backlog Clearing Time

The backlog clearing time is a measure of how long it takes each network topology to clear the backlogged packets at all its nodal queues where this measure also provides an insight as to the average queue buildups at all the different nodal queues. Figure 4.16a shows how the topologies respond in clearing the backlogged packets after the entry of new packets into the network is terminated at a network operating time of 1 *second*. It is observed that under low to medium traffic,

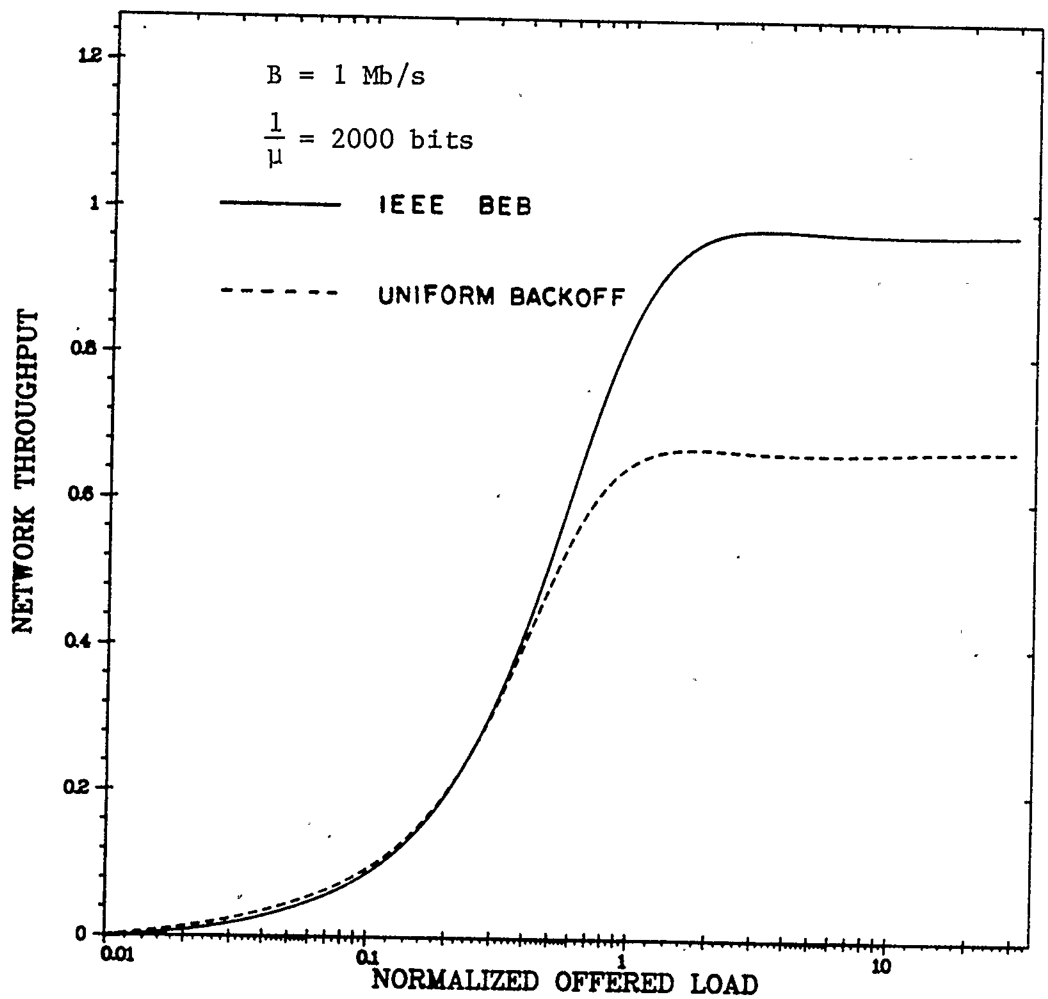

Fig. 4.15 (a) Effect of Backoff algorithm on Network Throughput for STARNET

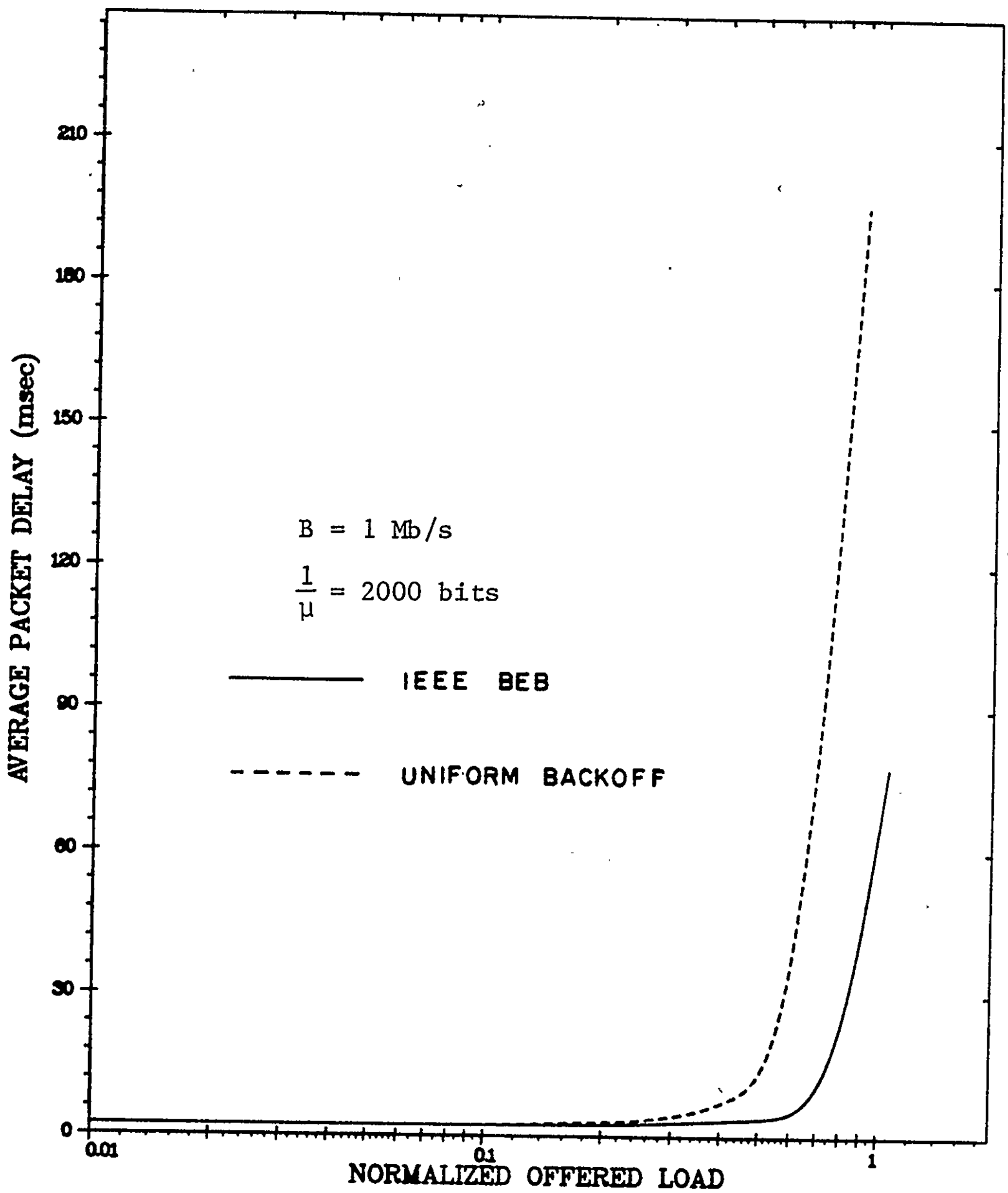

Fig. 4.15 (b) Effect of Backoff algorithm on Average Packet Delay for STARNET

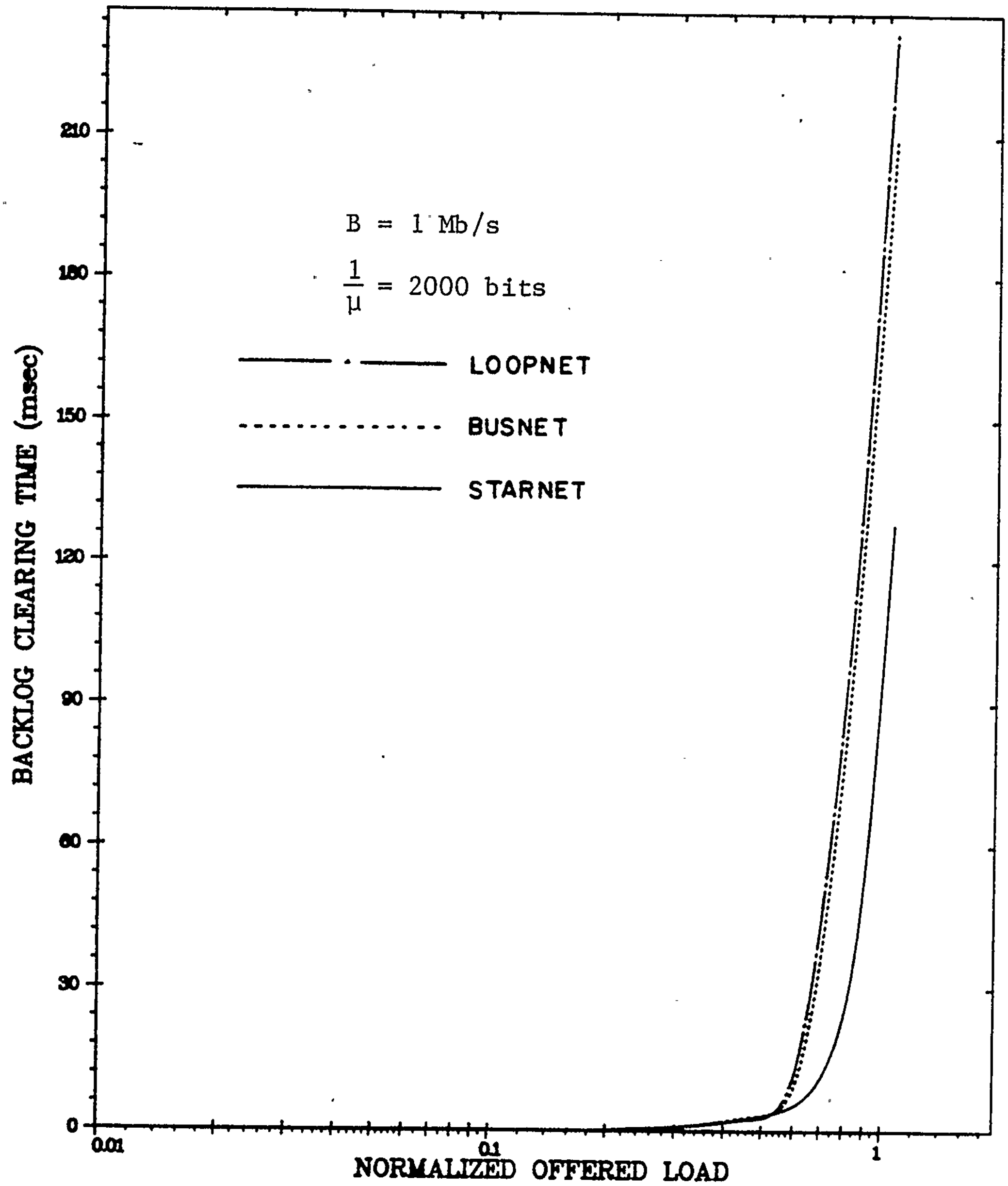

Fig. 4.16 (a) Backlog Clearing Time Versus Offered Load for B = 1 Mb/s , $\frac{1}{\mu}$ = 2000 bits

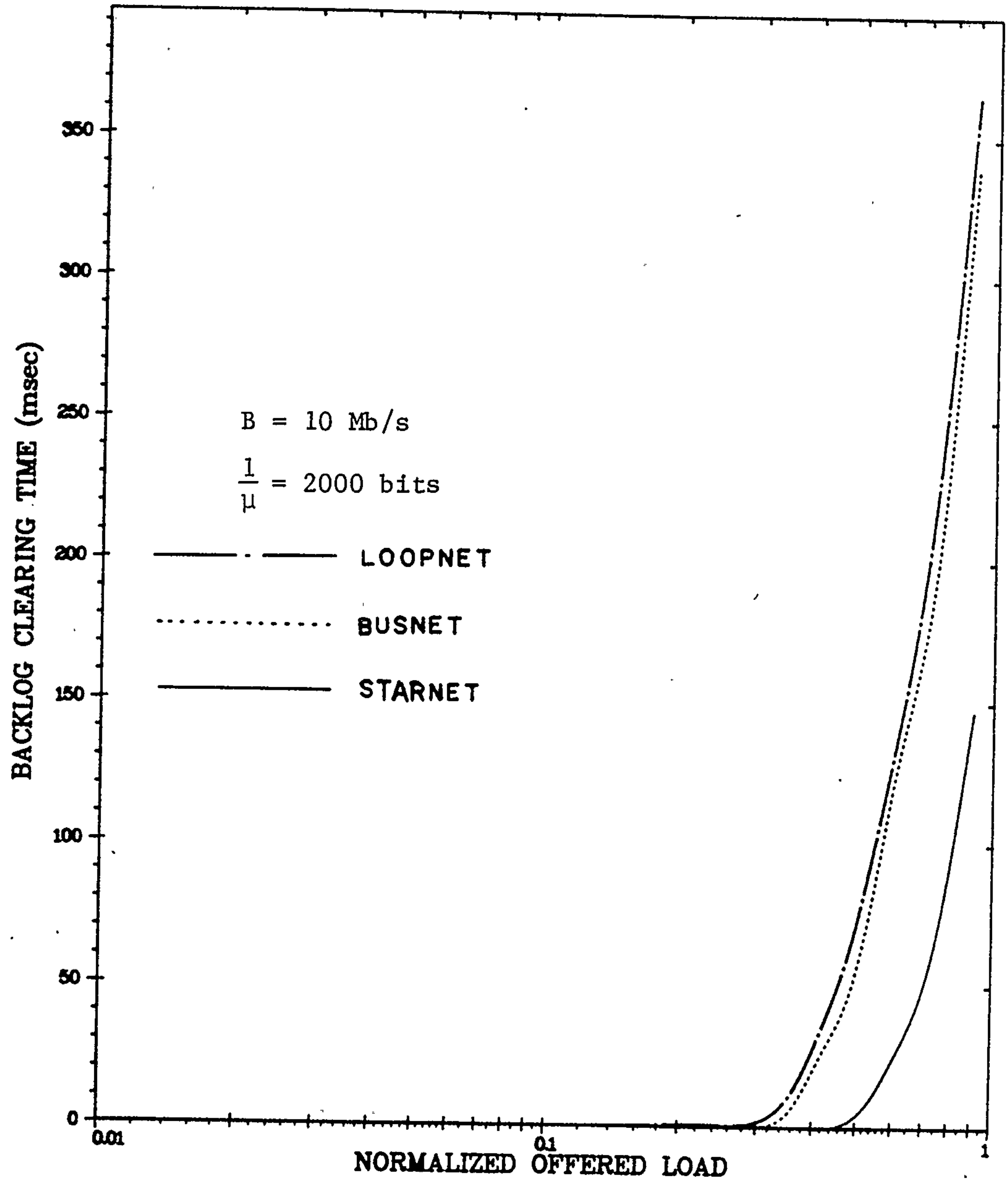

Fig. 4.16 (b) Effect of higher channel capacity on Backlog clearing time

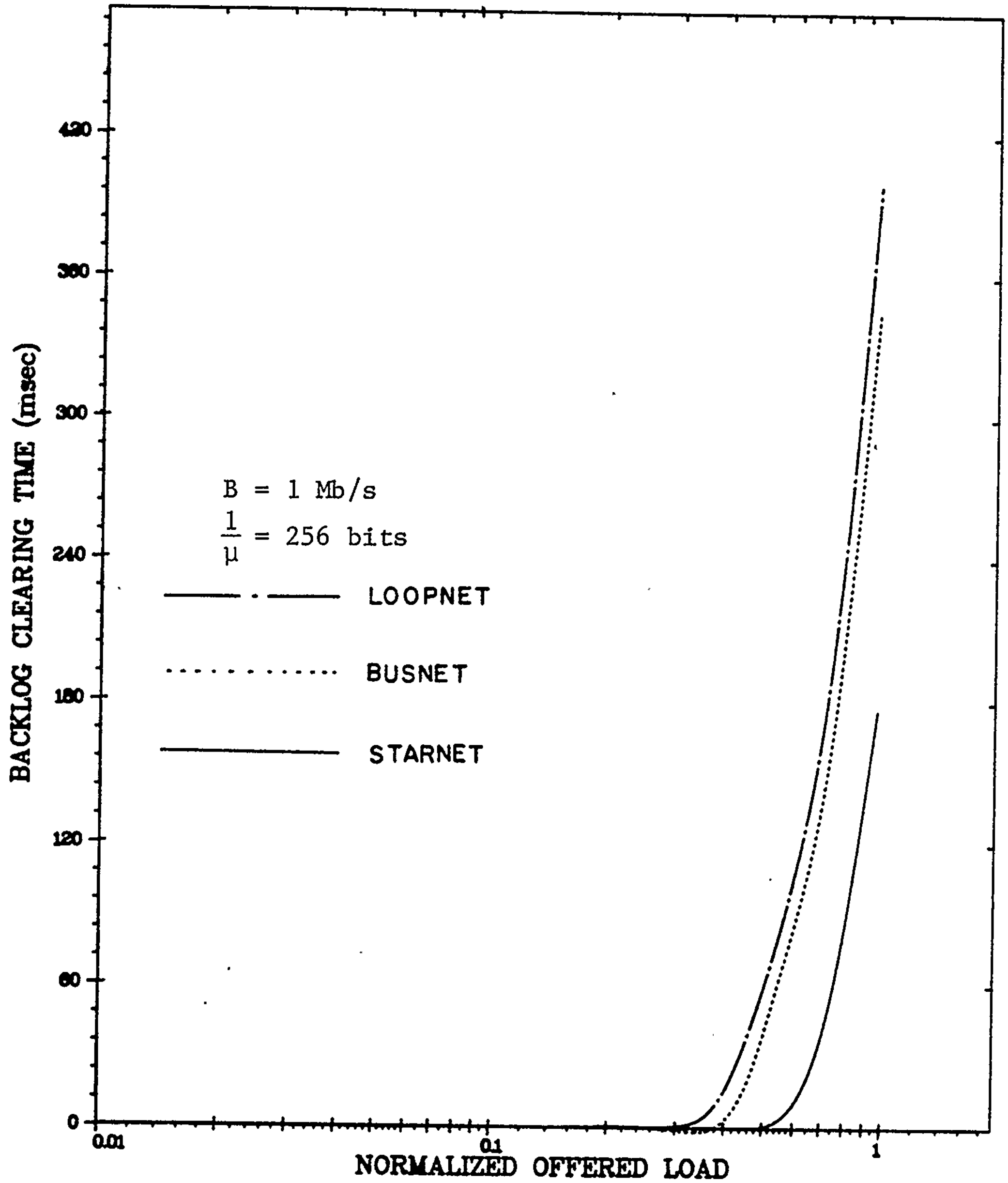

Fig. 4.16 (c) Effect of lower mean packet length on Backlog Clearing time

the backlog clearing time is zero due to a lack of queue buildups at the network nodes. Under high traffic, the STARNET is seen to have the smallest clearing time, the explanation for this being the small propagation delay that is associated with this topology. In like manner to the results obtained for the mean packet delay, the effects of either increasing the channel capacity at a constant mean packet length or lowering the mean packet length at a constant channel capacity lead to large backlog clearing times (Figure 4.16b and Figure 4.16c).

4.6. Summary

This Chapter begins with a justification for the use of the simulation approach in the evaluation of the performance of planned passive optical fiber local area networks (POFLAN's) and the capabilities and a detailed description of the software package developed for this purpose are then presented. The software package is satisfactorily verified and validated in order to build a high confidence level in the output results obtained. The usefulness of the package is then illustrated by its application in evaluating the performance of two network examples. Several results and the discussions on these results are then presented.

CHAPTER 5

CONCLUSIONS AND SUGGESTIONS FOR FUTURE DEVELOPMENTS

5.1. Conclusions

Digital computer-aided network design tools are becoming very popular in the communications industry. Of particular interest to this thesis is the development of a tool named Fiber Optic Network SIMulator (FONSIM) to be used in the evaluation of the performance of passive optical fiber local area networks (POFLANs') for broadcast data communication applications.

In developing a framework for the FONSIM package, each of the conventional local area network topologies-Star, Loop, and Linear Bus is first implemented as a POFLAN topology using currently available optoelectronic devices, optical fiber and optical interconnecting components such as couplers and connectors.

Five network performance parameters, namely, the total network path length, the network attenuation, the dynamic range, bandwidth capability and network traffic characteristics have formed the basis of the performance evaluation of all the POFLAN topologies considered in this thesis. The path length parameter is important because the costs of the optical fiber and its installation often form a significant part of the total system cost thus minimizing the total fiber length will lead to a more cost-effective system. The optical fiber, the optical connectors and the optical couplers account for all the transmission losses in an optical fiber system and it is therefore important to ensure that these transmission losses are lower than the allowable system power budget. The attenuation parameter is used as a measure of the above condition and it is also used to determine the total number of nodes which can be supported by each network topology. The network dynamic range parameter determines the maximum variation in a nodal received power, moreover, the total number of nodes that can be supported by a network topology is also dependent on the network dynamic range. The network bandwidth determines the information carrying capability of each network topology. The network traffic characteristics provide an insight on the amount of the available channel capacity that is useful for transmitting packets at a given network traffic level and also the average delay suffered by the transmitted packet before it is received at its destination.

Appropriate equations, algorithms and procedures which are required in the evaluation of these performance parameters have been presented.

A description of the features, capabilities, and structure of the FONSIM package which has been developed to facilitate the task of network design is provided and this package is specifically designed for the simulation of the different POFLAN topologies. The software package is well structured to allow flexible interactive use by network design experts and nonexperts and its modular structure allows any of the available package modules to be modified without affecting any of the other modules. Due to the relative complexity of the package, it is designed to run on a large computer system. Currently the package may be executed on a VAX 11/780 computer system or on a CDC CYBER 205 Supercomputer. The codes are written in FORTRAN 77 programming language so as to allow a sufficient degree of portability to other programming environments.

In Chapter Four, the usefulness of the FONSIM package developed has been demonstrated using two network examples. The main conclusions from these examples are summarized as follows:

(i) Under identical conditions for all the topologies considered, the Star topology can support a far greater number of nodes than the Linear Bus or the Loop topology. High coupling losses limit the number of nodes which can be supported by the Linear Bus and Loop topologies.

(ii) The Star topology has a smaller transmission loss than either of the other two topologies.

(iii) While the dynamic range requirements of the Loop and Linear Bus topologies are high and linearly increasing with the number of nodes supported, the dynamic range requirement by the Star topology is very low and invariant with the number of nodes, where this has the advantage of a reduced design constraint on the optical receiver at each of the Star network nodes.

(iv) Large size networks or networks operating at high bit rates require high quality fibers (fibers with low attenuation coefficients) for network interconnections.

(v) The Star topology has the largest bandwidth capability of all the topologies.

(vi) For the 6-node network example, the Star topology requires a greater fiber length than either the Loop or Linear Bus topology whereas in terms of the other criteria, it exhibits a superior performance. With regard to the traffic characteristics, the Star topology attains the maximum network throughput and it is determined that the packets transmitted on the Star topology experience the least delay. The Star topology has the shortest backlog clearing time of all the topologies. It follows that both increasing the channel capacity while the mean packet length remains constant and lowering the mean packet length at a constant channel capacity have a declining effect on the network throughput and on the mean packet delay. The CSMA/CD protocol is the simulated access protocol for all the POFLANs' and it is confirmed that the performance of this protocol is sensitive to the propagation delay. It is observed that the type of backoff algorithm which is applied for selecting the retransmission delays of the colliding packets also affects the protocol performance. In particular, the results obtained indicate that the IEEE BEB algorithm is superior to the Uniform backoff algorithm.

In summary, it is clear from these examples that the Star topology is the overall optimum choice of the three POFLAN topologies considered and this explains why much current research efforts are being geared towards the development and improvement of this topology [4,36]. The performance of the Loop and Linear bus topologies can be significantly improved if interconnecting component losses are significantly reduced, thus making them more competitive with the Star topology. Much effort is presently being spent in this area.

Finally, it is very important to stress that in a network design process, there are other subtle design criteria which must be taken into consideration before a final decision is made on the most suitable network topology to be employed. Such considerations include the type of application the network is to serve, the cost-effectiveness, the geographical distribution of the network nodes and political considerations. Decisions on some of these factors are beyond the scope of network designers as they are made by management. It is however essential that those directly involved in network design should be able to provide the policy makers with exact and accurate technical details on which subsequent decisions will be based and the FONSIM package that has been developed in this thesis will serve as an invaluable network design tool for determining these technical details.

5.2. Suggestions for Future Developments

The development of any simulation package is an ongoing process and a good simulation package must therefore allow for upgradability when the need arises. The FONSIM package developed in this thesis is no exception to this fact and its modular structure facilitates the addition of new modules without affecting the existing ones. At present, the package handles only digital transmissions and single-packet messages, the CSMA/CD protocol is the one access protocol considered for all the network topologies and furthermore the package can analyze only one type of network topology at a time.

Suggestions on future developments of the FONSIM package should be directed into the following areas:

(i) The handling of analog voice and video transmissions

(ii) The transmission of multiple packet messages

(iii) It is well known that some topologies perform better with a specific type of access protocol, therefore the incorporation of other types of access protocols such as the token ring or the token bus into the package will allow a direct comparison with the CSMA/CD protocol, alternatively, an entirely new protocol which is more suitable for all the POFLANs' may be proposed.

(iv) For a very complex network which consists of many nodes which cannot be well fitted to one of the regular local area network (LAN) topologies, such a network can be analyzed by partitioning it into two or more sections, where each section represents one of the conventional LAN topologies. The FONSIM package should therefore be upgraded to handle the analysis of such hybrid networks.

(v) Another important area that requires refinement is how to increase the program running speed and also to reduce the computer storage requirements. At present, the average running speed of the traffic modules is about 100 cpu seconds on the CDC CYBER 205 Supercomputer. The improvement gained on the run time on the CYBER 205 Supercomputer over the run time on the VAX 11/780 system is of the order of 100 to 150. The running speed on the CYBER 205 Supercomputer can be increased by vectorizing the codes and this will allow larger networks to be analyzed.

REFERENCES

(1) P. Baues, "Local Area Networks Based on Fiber-Optic Communication Technology," *Siemens Forsch. -u. Entwickl. -Ber.* Bd. 12, pp.3-10, January 1983.

(2) R. Maciejko, "Fiber Optics for local area networks," *Telesis,* Vol.2, pp.15-19, February 1984.

(3) R.V. Schmidt, E.G. Rawson, R.E. Norton Jr., S.B. Jackson, and M.D. Bailey, "Fibernet II: A Fiber Optic Ethernet," *IEEE Journal on Selected areas in Communications,* Vol. SAC-1, pp.702-711, November 1983.

(4) Y. Hakamada and K. Ogushi, "32 *Mbit/s* Star Configured Optical Local area network design and performance," *Journal of Lightwave Technology,* Vol. LT-3, pp.511-524, June 1985.

(5) P.W. Shumate and M.D. Domenico, Jr., "Lightwave Transmitters," *in Semiconductor Devices for Optical Communication.* New York: Springer-Verlag, 1980, Chapter 5.

(6) J.K. Butler, "The effect of Junction Heating on Laser linearity and harmonic distortion," *in Semiconductor Devices for Optical Communication.* New York: Springer-Verlag, 1980, Chapter 8.

(7) S.D. Personick, *Optical Fiber transmission Systems,* New York: Plenum Press, 1981.

(8) J. Gowar, *Optical Communication Systems,* Englewood Cliffs: Prentice-Hall International Series in Optoelectronics, 1984.

(9) S. Geckeler, "Modelling of Fiber-Optic transmission Systems on a Desk-Top Computer," *Siemens Forsch. -u. Entwickl. -Ber.* Bd.12, pp.127-134, February 1983.

(10) A.H. Cherin, *An Introduction to Optical Fibers,* New York: McGraw-Hill, Inc., 1983.

(11) D.G. Duff, "Computer-Aided Design of Digital Lightwave Systems," *IEEE Journal on Selected Areas in Communications,* Vol.SAC-2, pp.171-185, January 1984.

(12) S.D. Personick, "Receiver design for digital fiber optic Communication systems, Part I and II," *Bell System Technical Journal,* Vol.52, pp.843-886, July-Aug. 1973.

(13) D.R. Smith and I. Garett, "A simplified approach to digital optical receiver design," *Optical and Quantum Electronics,* Vol.10, pp.211-221, October 1978.

(14) D.R. Smith, R.C. Hooper and I. Garett, "Receivers for optical communications: A comparison of avalanche photodiodes with PIN-FET hybrids," *Optical and Quantum Electronics,* Vol.10, pp.293-300, October 1978.

(15) Kaptron Inc., "Fiber Optics Couplers, Monitors, Switches, Multiplexers," *Application Notes,* 1984.

(16) G.R. Elion and H.A. Elion, *Fiber Optics in Communication Systems,* New York: Marcel Dekker, Inc., 1978.

(17) P.K. Cheo, *Fiber Optics: Devices and Systems,* Englewood Cliffs: Prentice Hall, 1985.

(18) S. Geckeler, "Pulse broadening in Optical fibers with mode mixing," *Applied Optics,* Vol.18, pp.2192-2198, July 1979.

(19) A. Papoulis, *Probability, Random variables, and Stochastic Processes,* New York: McGraw-Hill, 1984.

(20) F.A. Tobagi and V.B.Hunt, "Performance analysis of carrier sense multiple access with collision detection," *Computer Networks*, Vol.4, pp.245-259, 1980.

(21) S.S. Lam, "A carrier-sense multiple access protocol for local networks," *Computer networks*, Vol.4, pp.21-32,1980.

(22) W. Stallings, *Local Networks*, New York: Macmillan Publishing Company, 1984.

(23) IEEE 802.3, "CSMA/CD Access Method and Physical Layer Specifications," *in Local Network Standards*, IEEE Project 802, 1983.

(24) W.J. Graybeal and U.W. Pooch, *Simulation: Principles and Methods*, Cambridge: Winthrop Publishers, Inc., 1980.

(25) D. Irvine-Halliday and A.O. Fapojuwo, "Performance Evaluation of Passive Optical Fibre LAN's," *in Proc.* 10th *Australian Conference on Optical Fibre Technology*, Perth, pp.197-201, December 1985.

(26) H. Kobayashi, *Modeling and Analysis: An Introduction to System Performance Evaluation Methodology*, Reading: Addison-Wesley Publishing Company, 1978.

(27) A.M. Law and W.D. Kelton, *Simulation Modeling and Analysis*, New York: McGraw-Hill Book Company, 1982.

(28) W.H. Beyer, *CRC Standard Mathematical Tables*, Boca Raton: CRC Press, Inc., 1984.

(29) R. Page, R.Didday and E. Alpert, *FORTRAN 77 for Humans*, New York: West Publishing Company, 1983.

(30) L. Kleinrock, *Queueing Systems, Vol.1: Theory,* New York: John Wiley, 1975.

(31) J.F. Shoch and J.A. Hupp, "Measured performance of an Ethernet Local Network," *in The Ethernet Local Network: Three Reports,* CSL-80-2, Xerox Palo Alto Research Center, 1980.

(32) General Optoelectronics Corp., "Application Notes on LED Modules," 1984

(33) T.V. Muoi, private communication, TRW Electrooptics Research Center, El Segundo, CA, 1984.

(34) E.G. Rawson, private communication, Xerox Corporation, Palo Alto Research Center, Palo Alto, CA, 1985.

(35) L. Kleinrock and F.A. Tobagi, "Packet Switching in Radio Channels: Part I-Carrier Sense Multiple-Access Modes and their Throughput-Delay Characteristics," *IEEE Transactions on Communications,* Vol. COM-23, pp.1400-1416, December 1975.

(36) E.G. Rawson, "The Fibernet II Ethernet-Compatible Fiber-Optic LAN," *Journal of Lightwave Technology,* Vol. LT-3, pp.496-501, June 1985.

APPENDIX

DERIVATION OF THE PERFORMANCE MEASURES FOR THE *M/M/*1 SYSTEM

The *M/M/*1 system (Fig.4.4) is a single-server system whose interarrival and service times are exponentially distributed with parameters $\frac{1}{\lambda}$ and $\frac{1}{\mu C}$ respectively. There is no restriction on the queue size and the queue discipline is a first-in, first-out discipline.

(i) Expected Number of Packets in the System:

Let X denote the random variable that counts the number of packets entering the system. The steady state probabilities for an *M/M/*1 system having the traffic intensity less than unity ($\rho = \frac{\lambda}{\mu C} < 1$) is given by [30]

$$P_n = \rho^n(1-\rho) \quad n = 0,1,2,... \tag{A1.1}$$

Thus,

$$P(X = x) = P_x = \rho^x(1-\rho) \quad x = 0,1,2,... \tag{A1.2}$$

The expected value of X is defined by

$$E(X) = \sum_{x=0}^{\infty} xP_x \tag{A1.3}$$

Substituting P_x into Equation (A1.3) gives

$$E(X) = (1-\rho)\sum_{x=0}^{\infty} x\rho^x \tag{A1.4}$$

Noting that $\rho < 1$ and by simple algebraic manipulation

$$E(X) = L = \frac{\rho}{1-\rho} \tag{A1.5}$$

(ii) Expected Number of Packets in the Queue:

Let Q_m denote the random variable that counts the number of packets waiting in the queue for transmission. Then the expected value of Q_m is given by

$$E(Q_m) = 0P_o + \sum_{j=1}^{\infty}(j-1)P_j \tag{A1.6}$$

Simplifying,

$$E(Q_m) = \sum_{j=0}^{\infty} jP_j - \sum_{j=1}^{\infty} P_j \tag{A1.7}$$

Applying Equation (A1.3) to the first term on the right hand side results in

$$E(Q_m) = L - \sum_{j=1}^{\infty} P_j \tag{A1.8}$$

But

$$\sum_{j=0}^{\infty} P_j = 1$$

so

$$\sum_{j=1}^{\infty} P_j = 1 - P_o$$

Hence,

$$E(Q_m) = L - (1 - P_o) \tag{A1.9}$$

Since $P_o = 1 - \rho$, the expected number of packets in the nodal queue is obtained as

$$E(Q_m) = L_q = \frac{\rho^2}{1-\rho} \tag{A1.10}$$

(iii) Expected Packet Delay in the System:

The expected delay experienced by a packet in the system consists of the nodal delay and the transmission time. The expected delay is usually computed by using Little's formula [30]. If W is the expected packet delay in the system, L the expected number in the system and λ the packet arrival rate, then

$$L = \lambda W \tag{A1.11a}$$

or

$$W = \frac{L}{\lambda} \tag{A1.11b}$$

Substituting the expression for L gives

$$W = \frac{1}{1-\rho}\left(\frac{1}{\mu C}\right) \tag{A1.12}$$

(iv) Expected Packet Delay in Queue:

Little's formula also relates the average packet delay in the queue to the average length of the queue:

$$L_q = \lambda W_q \tag{A1.13}$$

Substituting the expression for L_q and solving for W_q gives

$$W_q = \frac{\rho}{1-\rho}\left(\frac{1}{\mu C}\right) \tag{A1.14}$$